JAIST Repository
https://dspace.jaist.ac.jp/

Title	時間対称な制御入力信号と引き込み効果に基づく2脚ロボットの高効率かつ頑健な歩容生成
Author(s)	顔, 聡
Citation	
Issue Date	2023-03
Type	Thesis or Dissertation
Text version	ETD
URL	http://hdl.handle.net/10119/18419
Rights	
Description	Supervisor:浅野 文彦, 先端科学技術研究科, 博士

JAIST
JAPAN
ADVANCED INSTITUTE OF
SCIENCE AND TECHNOLOGY

Japan Advanced Institute of Science and Technology

Efficient and Robust Gait Generation for Biped Robots Based on Time-symmetric Control Input Signals and Entrainment Effects

Cong Yan

Japan Advanced Institute of Science and Technology

Doctoral Dissertation

Efficient and Robust Gait Generation for Biped Robots Based on Time-symmetric Control Input Signals and Entrainment Effects

Cong Yan

Supervisor: Associate Professor Fumihiko Asano

Graduate School of Advanced Science and Technology
Japan Advanced Institute of Science and Technology
Information Science

March 2023

Abstract

Bipedal robots can operate in more restricted environments than multi-legged and wheeled robots, and most conventional bipedal robots are driven by actuators at each joint with precise joint angle control to follow a target trajectory for walking motion. In typical motion control methods for bipedal robots, the ZMP (zero moment point), the point at which the combined forces of gravity and inertia are projected onto the road, is the standard for stable walking, but it is commonly noted that this control method does not make excellent use of its own EI (embodied intelligence) to improve walking efficiency and to obtain a natural gait. Moreover, the robot requires precise real-time feedback control to achieve stable walking in a fully-actuated manner, which results in huge energy loss and cannot be sustained for long periods of time in real-world environments. Therefore, in recent years, numerous researchers have focused on how to use body dynamics to control robots to maintain efficient motion. The most significant challenge in this research direction is to improve walking efficiency while having available robustness.

By exploiting the dynamics dictated by the robot's body structure, the robot can not only considerably improve the efficiency of its motion but also considerably reduce its computational effort and thus the difficulty of control. Nonetheless, the fundamental problem with this approach is that the expected behavior of the system is highly dependent on environmental conditions, which leads to a lack of robustness. For example, a passive walking robot could use its body dynamics to walk down a slope in a deep natural way without any input. However, it can only function under the constraints of a suitable slope angle and ground friction. Another example is the CPG (central pattern generator), a local oscillatory network composed of neurons, which generates stable phase-locking relationships through mutual inhibition between neurons and produces rhythmic movements at relevant parts of the soma through self-excited oscillations. The CPG-based approach to motion control simulates the temporal sequencing of animal walking, which is a more natural approach for robotic motion control problems. However, an extremely large number of term conditions typically require attention when constructing CPG models, resulting in control methods that are still not concise enough.

In this paper, the author aims to explore more underlying mechanisms of walking and achieve a more simple and more efficient method of motion control for bipedal robots. We can draw on two signal systems acquired by humans during evolution, namely the first and the second signal system. A similar classification of signal systems can be made for the generation of robotic motion. The former is used to reliably generate and maintain elementary motions, while the latter is used to adapt flexibly to complex environments where each system operates in a shared and coordinated manner. First, a minimalist compass-like bipedal robot where only the hip torque can be applied, so the robot is an underactuated system. Here the bipedal robot can be made to walk efficiently and stably on downhill as well as horizontal surfaces by means of entrainment effects, using a reasonable feedforward input waveform (e.g., a sine wave). It can be regarded as the motion generation of the control signal (first signal system) generated at the level of human reflexes without any feedback control, which greatly reduces the cost of control. At the same time, step length, walking frequency, and walking speed, which are important indicators of walking within the entrainment range, can be simply tuned by controlling the parameters.

To ensure the practical feasibility of the proposed method, it is necessary to conduct an experimental study to verify whether entrainment effects can successfully control a robot to generate dynamic walking in a realistic environment. A bipedal walker was designed and fabricated to allow for practical experiments. The control method is consistent with that used in the simulation, where a designed planetary gear mechanism is used to complete gait generation on a horizontal road surface by feeding a preset feed-forward waveform through a hip-only servo motor. It should be noted that in order to avoid gait failure due to foot scuffing while swinging the leg, the rotator foot is designed to circumvent it. Although the 1:1 entrainment between the input waveform frequency and the actual

walk frequency is only achieved due to hardware conditions, the experimental results are in good agreement with the numerical simulations.

In order to pursue higher walking performance, such as high-speed walking, and to obtain the highest energy utilization while limiting the walking speed, the author performs a global optimization of the control parameters, as well as the physical parameters of the robot itself, by means of Bayesian optimization. The results show that the fastest walking speed occurs in a 2:1 entrainment waveform when only the control parameters are changed, while the fastest walking speed can be achieved in a 1:1 entrainment waveform after optimizing the foot shape, which indicates that the structural design of the robot itself, such as the foot shape and the overall center of gravity distribution, is also important. The results for walking efficiency show that while maintaining a walking speed of 0.5 [m/s] or more, SR can be as low as 0.007 (lower values indicate higher walking efficiency) by the proposed control method, which is much lower than the current robots by conventional control methods and even better than humans.

In bipedal dynamic walking, one also usually expects the gait to converge to a limit cycle gait. From another point of view, the most basic requirement for achieving stable bipedal walking is not to fall, which requires a large BOA (basin of attraction) to tolerate disturbances. Chaotic oscillators tend to have larger basins of attraction compared to the limit cycle. Correspondingly, it is hypothesized in this paper that a properly generated chaotic bipedal gait due to entrainment effects may be more robust to perturbations such as walking on uneven ground. Based on this consideration, a chaotic gait is generated by employing a typical chaotic oscillator Rössler attractor. It was shown that the chaotic bipedal gait has a larger BOA than the limiting periodic walk with the same input strength, and the domain of stable walking was further explored by varying the control parameters of the chaotic bipedal gait.

Work so far has focused on exploring the robot's walking conditions under the first signal system and generating relatively stable and efficient gaits. The judgment of more complex road conditions requires advanced signal processing capabilities corresponding to a second signaling system. The present work lays the groundwork for further research, not only by enabling bipedal walking on uneven ground with extremely simple control methods but also by showing the positive side of chaos in dynamic walking and providing a new perspective on the stability of bipedal gait.

Keywords: Bipedal robot, Passive walking, Entrainment, Rimless wheel, Semicircular feet, Chaotic gait, Stability, Efficiency

Acknowledgments

First, I would like to express my sincere gratitude to my main supervisor, Associate Professor Fumihiko Asano, for guiding me, encouraging me, and setting me an excellent example over the years. I am fortunate to have joined the Asano lab and to have had the opportunity to be guided and cared for by Asano sensei. He acted not only as my supervisor but as a friend, with whom I corresponded regularly in my daily life as we shared numerous common interests. I believe that without his careful guidance and full support, my research life at JAIST would have been difficult. Second, I would like to express my sincere gratitude to Professor Isao Tokuda, my supervisor of minor research for the out-of-school program. Through the direction of my minor research project, Tokuda sensei taught me a lot of fascinating knowledge related to nonlinear mechanics and opened the door to a new world by conducting experiments to observe the exciting phenomenon of noise-induced synchronization.

Then, I would especially like to thank my Second Supervisor, Professor Kazuhiro Ogata, and my on-campus minor research advisor, Associate Professor Yonghoon Ji, who not only gave me extremely helpful advice at critical times but also regularly cheered me up by e-mail. I would also like to thank Professor Kunihiko Hiraishi and Associate Professor Yuji Harada for their willingness to devote their energy to reviewing my doctoral dissertation despite their busy schedules, and I believe that I will submit a better final draft through their professional comments on the revision of my dissertation.

Next, I would like to focus on thanking my senior, Associate Professor Longchuan Li, without whose introduction I would not have had the opportunity to enter the Asano lab and meet so many wonderful people. From the beginning of my master's degree, Dr. Li taught me a lot of basic research by hand. His frequent correspondence with me on the latest developments in research opened my eyes to this day. I am more than willing to pass on Dr. Li's helpful spirit. In addition, I would like to thank the members of my lab, especially Haosong Chen and Yuxuan Xiang for helping me with my experiments, Yanqiu Zheng for discussing my project, and my senior Masatsugu Nishihara for teaching me a lot about lab management. Furthermore, I would

like to thank Yuetong He, Runyu Liu, Qiukai Qi, Sixia Li, Bowen Cui, Zhaolun Huang, Kai Li, and all my other friends at JAIST.

I would also like to thank the Japan Student Services Organization(Jasso) for providing me with a scholarship, JAIST for providing me with research grants (Houga), and all the JAIST staff for their help. Most of all, I am grateful to my parents and wife for their support, tolerance, and understanding. It would have been particularly tough for me to have gotten this far without their constant inspiration and companionship.

List of Figures

List of Tables

Acronym and Abbreviation

ZMP	Zero moment point
EI	Embodied intelligence
CPG	Central pattern generator
BOA	Basin of attraction
BO	Bayesian optimization
DOF	Degrees of freedom
RW	Rimless wheel

Table of Contents

Chapter 1

Introduction

1.1 Background

With the rapid development of modern science and technology, especially the maturing of robotics, the use of robots to assist human workers has become increasingly close to reality [1]. Although mature robotics and applications are still mainly focused on robotic arms and wheeled mobile robots, most people's first impression of robots should still be like the bionic anthropomorphic form of the classic Japanese anime Iron Arm Astro Boy, which is believed to be the original intention of numerous robotics researchers. Bipedal robots benefit from their human-like body structure and are expected to walk on a variety of surfaces, something that alternative methods of locomotion cannot replace. One of the main control methods thus far is the standard one with Zero Moment Point(ZMP), defined by Vukobratović et al. [2]. ZMP refers to the point on the sole of the foot where the combined forces acting on the sole of the foot are applied. For a motion to be realizable, the ZMP must be guaranteed to lie within the support polygon, a common stability criterion for footed robots. ASIMO [3], which Honda has announced it is discontinuing development of, is a prime example of a vehicle based on this traditional control approach. However, the ZMP control approach requires the use of a variety of high-precision sensors to acquire data in real-time, a high-performance chip to quickly compute the robot's center of gravity and position, and finally a costly actuator to precisely track the target trajectory and thus stabilize the gait. This results in severely elevated control costs and extremely inefficient walking, while we humans walk in ordinary road conditions, with near-unconscious movements, and do not need to precisely control the swing speed and angle

of our legs. Thus, humans are approximately 16 times more efficient than ASIMO walkers. Therefore, from the point of view of natural dynamics, it is desirable to have a natural and efficient control method that can completely exploit the inherent dynamical properties of bipedal robots. Specifically, underdriven robot control requires that the dynamics of the robot be utilized more in the controller design rather than ignored [4, 5].

Passive walking was proposed by McGeer et al. in 1990 [6] to mimic a human gait with no input during downhill, relying only on the conversion between gravitational potential energy and kinetic energy. Since then, people inspired by passive dynamic walking have devised various efficient gait control methods based on passive walking. Goswami et al., and Collins et al. also made great contributions to the performance analysis of passive walking [7–11]. Although passive walking has far-reaching implications and impacts on optimizing the walking efficiency of walking robots. However, in practical walks, it is not possible to achieve input-free. Even if only the gravitational potential energy is used in the descent, only a single gait can be generated, and it is not possible to modify the speed, stride length, or obstacle crossing. Thus, while this concept is well accepted theoretically by walking robotics scholars, it is difficult to be applied and promoted in the real world with sincerity and effectiveness. In order to make the passive walking theory applicable to ordinary road surfaces, robotics researchers have also conducted a lot of research, such as the torque compensation-based approach by Spong et al. [12, 13], the energy constraint-based control approach proposed by Asano et al. [14, 15], an efficient walking method based on parametric excitation by Harata et al. and applied to a robot with knees [16, 17].

Moreover, another similar method is CPG (Central pattern generator), which is a local oscillatory network of neurons that can generate stable phase-locking relationships through mutual inhibition between neurons and generate rhythmic movements in the relevant parts of the soma through self-excited oscillations [18, 19]. Furthermore, the output properties of the CPG can be modulated by the animal's abundant feedback network and higher-level neural centers, so that the CPG can output rhythmic control signals adapted to the environment. The CPG-based approach to humanoid robot motion control, which mimics the time-series properties of bipedal walking, is also a more natural approach to the robot motion control problem, but still requires angle-based feedback and the control cost is still not low enough.

One of the most fundamental issues that need to be addressed when controlling bipedal

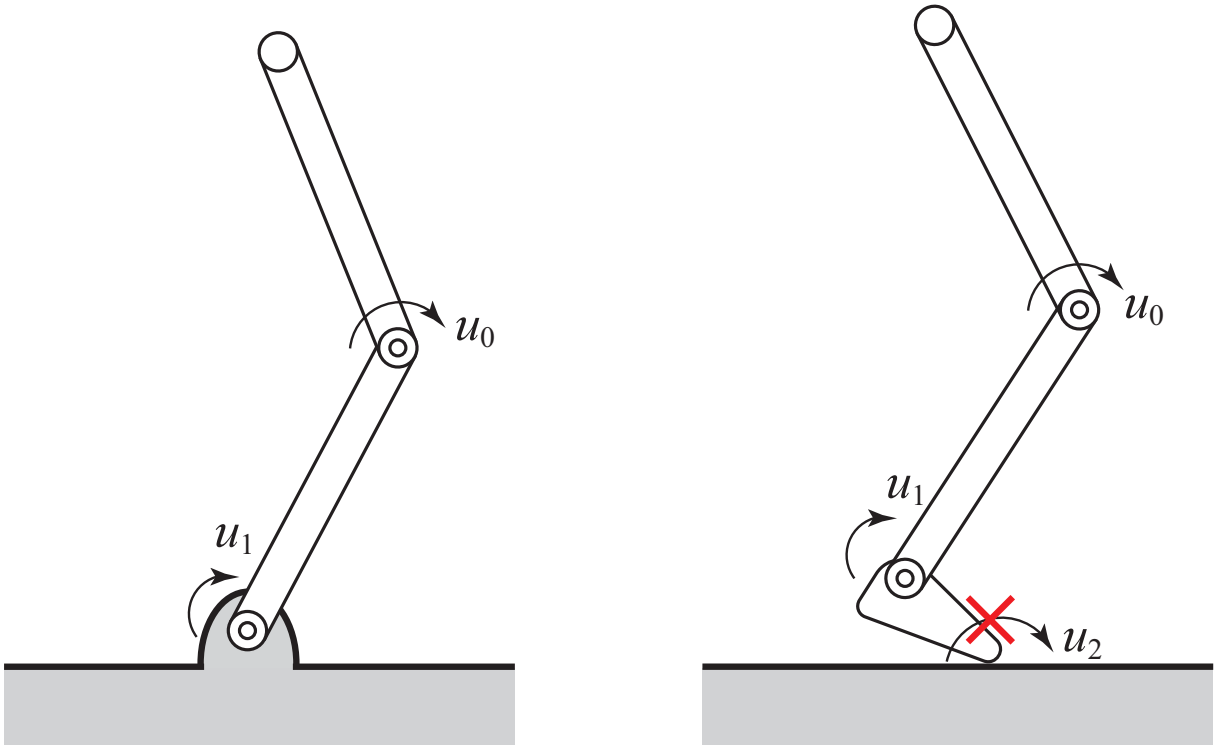

Figure 1.1: Fully-actuated and underactuated

robots with ease and efficiency based on the above ideas is overcoming underactuation without feedback. When the center of gravity changes at any time, it is clear that methods based on precise angular control cannot take full advantage of the dynamic characteristics of the bipedal robot, and only appropriate moment-based feedforward control can do so [20, 21]. This idea has also been proven by dynamical principles and mathematical means [22].

1.1.1 Fully actuated and underactuated

Fully actuated systems refer to a class of mechanical systems in which the number of control inputs in the system is equal to the number of controlled degrees of freedom, and it should be noted that the number of controlled degrees of freedom is not the number of system states. The corresponding two types of systems are underactuated systems (where the number of control inputs is less than the number of controlled degrees of freedom) [12] and over-actuated systems (where the number of control inputs is greater than the number of controlled degrees of freedom) [23]. For a given mechanical system, the driving case is normally determined by the configuration of the specific actuation structure. As shown in Fig. 1.1, the left side uses a

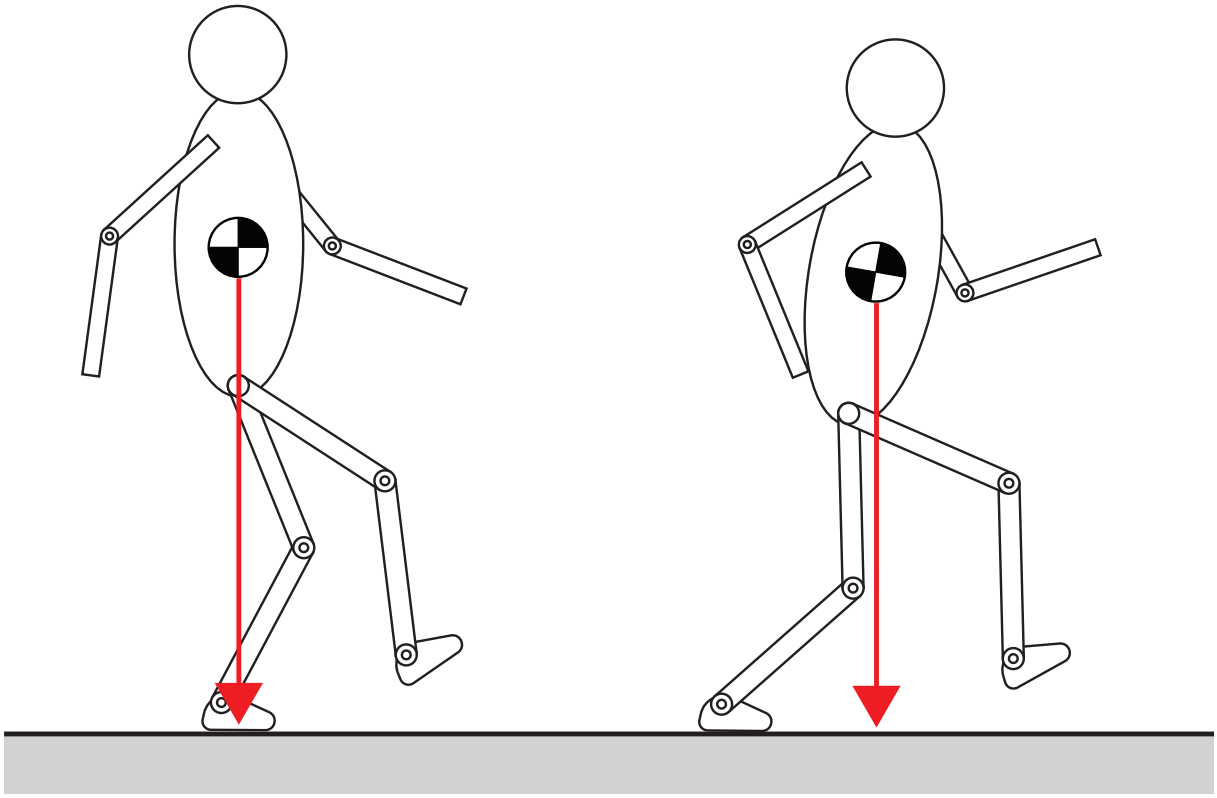

Figure 1.2: Static and dynamic walking

2-rod system as an example, by fixing the bottom to the ground, when the system has only two degrees of freedom and there are two inputs in the system corresponding to each of these two degrees of freedom, the system becomes a fully actuated system. The right side adds a foot to the left to simulate a human leg. At this time, the number of inputs does not alter (u_2 can not work), but the degree of freedom has increased by one, so it becomes an underactuated system. In general, unless the feet can be forcibly constrained to the ground, bipedal walking robots are underactuated systems, which makes it extremely difficult to efficiently and stably control a bipedal robot to achieve the desired motion [24–26].

1.1.2 Static and dynamic walking

Static walking is walking so that with each step the center of gravity of the body is constantly within the range of the soles of the feet (as shown on the left side of Fig. 1.2). For example, a large number of older people also have static walking, they shift their weight carefully, their step length is short, and their walking speed is moderate. In the early days of bipedal robotics

research, most of them used the static walking method [27], including the toys of bipedal robots that are now sold on the market, which makes the sole of the foot extremely large, which makes the grounding area extremely wide and makes it easier to keep the center of gravity within the sole of the foot. When a normal human walks, he or she has a dynamic walking in which the center of gravity is constantly moving forward (As shown on the right side of Fig. 1.2). Dynamical walking [28] is a perfect combination of various factors, such as the relationship between gravity and center of gravity shift, the maintenance of balance, and the parameters of the body that allow us to walk in a stable manner. In other words, in dynamic walking, which uses the body's momentum to move smoothly, the center of gravity is not always on the sole of the foot. It is necessary to increase walking speed and also to achieve dynamic walking when considering walking over uneven or sloping surfaces or any other type of ground. The specific differences between static and dynamic walking are shown in Table 1.1.

1.1.3 Zero moment point

When the robot is walking, it is subject to gravitational forces from the Earth and inertial forces from the acceleration and deceleration of the walk. These combined forces are called total inertial forces. On the other hand, the robot's landing foot is subject to the ground reaction force as a reaction from the ground. The intersection of the axis of total inertia force and the

Table 1.1: Difference between the static and dynamic walking

	Static walking	Dynamic walking
Balance	Walking with constant balance	Intermittently shifts weight by off-balance
Environment	Only can walk on flat ground	Can walk stably on slopes, stairs, uneven floor surfaces, etc
Speed	Slow	Fast
Stop	Can be stopped at any time	Cannot be stopped in the middle
Motion	Walking with upper body move back or forward	Walking with Upper body usually remains fixed

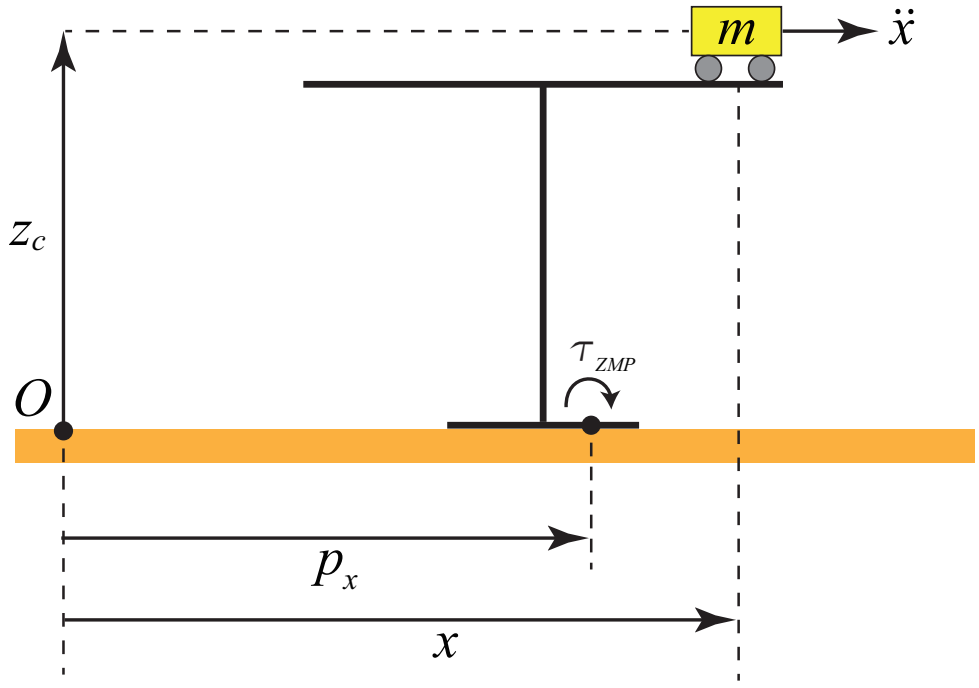

Figure 1.3: Zero moment point

ground is called the Zero Moment Point(ZMP) because the moment of total inertia force is zero. The point where the ground reaction force acts are called the ground reaction force action point. For example, if we focus on our toes, we can stand on our toes or we can stand on our heels. In the former case, the ZMP is located at the toe, and in the latter case, the ZMP is located at the heel.

Simplifying the bipedal robot to a Cart-Table model would be more convenient for dealing with the ZMP problem [29]. As shown in Fig. 1.3, there is a cart moving along the surface of the table on the horizontal ground, and the table presents a top-heavy situation and is prone to tip over due to the limited area of support in contact with the table and the ground. However, the car can be controlled to perform an accelerated motion on the tabletop, generating a corresponding acceleration, relying on inertial forces to obtain an instantaneous equilibrium of the table, at which point the ZMP is within the range of the table support legs. The figure shows a car model moving along the horizontal direction of X. In the 3D setting, a car model moving along the Y direction is also required, and the situation is similar, so the car moving in the horizontal direction is used here as an example for analysis. Since we require that the moment around the

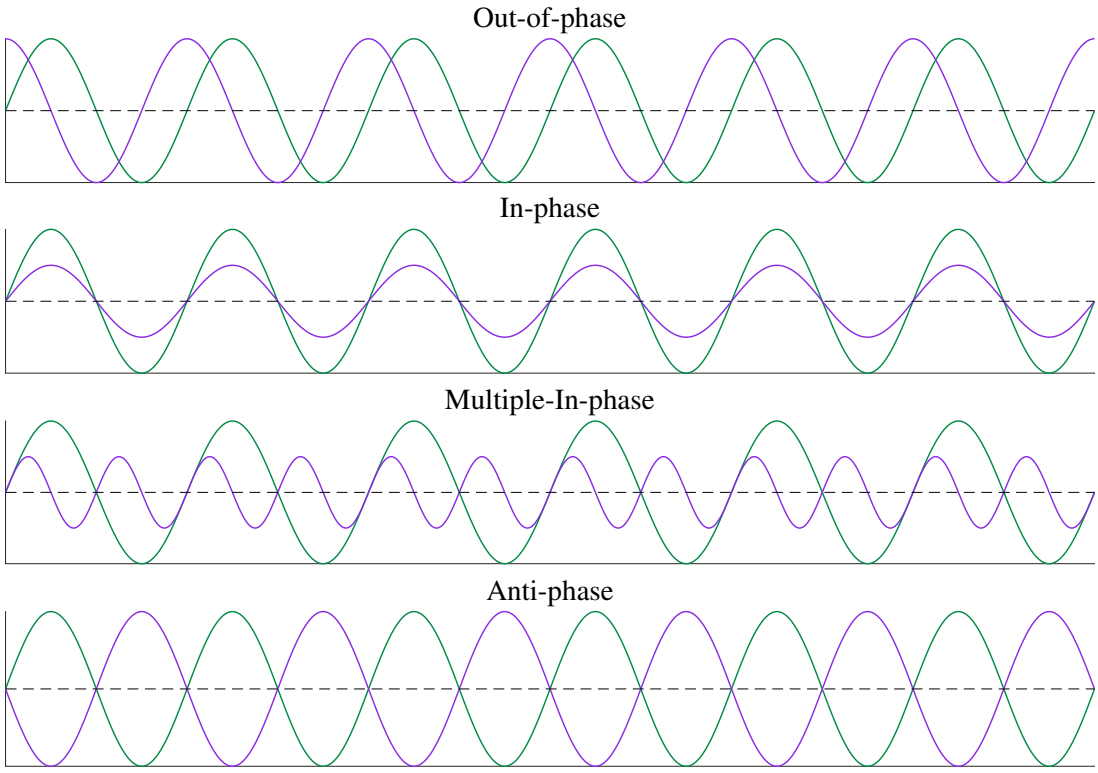

Figure 1.4: Entrainment effect

ZMP must be zero (otherwise it would cause the table to tip over), therefore,

$$\tau_{\text{ZMP}} = mg(x - p_x) - m\ddot{x}z_c = 0. \tag{1.1}$$

The equation implies that the acceleration generated by the car is equivalent to the moment effect at the ZMP in order to be able to cancel the moment effect at the ZMP after the mass of the car has been subjected to gravity, thus ensuring that the table is balanced.

1.2 Research Methodology

1.2.1 Entrainment effect

It is an Entrainment effect two oscillators, which, if no external force were applied, should have their own natural frequencies, are compelled to vibrate in concert when their frequencies are close to each other, and to synchronize at a common frequency slightly deviating from

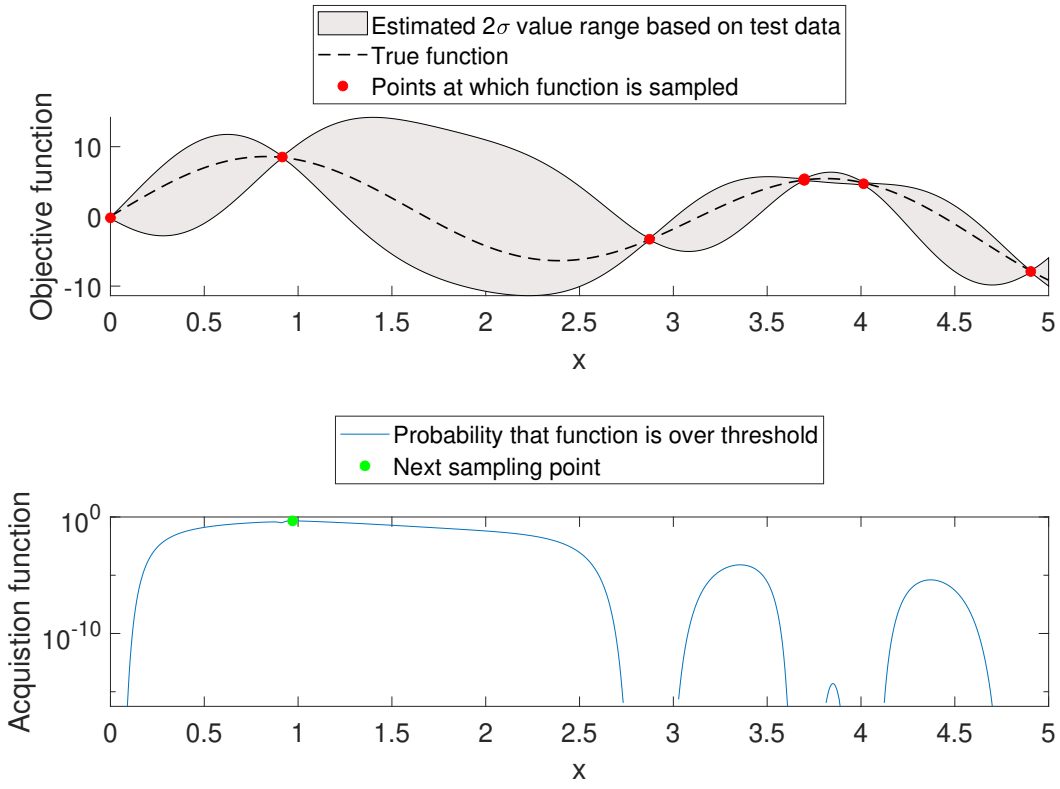

Figure 1.5: Bayesian optimization

their original natural frequency [30,31]. For example, if two metronomes with slightly different frequencies are placed on the same table, they will move at the same frequency. Humans operate on a 24-hour cycle (the original biological clock is about a 25-hour cycle, but it is entrained to the sun). As shown in Fig. 1.4, the two oscillators can be represented as Out-of-phase, In-phase, Multiple-In-phase, and Anti-phase. If the two oscillators are linear systems, then an accurate algebraic model can be constructed such that the state of the system can be predicted from the solution of the model. However, it is common that most of the oscillators, in reality, are nonlinear systems, which require the use of nonlinear mechanics for analysis.

1.2.2 Bayesian optimization

BO (bayesian optimization) is effective in finding global maxima or minima in the case of high-dimensional parameter spaces and unknown or non-reducible cost functions [32]. The specific process is as follows:

- Gaussian process
  - Definition: express the cost function/function to be optimized as a probability distribution and update the probability distribution using the observed values
  - Purpose: to obtain the optimal value by iteration
  - Inputs: combinations of parameters
  - Outputs: vector of means, the covariance matrix
- Collection function
  - Definition: function used to evaluate the probability of a favorable performing observation (a function that predicts which set of parameters will yield the optimal value)
  - Purpose: to select the next point of observation
  - Inputs: vector of means, the covariance matrix
  - Outputs: current combination of parameters
- Procedure
  - Randomly set the initial value of the Gaussian process (combination of parameters), then substitute into the unknown function to get the observed value, after using the newly obtained Gaussian distribution (mean vector covariance matrix) to substitute into the sampling function, through the sampling function to get the next observation of the combination of parameters finally brought into the original function, and thus on, until the global maximum or minimum value is found.

Since the bipedal robot needs to optimize numerous parameters, not only the input parameters but also the physical parameters of the system itself, it is excellent to use Bayesian optimization when doing high-dimensional parameter optimization, and the algorithm part of this paper, referring to the previous work of Saar et al. [33].

1.2.3 Rössler attractor

Currently, chaotic phenomena are mostly believed to have a negative effect on bipedal walking. Therefore, some work has been carried out to avoid the creation of chaotic gaits or to

control chaotic gaits directly to limit cycle walking [34, 35]. However, from another point of view, the most fundamental requirement for bipedal walking is the ability to continue walking without falling, and thus larger BOA (basin of attraction) is required to tolerate external perturbations. In this sense, chaotic oscillators tend to have larger BOA compared to the limit cycle. With these considerations in mind, a reasonably generated chaotic bipedal gait may be more robust to perturbations. To investigate the performance of chaotic gaits, the Rössler attractor [36] generates a chaotic control waveform suitable as a robot input torque.

1.3 Research Aim

Simultaneously achieving natural and efficient gait generation and robust adaptation to the environment is a challenging problem for bipedal robots. The current, mature approach to bipedal robot control, like ZMP, enables real-time feedback control of poses by using a large number of sensors and high-priced high-performance actuators. Although stability and walking speed are guaranteed to some extent, walking efficiency is particularly low. In reality, working hours are too short and the energy consumption is overly steep, a problem that cannot be ignored. Therefore, it is extremely essential to apply a reasonable torque control so that the robot can take full advantage of the inherent dynamics and achieve an efficient and controllable gait.

The purpose of this study is to advocate an efficient and robust theory of motion generation for bipedal robots. Such as a biped robot, to which only hip torque can be applied, can continue to walk stably on a horizontal surface by devising a mechanism (foot shape, mass balance, etc.) to reduce kinetic energy loss during a swing leg collision. Moreover, when stepping over low steps, the hip torque can be correctly set to break the potential barrier in the mid-step phase. These can be viewed as motion generation by control signals generated at the human reflex level (first signal system). However, a bipedal robot without sufficient DOF (degrees of freedom) is practically incapable of adapting to more complex environments, forcing it to add additional DOF or integrate with advanced signaling systems. This study aims to address the properties of the first signal system needed to generate bipedal locomotion and the optimization problem of the control signals it generates. The stable and efficient motion of an underactuated bipedal robot using an entrainment control method. Therefore, nonlinear analysis on numerical simulations, experimental validation in realistic environments, and optimization of the entrainment waveform should be performed.

On the other hand, it is also essential to generate chaotic gaits similar to human walking and investigate their properties. In this study, the author indirectly generated chaotic gaits by Rössler attractor to compare single-cycle limit cycle gait, which provides a basis for additional characterization of chaotic gaits in the future.

1.4 Organization of Dissertation

This dissertation consists of 3 main parts. The first part uses a nonlinear analysis approach for the feasibility of entrainment control and validates it with different pavements, corresponding to chap. 2, 3, and 4. The second part is devoted to experimental validation and parameter optimization, corresponding to chap. 5 and 6. The third part investigates whether the chaotic gait achieved by the entrainment method can achieve stable and efficient motion in comparison with the limit cycle gait, corresponding to Chapter 7. The details are described below.

Chapter 2 : By using the rimless wheel as the simplest example, explored the possibility of gait generation by applying periodic inputs through the reaction wheel and analyzed it through numerical simulations. It was clarified that it is only possible for a rimless wheel to walk on a horizontal surface when equipped with extremely circular feet and that varying the input frequency does not effectively affect the rimless wheel's walking frequency, providing a reference for general bipedal robots in the sequel.

Chapter 3 : The entrainment control method is presented and illustrated using a passive walking robot as an example, and a typical nonlinear analysis is performed through numerical simulations. Demonstrates the effectiveness of entrainment control in a general bipedal robot model. Preparations were made for the next application on non-downhill surfaces.

Chapter 4 : Detailed gait analysis of the biped robot was used to verify the effect of entrainment on level ground as well as on uneven ground. Efficiency and stability are also evaluated for the generated gait. It was found that the walk performance can be effectively improved in the entrainment range by using a time-symmetric input signal.

Chapter 5 : The effectiveness of the proposed control method was demonstrated through fabrication and experiments on real machines, where a robot using the same method was able to successfully walk on a horizontal road surface in a real environment. The difference between experiment and simulation is illustrated by comparing the experimental results with the simulation results.

Chapter 6 : By using a BO approach, the control and physical parameters of the entire system are optimized, mainly for walking speed and walking efficiency. The results show that the walking performance of the robot can be enhanced by both its own physical and control parameters.

Chapter 7 : To investigate whether a reasonably generated chaotic bipedal gait might be more stable. The Rössler attractor is used to generate chaotic control waveforms suitable for use as robot input torques, and the differences between the generated chaotic gaits and the limit cycle gaits are analyzed to clarify that the rationally generated chaotic gaits are in some cases more robust.

Chapter 8 : Summarize the dissertation and lead to the next work.

Chapter 2

Modeling, Control, and Analysis of Rimless Wheel Walking on Horizontal Road Surface Based on Periodic Input Signal

2.1 Overview

Limit cycle walking [7, 9] inspired by passive walking is a favorable way for biped robots. Various types of limit cycle walkers such as biped [37–39], quadruped [40–42], and multilegged robots [43, 44] have been studied and developed. The easiest way to achieve efficient horizontal walking is to add a slight torque input to the passive walker. Because of its inherent stability, the resulting gait will converge to a stable periodic orbit in most cases. From previous work, it is not difficult to generate a stable limit cycle, but how to effectively control the gait of the robot through only one periodic input has not been explored. The rimless wheel, as the simplest model that can simulate biped walking, is a great example to study the characteristics and mechanism of limit cycle walking, such as efficiency [45], stability [46, 47], and gait symmetry [48, 49].

In this chapter, the author studies the gait generation of the rimless wheel on a horizontal surface by applying periodic input. First of all, the numerical simulation shows that when the input signal is time symmetrical (that is, the time integral of each walking cycle is 0), the rimless wheel with a large sufficiently semicircular foot is needed to generate the limit cycle

gait, and the larger the radius of the semicircular foot is, the greater the walking speed is. Moreover, the walking frequency of RW is practically not affected by the input frequency, so the entrainment effect is difficult to produce. When the input signal is time asymmetry (that is, the time integral of each walking cycle is greater than 0), the radius of the smaller semicircular foot can also generate the limit cycle gait. At this time, although part of the input frequency is consistent with the walking frequency, the walking performance has not been significantly improved. Therefore, periodic input does not bring obvious advantages when using the RW model.

2.2 Dynamics Modeling and Control Method

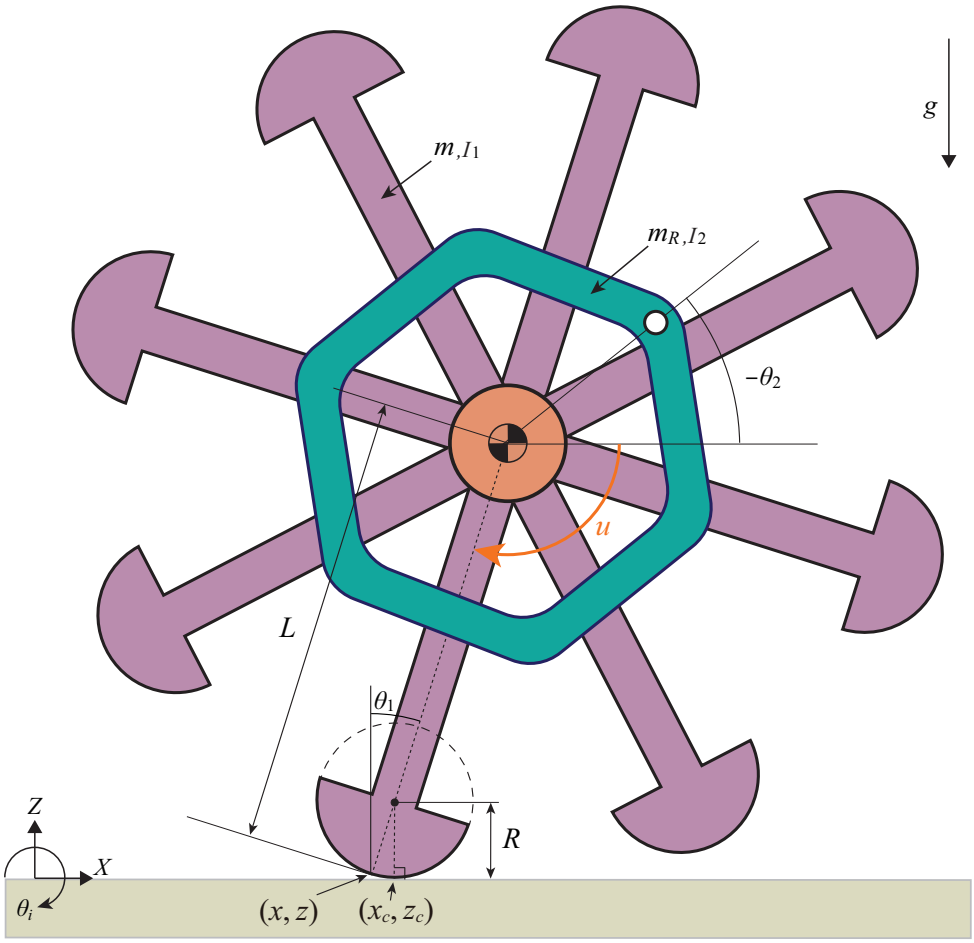

Figure 2.1: Underactuated rimless wheel with semicircular feet driven by reaction wheel

The mathematical model is shown in Fig. 2.1, which is specified as:

- The angular position of the stance leg to the vertical direction is θ_1 [rad]. The rimless

wheel has 8 identical legs, and the length of each leg is L [m]. So the angle of each two legs is $\pi/4$ [rad].

- The radius of semicircular feet is R [m] and the position of the midpoint of the semicircular feet is (x, z). The coordinate of the grounding point of the stance leg is set to (x_c, z_c).
- The masses of each leg are m [kg] and the inertial moment of the RW is I_1 [kg·m^2]. The weight of the reaction wheel is m_R [kg] and the inertial moment of the reaction wheel is I_2 [kg·m^2].
- The only control input u [N·m] acts between the RW and the reaction wheel.

2.2.1 Equation of motion

The generalized coordinate vectors is set to $\boldsymbol{q} = \begin{bmatrix} x & z & \theta_1 & \theta_2 \end{bmatrix}^{\mathrm{T}}$. The equation of motion about the robot then becomes

$$\boldsymbol{M}\ddot{\boldsymbol{q}} + \boldsymbol{h} = \boldsymbol{J}^{\mathrm{T}}\boldsymbol{\lambda} + \boldsymbol{S}u, \tag{2.1}$$

$$\boldsymbol{J}\dot{\boldsymbol{q}} = \boldsymbol{0}_{2\times 1}, \tag{2.2}$$

where $\boldsymbol{M}$ represents the inertia matrix, $\boldsymbol{h}$ is the combination of the central force, Coriolis force, and gravity terms. On the right side of Eq. (2.1), $\boldsymbol{J}^{\mathrm{T}}\boldsymbol{\lambda}$ is the holonomic constraint. In addition, the driving vector becomes

$$\boldsymbol{S} = \begin{bmatrix} 0 & 0 & 1 & -1 \end{bmatrix}^{\mathrm{T}}. \tag{2.3}$$

The author assumes that the robot is in non-sliding contact with the ground. Due to the semicircular feet, the velocity constraint at the contact point between the stance leg and the ground during the walking period should satisfy the following conditions:

$$\dot{x}_c = R\dot{\theta}_1, \quad \dot{z}_c = 0. \tag{2.4}$$

Therefore, the location of the grounding point can be obtained by the following equation:

$$\begin{bmatrix} x_c \\ z_c \end{bmatrix} = \begin{bmatrix} x + R\sin\theta_1 \\ z + R\cos\theta_1 - R \end{bmatrix}. \tag{2.5}$$

After differentiation, we can obtain the velocity of the point as:

$$\frac{\mathrm{d}}{\mathrm{d}t}\begin{bmatrix} x_c \\ z_c \end{bmatrix} = \begin{bmatrix} \dot{x} + R\dot{\theta}_1 \cos\theta_1 \\ \dot{z} - R\dot{\theta}_1 \sin\theta_1 \end{bmatrix}. \tag{2.6}$$

Therefore, Jacobians $\boldsymbol{J}$ are determined as

$$\boldsymbol{J} = \begin{bmatrix} 1 & 0 & R\cos\theta_1 - R & 0 \\ 0 & 1 & -R\sin\theta_1 & 0 \end{bmatrix}. \tag{2.7}$$

In addition, the ground reaction force $\boldsymbol{\lambda}$ [N] is the simultaneous solution of Eqs. (2.1) and (2.2) as follows:

$$\begin{aligned} \boldsymbol{\lambda} &= -\boldsymbol{X}^{-1}(\boldsymbol{J}\boldsymbol{M}^{-1}(\boldsymbol{S}u - \boldsymbol{h}) + \dot{\boldsymbol{J}}\dot{\boldsymbol{q}}), \\ \boldsymbol{X} &:= \boldsymbol{J}\boldsymbol{M}^{-1}\boldsymbol{J}^{\mathrm{T}}. \end{aligned} \tag{2.8}$$

The ground reaction force must always be positive during walking, otherwise, a normal walking gait cannot be generated. By substituting Eq. (2.8) into Eq. (2.1), we can obtain

$$\begin{aligned} \ddot{\boldsymbol{q}} &= \boldsymbol{M}^{-1}\boldsymbol{Y}(\boldsymbol{S}u - \boldsymbol{h}), \\ \boldsymbol{Y} &:= \boldsymbol{I}_4 - \boldsymbol{J}^{\mathrm{T}}\boldsymbol{X}^{-1}\boldsymbol{J}\boldsymbol{M}^{-1}, \end{aligned} \tag{2.9}$$

where $\boldsymbol{I}_4$ is the identity matrix of size 4.

2.2.2 Equation of collision

According to the inelastic collision model, the foreleg neither slides nor bounces when it touches the ground. Therefore, the foreleg and rear leg are immediately exchanged at the moment of ground-contacting. Since each leg is identical, the zero crossing of the following function becomes:

$$f(\theta_1) := \theta_1 - \alpha/2, \tag{2.10}$$

The transition that occurs before and after the collision is shown below:

$$\boldsymbol{M}\dot{\boldsymbol{q}}^{+} = \boldsymbol{M}\dot{\boldsymbol{q}}^{-} + \boldsymbol{J}_I^{\mathrm{T}}\boldsymbol{\lambda}_I \tag{2.11}$$

$$\boldsymbol{J}_I\dot{\boldsymbol{q}}^{+} = \boldsymbol{0}_{2\times 1}. \tag{2.12}$$

Here, the superscripts "−" and "+" mean immediately before and after a collision. Due to the semicircular feet, When the leg change condition is triggered, the foreleg is grounded at the

point of the foot as $(\bar{x}_c, \bar{z}_c)$. Therefore, the velocity constraint condition for the landing point of the forefoot is determined as

$$\dot{\bar{x}}_c^{\,+} = R\dot{\theta}_2, \quad \dot{\bar{z}}_c^{\,+} = 0, \tag{2.13}$$

with the details of

$$\frac{\mathrm{d}}{\mathrm{d}t}\begin{bmatrix} \bar{x}_c \\ \bar{z}_c \end{bmatrix}^+ = \frac{\mathrm{d}}{\mathrm{d}t}\begin{bmatrix} x + L\sin\theta_1 + (L-R)\sin(\alpha-\theta_1) \\ z + L\cos\theta_1 - (L+R)\cos(\alpha-\theta_1) - R \end{bmatrix}^+$$

Accordingly, the velocity constraint $\boldsymbol{J}_I$ can be derived as

$$\boldsymbol{J}_I^{\mathrm{T}} = \begin{bmatrix} 1 & 0 \\ 0 & 1 \\ (-L+R)\cos(\alpha-\theta_1^-) + L\cos\theta_1 - R & -L\sin\theta_1^- - (L-R)\sin(\alpha-\theta_1^-) \\ 0 & 0 \end{bmatrix}. \tag{2.14}$$

By solving Eqs. (2.11) and (2.12) simultaneously, the Lagrange multiplier vector $\boldsymbol{\lambda}_I \in \mathbb{R}^2$ can be derived as

$$\begin{aligned} \boldsymbol{\lambda}_I &= -\boldsymbol{X}_I^{-1}\boldsymbol{J}_I\dot{\boldsymbol{q}}^-, \\ \boldsymbol{X}_I &:= \boldsymbol{J}_I\boldsymbol{M}^{-1}\boldsymbol{J}_I^{\mathrm{T}}. \end{aligned} \tag{2.15}$$

By substituting Eq. (2.15) into Eq. (2.11), we can also obtain

$$\dot{\boldsymbol{q}}^+ = \left(\boldsymbol{I}_4 - \boldsymbol{M}^{-1}\boldsymbol{J}_I^{\mathrm{T}}\boldsymbol{X}_I^{-1}\boldsymbol{J}_I\right)\dot{\boldsymbol{q}}^-. \tag{2.16}$$

2.2.3 Control methods

To take advantage of the inherent dynamics of the robot as much as possible, the feedforward periodic input waveform is used in this chapter, as shown below.

$$u(t) = u_0 + A_m\sin(2\pi f_c t) \tag{2.17}$$

where A_m [N·m] and f_c [Hz] are the amplitude and frequency of the sine wave, respectively. It is essential to note here that this input signal is time-symmetric when $u_0 = 0$, i.e., the time integral of each walking cycle is 0, as shown below.

$$\int_0^T u(t)\mathrm{d}t = 0. \tag{2.18}$$

At this point, the energy compensated by the input must be greater than 0 for the robot to generate a gait after each collision with the ground. The details are as follows,

$$\Delta E = \int_0^T \dot{\theta}_1 u \mathrm{d}t = \int_{-\alpha/2}^{\alpha/2} u(\theta_1)\mathrm{d}\theta_1 > 0. \tag{2.19}$$

If this condition cannot be met, RW will not be able to cross the potential barrier.

2.3 Numerical Simulation Results

2.3.1 Motion generation

Numerical simulation needs to use the physical and control parameters shown in Table 2.1. Here, it should be noted that the location of the grounding point of the foot is not the generalized coordinate system in x, z but x_c and z_c, so the need to calculate the actual role of the arc foot through the geometric relationship to the initial conditions of the ground. The easiest way to do that is to start at 0 [rad] so that x, z can also start at 0 as shown below.

$$\boldsymbol{q}(0) = \begin{bmatrix} 0 & 0 & 0 & 0 \end{bmatrix}^{\mathrm{T}} \qquad \dot{\boldsymbol{q}}(0) = \begin{bmatrix} 0 & 0 & 1 & 0 \end{bmatrix}^{\mathrm{T}} \tag{2.20}$$

Since the initial state gives the right angle as well as sufficient speed, the robot can cross the potential barrier.

Figure 2.2 shows the simulation results of the limit cycle walking of the RW for the first 10 seconds. In Fig. 2.2(a), it can be seen that RW is affected by the initial velocity and the input

Table 2.1: Physical and Control Parameters

Symbol	Value	Unit
m	1	kg
m_R	1	kg
L	1	m
R	0.1	m
α	$\pi/4$	rad
g	9.81	m/s^2

Symbol	Value	Unit
I_1	0.25	kg·m^2
I_2	0.09	kg·m^2
u_0	1	N·m
A_m	1	N·m
f_c	1	Hz

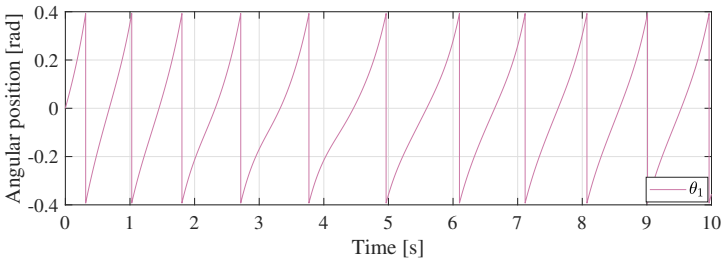

(a) Angular position

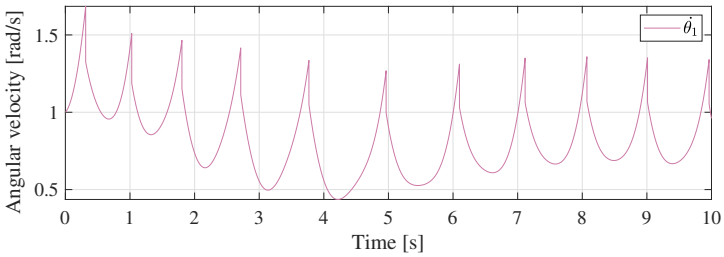

(b) Angular velocity

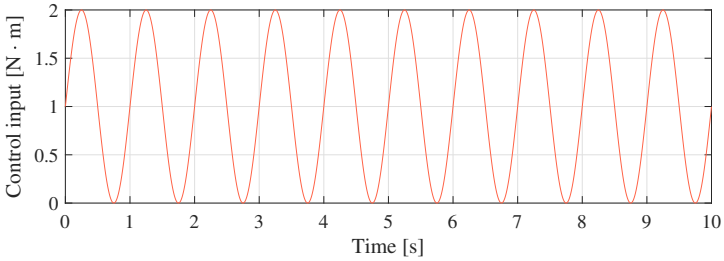

(c) Control input

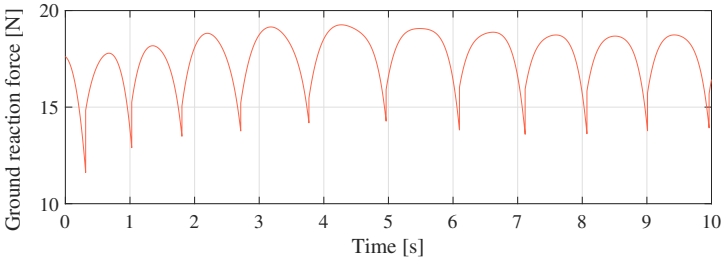

(d) Vertical ground reaction force

Figure 2.2: Simulation results of typical gait generation where $u_0 > 0$

waveform, which first becomes slower and then gradually stabilizes. Moreover, since RW is a fixed step, the angular magnitude of each step is also fixed. The shift of RW angular velocity can be observed in Fig. 2.2(b), it is also found that it decelerates first and then tends to shift at a uniform speed. Fig. 2.2(c) shows the variation of the torque given by the sine input. Note that u_0 is not zero, so the input signal is not time-symmetric. The last Fig. 2.2(d) shows the time variation of the vertical ground reaction force. Since the weight of the whole system is 2 [kg],

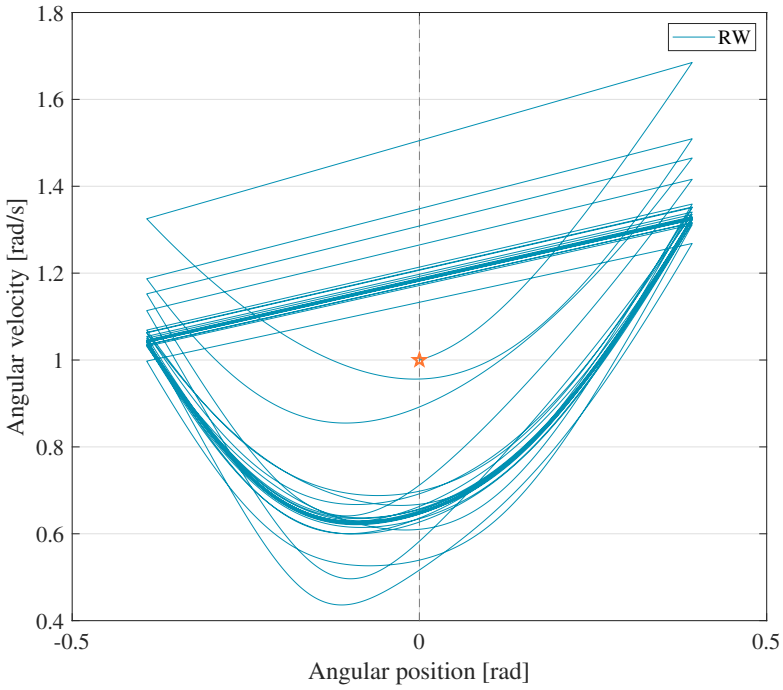

Figure 2.3: Phase plane plot of RW where $u_0 > 0$

the ground reaction force is thought to correspond to it. In addition, the value of the vertical ground reaction force is consistently positive, indicating that the stance leg does not leave the ground.

To confirm that the robot converges to a stable limit cycle gait after applying this input signal, the phase plane diagram of the gait after a sufficient time (after 300 [s]) is shown in Fig. 2.3. The five-pointed star in the figure represents the initial position. It can be seen that the RW is able to converge to the limit cycle gait on the horizontal pavement with the application of a time-asymmetric sinusoidal input signal.

2.3.2 Analysis of time-symmetric control input

In the previous subsection, the authors successfully generated the limit-loop gait by a time-asymmetric input signal. Then, whether RW can also generate a stable gait when $u_0 = 0$, i.e., when the input signal is time-symmetric, needs to be verified by numerical simulations. According to Algorithm 1, the results are shown in Fig. 2.4. Figure 2.4(a) indicates the size of R for which the limit cycle gait can be generated for a radius R of the semicircular foot in the range from 0 to 1 [m]. We can find that the only way to walk successfully is when R is greater

Algorithm 1 Calculate walking frequency f_w and walkable R

Require: The walking frequency f_w of the bipedal robot when it gets stabilized

Input: Initial state $\boldsymbol{q}(0)$, $\dot{\boldsymbol{q}}(0)$, A_{m} and f_{c}

Output: Walking frequency f_w of the next 30 steps after 100 seconds

Initialization $f_w[l][m][30] = 0$, $f_{\mathrm{c}} = 1$, $A_{\mathrm{m}} = 0.1$
for $i = 1; i <= l : i++$ **do**
  for $j = 1; j <= m : j++$ **do**
    Run simulation for 100 seconds.
    Save the next 30 walking frequency to f
    $f_w[i][j] = f$
    $f_c = f_c + 0.05$
  end
  $R = R + 0.05$
end
Return f_w

than 0.86 [m]. This is extremely demanding, and the leg length of RW is only 1 [m]. It is easier to walk because when RW has a large semicircular foot radius, which considerably reduces the location of the potential barriers. Figure 2.4(b) is the result of the effect of changing the input frequency on the walking frequency when set to the smallest radius that can generate a gait. The circles represent 30 gait steps, and the middle dots indicate the average value, and it can be seen that the RW can walk even at extremely minor input frequencies, but by changing the input frequency, the walking frequency of the RW does not alter significantly and does not produce the expected entrainment phenomenon. In the Fig. 2.4(c), the author takes the R close to the leg length to explore the effect of the input frequency on the walking frequency, and although the same entrainment phenomenon is not observed, the variance of the walking frequency becomes smaller for each input frequency.

2.3.3 Analysis of time-asymmetric control input

For comparative analysis, when u_0 is greater than 0, the simulation results are shown in Fig. 2.5. In Fig. 2.5(a), each dashed line represents the case where f_w: f_c is 1: n (n is a positive integer), respectively. When the input signal is time-asymmetric, i.e., both u_0 and A_m are 1 [N·m],

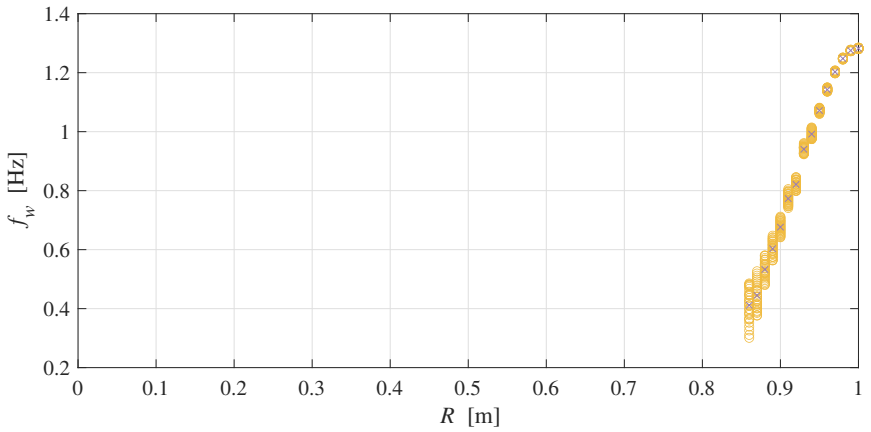

(a) Walkable R

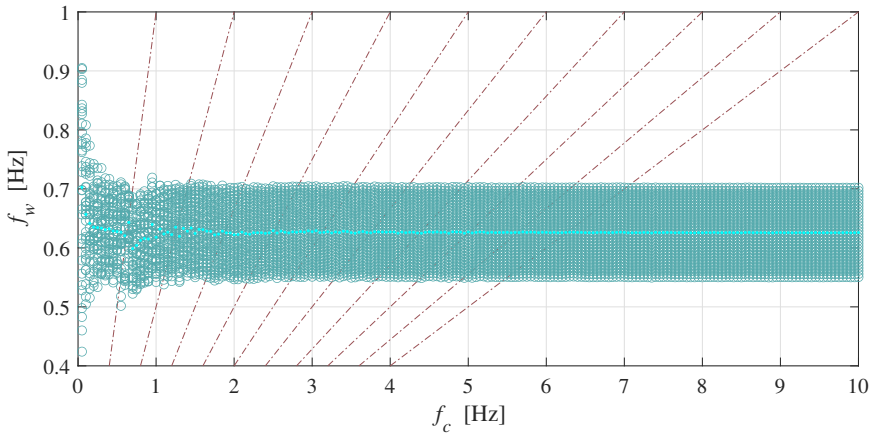

(b) Walking frequency where R=0.86 [m]

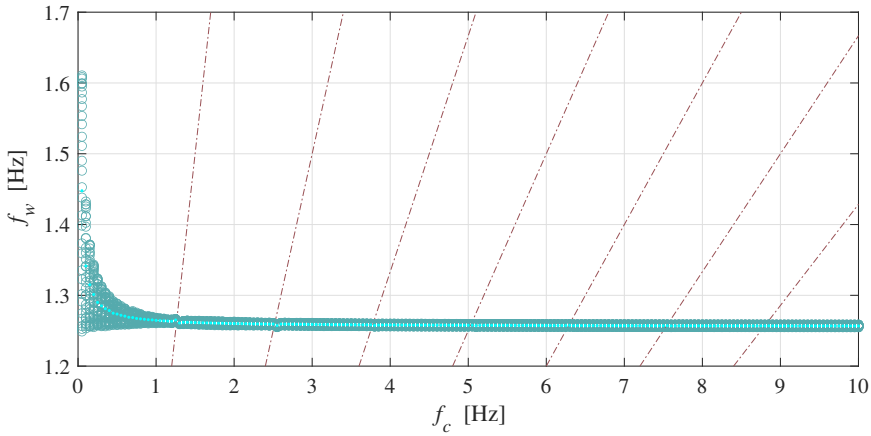

(c) Walking frequency where R=0.98 [m]

Figure 2.4: Walkable R and walking frequency by the sine wave input where $u_0 = 0$

at this time, by varying the input frequency, we can find that the entrainment phenomenon is

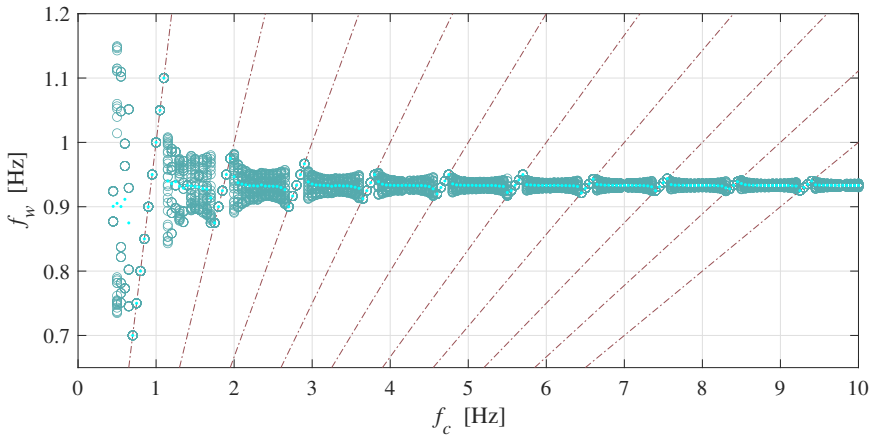

(a) Walking frequency where R=0.1 [m] and u_0=1 [N·m]

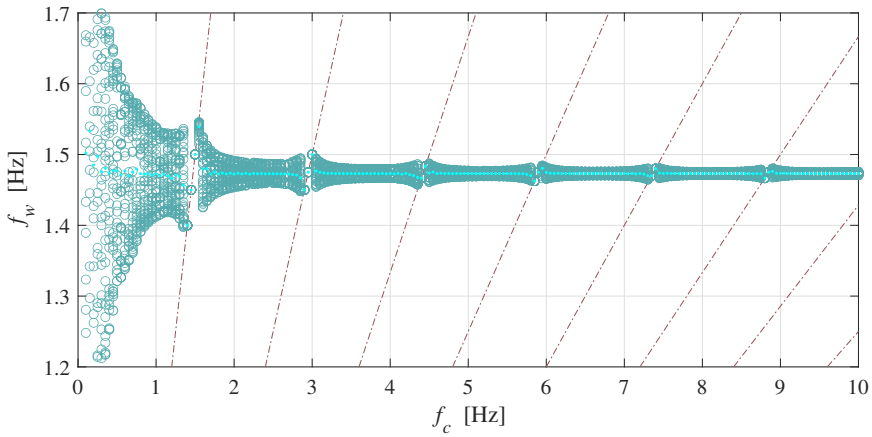

(b) Walking frequency where R=0.1 [m] and u_0=1.5 [N·m]

Figure 2.5: Walking frequency by the sine wave input where $u_0 > 0$

generated sequentially, but the individual entrainment ranges are tiny. In the entrainment range of 1:1, there is a slight increase in the walking frequency and a corresponding slight increase in the walking speed due to the fixed step characteristic of RW. The subsequent entrainment intervals did not show any significant shift in walking performance. The simulation results for increasing u_0 to 1.5 [N·m] are shown in Fig. 2.5(b). Compared with Fig. 2.5(a), the overall average walking frequency of the RW increases due to the larger input torque, and the gait can be generated at a smaller input frequency. However, the entrainment effect is not satisfactory at this point, and changing the input frequency does not bring significant performance improvement.

2.4 Summary and Discussions

In this chapter, to investigate the walking characteristics of a bipedal walking robot under periodic input signals, a minimal model RW is used and simulates the swing leg motion of an ordinary bipedal robot by carrying a reaction wheel. The simulation results show that the RW requires an extremely large semicircular foot to generate a limit cycle gait under a time-symmetric input signal, and the walking frequency of the RW is not well affected by changing the input frequency at this time. In contrast, with a time-asymmetric input signal, the RW can easily cross the potential barrier when paired with a smaller semicircular foot. A weak entrainment effect is generated at this point, but the walking performance of RW cannot be significantly improved within each entrainment interval.

Due to the fixed step length nature of the RW, the fewer the legs, the more energy is required to break through the potential barrier after each impact on the ground, and in a general bipedal walking robot, the author speculates that this control method is more advantageous in a compass-like bipedal robot due to the presence of swinging leg, thus extending this control method to a more general bipedal robot is necessary. The next chapter is dedicated to discussing whether this method can be used to produce a stable and controllable gait when the robot is walking on a slope.

Chapter 3

Motion Analysis of Quasi-passive Dynamic Walking Robot Based on Entrainment Effect

3.1 Overview

If we want to generalize the idea of passive walking, the most crucial and difficult point is to actively exploit the natural dynamics of the system. That is, the effect of the control input on the system should be efficiently coupled with the dynamics of the system itself. Inspired by resonant phenomena in nature, Asano and Tokuda proposed an indirectly controlled connected rimless wheel walk system consisting of two connected rimless wheels and a wobbling mass [50]. This system is characterized by the fact that there is no conventional torque input between the rimless wheels and the connecting rod, yet the wobbling mass can be controlled to oscillate periodically. Li et al. additionally analyzed this mechanism based on the fact that it allows for efficient walking by actively exploiting the natural dynamics of the system [51–53] and the fact that periodic oscillations of the oscillator induce resonances in the robot, offering the possibility of convergence to a steady state.

Connected rimless wheel systems are inherently stable, and it is extremely difficult to achieve similar results in bipedal robots. However, from the point of view of the signal system, a human unconsciously and periodically steps forward during a normal walk. Then it seems feasible to use only a suitable torque applied to the hip. If a constant torque is given to

make the legs step forward, it can be achieved. Still, the bipedal robot has zero dynamics for both legs with only one feed-forward input torque and based on the fact that the walking action is a periodic motion, it is critical to design a reasonable input waveform. In Chap. 3, the author explores the feasibility of entrainment control using the feed-forward torque exerted by the sine wave like in Chap. 2. Moreover, explore the advantages of a compass liked biped robot under this input condition.

3.2 Dynamics Modeling and Control Method

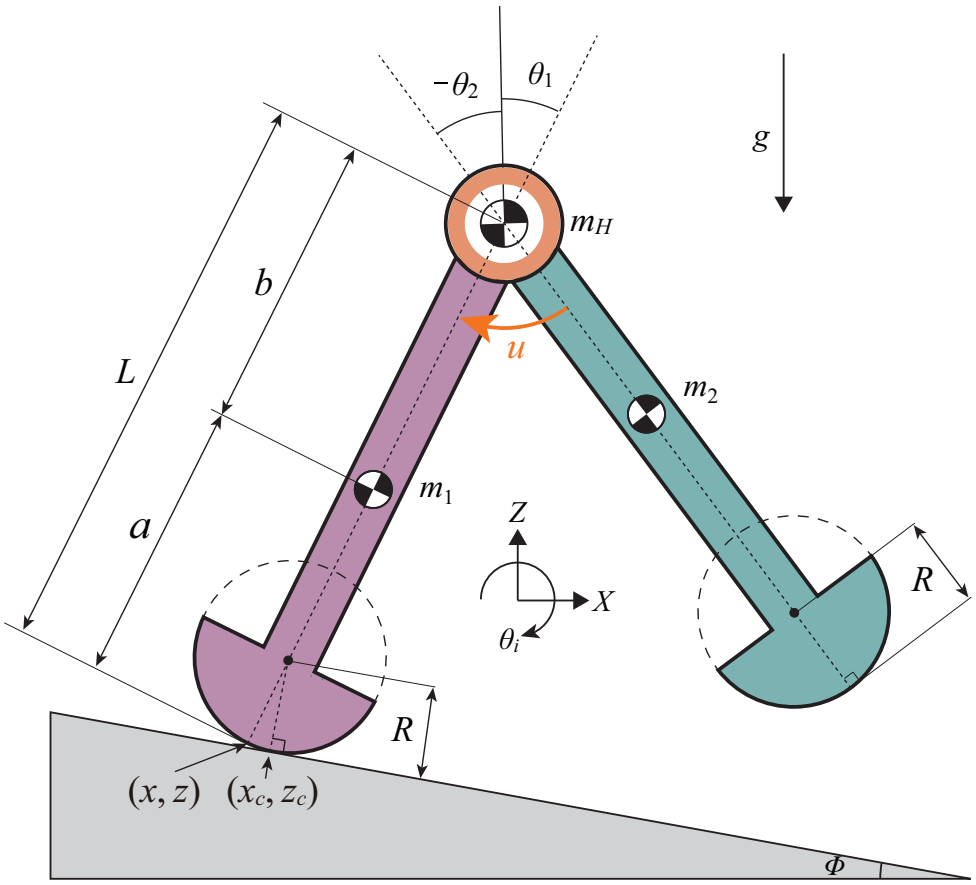

Figure 3.1: Quasi-passive dynamic bipedal robot with semicircular feet

To facilitate comparison with previous studies, the widely studied compass-like bipedal robot is used in this paper. In order to reduce the energy loss due to conflict and increase the virtual gravity effect due to rolling, the model uses semi-circular feet with adjustable radii. The mathematical model is shown in Fig. 3.1, which is specified as:

- The angular positions of the stance and swing legs to the vertical direction are θ_1 and θ_2 [rad] respectively. The length of each leg is $L(= a + b)$ [m].
- The radius of semicircular feet is R [m] and the position of the midpoint of the semicircular feet is (x, z). The coordinate of the grounding point of the stance leg is set to (x_c, z_c).
- The masses of two identical rigid legs are m_1 and m_2 [kg] and the inertial moment of the legs is ignored. The weight of the hip is m_H [kg] and the friction of the hip joint is neglected.
- The angle of the downslope is set as ϕ [rad]. The only control input u [N·m] for this underactuated bipedal robot is applied to the hip joint.

3.2.1 Equation of motion

The generalized coordinate vectors is set to $\boldsymbol{q} = \begin{bmatrix} x & z & \theta_1 & \theta_2 \end{bmatrix}^{\mathrm{T}}$. The equation of motion about the robot then becomes

$$\boldsymbol{M}\ddot{\boldsymbol{q}} + \boldsymbol{h} = \boldsymbol{J}^{\mathrm{T}}\boldsymbol{\lambda} + \boldsymbol{S}u, \tag{3.1}$$

$$\boldsymbol{J}\dot{\boldsymbol{q}} = \boldsymbol{0}_{2\times 1}, \tag{3.2}$$

where $\boldsymbol{M}$ represents the inertia matrix, $\boldsymbol{h}$ is the combination of the central force, Coriolis force, and gravity terms. Moreover, the details about $\boldsymbol{M}$ and $\boldsymbol{h}$ can be calculated as follows:

$$\boldsymbol{M} = \begin{bmatrix} M_{11} & 0 & M_{13} & -bm_2\cos\theta_2 \\ & M_{22} & M_{23} & bm_2\sin\theta_2 \\ & & M_{33} & -b(a+b)m_2\cos(\theta_1-\theta_2) \\ \text{Sym.} & & & b^2m_2 \end{bmatrix},$$

$$\begin{aligned} M_{11} &= M_{22} = m_1 + m_2 + m_H, \\ M_{13} &= (b(m_2 + m_H) + a(m_1 + m_2 + m_H))\cos\theta_1, \\ M_{23} &= -(b(m_2 + m_H) + a(m_1 + m_2 + m_H))\sin\theta_1, \\ M_{33} &= 2ab(m_2 + m_H) + b^2(m_2 + m_H) \\ &\quad + a^2(m_1 + m_2 + m_H). \end{aligned}$$

$$\boldsymbol{h} = \begin{bmatrix} h_1 & h_2 & h_3 & h_4 \end{bmatrix}^{\mathrm{T}},$$

$$\begin{aligned}
h_1 &= -\dot{\theta_1}^2(b(m_2+m_H)+a(m_1+m_2+m_H))\sin\theta_1 \\
&\quad +b\dot{\theta_2}^2 m_2 \sin\theta_2, \\
h_2 &= g(m_1+m_2+m_H) - \dot{\theta_1}^2(b(m_2+m_H) \\
&\quad +a(m_1+m_2+m_H))\cos\theta_1 + b\dot{\theta_2}^2 m_2 \cos\theta_2, \\
h_3 &= -g(b(m_2+m_H)+a(m_1+m_2+m_H))\sin\theta_1 \\
&\quad -b(a+b)\dot{\theta_2}^2 m_2 \sin(\theta_1-\theta_2), \\
h_4 &= bm_2((a+b)\dot{\theta_1}^2 \sin(\theta_1-\theta_2) + g\sin\theta_2).
\end{aligned}$$

On the right side of Eq. (3.1), $\boldsymbol{J}^{\mathrm{T}}\boldsymbol{\lambda}$ is the holonomic constraint. In addition, by letting u be the only control input applied to the hip joint, the driving vector becomes

$$\boldsymbol{S} = \begin{bmatrix} 0 & 0 & 1 & -1 \end{bmatrix}^{\mathrm{T}}. \tag{3.3}$$

The author assumes that the robot is in non-sliding contact with the ground. Due to the semi-circular feet, the velocity constraint at the contact point between the stance leg and the ground during the walking period should satisfy the following conditions:

$$\dot{x}_c = R\dot{\theta}_1 \cos\phi, \quad \dot{z}_c = -R\dot{\theta}_1 \sin\phi. \tag{3.4}$$

Therefore, the location of the grounding point can be obtained by the following equation:

$$\begin{bmatrix} x_c \\ z_c \end{bmatrix} = \begin{bmatrix} x + R\sin\theta_1 - R\sin\phi \\ z + R\cos\theta_1 - R\cos\phi \end{bmatrix}. \tag{3.5}$$

After differentiation, we can obtain the velocity of the point as:

$$\frac{\mathrm{d}}{\mathrm{d}t}\begin{bmatrix} x_c \\ z_c \end{bmatrix} = \begin{bmatrix} \dot{x} + R\dot{\theta}_1 \cos\theta_1 \\ \dot{z} - R\dot{\theta}_1 \sin\theta_1 \end{bmatrix}. \tag{3.6}$$

Therefore, Jacobians $\boldsymbol{J}$ are determined as

$$\boldsymbol{J} = \begin{bmatrix} 1 & 0 & R\cos\theta_1 - R\cos\phi & 0 \\ 0 & 1 & -R\sin\theta_1 + R\sin\phi & 0 \end{bmatrix}. \tag{3.7}$$

3.2.2 Equation of collision

According to the inelastic collision model, the swing leg neither slides nor bounces when it touches the ground. Therefore, the swing and stance legs are immediately exchanged at the moment of ground-contacting. Since the two legs are identical, the zero crossing of the following function becomes:

$$f(\theta_1, \theta_2) := \theta_1 + \theta_2 - 2\phi, \tag{3.8}$$

Moreover, it requires $\frac{\mathrm{d}}{\mathrm{d}t} f(\theta_1, \theta_2) := \dot{\theta}_1 + \dot{\theta}_2 > 0$ to detect collision. The transition that occurs before and after the collision is shown below:

$$\boldsymbol{M}\dot{\boldsymbol{q}}^+ = \boldsymbol{M}\dot{\boldsymbol{q}}^- + \boldsymbol{J}_I^{\mathrm{T}}\boldsymbol{\lambda}_I \tag{3.9}$$

$$\boldsymbol{J}_I\dot{\boldsymbol{q}}^+ = \boldsymbol{0}_{2\times 1}. \tag{3.10}$$

Here, the superscripts "−" and "+" mean immediately before and after a collision. Due to the semicircular feet, When the leg change condition is triggered, the foreleg is grounded at the point of the foot as $(\bar{x}_c, \bar{z}_c)$. Therefore, the velocity constraint condition for the landing point of the forefoot is determined as

$$\dot{\bar{x}}_c{}^+ = R\dot{\theta}_2 \cos\phi, \quad \dot{\bar{z}}_c{}^+ = -R\dot{\theta}_2 \sin\phi, \tag{3.11}$$

with the details of

$$\begin{aligned} \frac{\mathrm{d}}{\mathrm{d}t}\begin{bmatrix} \bar{x}_c \\ \bar{z}_c \end{bmatrix}^+ &= \frac{\mathrm{d}}{\mathrm{d}t}\begin{bmatrix} x + L\sin\theta_1 - (L-R)\sin\theta_2 - R\sin\phi \\ z + L\cos\theta_1 - (L-R)\cos\theta_2 - R\cos\phi \end{bmatrix}^+ \\ &= \begin{bmatrix} 1 & 0 & L\cos\theta_1^- & -(L-R)\cos\theta_2^- \\ 0 & 1 & -L\sin\theta_1^- & (L-R)\sin\theta_2^- \end{bmatrix}\dot{\boldsymbol{q}}^+. \end{aligned} \tag{3.12}$$

Accordingly, the velocity constraint $\boldsymbol{J}_I$ can be derived as

$$\boldsymbol{J}_I^{\mathrm{T}} = \begin{bmatrix} 1 & 0 \\ 0 & 1 \\ L\cos\theta_1^- & -L\sin\theta_1^- \\ (R-L)\cos\theta_2^- - R\cos\phi & (L-R)\sin\theta_2^- + R\sin\phi \end{bmatrix}. \tag{3.13}$$

By solving Eqs. (3.9) and (3.10) simultaneously, the Lagrange multiplier vector $\boldsymbol{\lambda}_I \in \mathbb{R}^2$ can be derived as

$$\begin{aligned} \boldsymbol{\lambda}_I &= -\boldsymbol{X}_I^{-1}\boldsymbol{J}_I\dot{\boldsymbol{q}}^-, \\ \boldsymbol{X}_I &:= \boldsymbol{J}_I\boldsymbol{M}^{-1}\boldsymbol{J}_I^{\mathrm{T}}. \end{aligned} \tag{3.14}$$

By substituting Eq. (3.14) into Eq. (3.9), we can also obtain

$$\dot{\boldsymbol{q}}^{+} = \left(\boldsymbol{I}_4 - \boldsymbol{M}^{-1} \boldsymbol{J}_I^{\mathrm{T}} \boldsymbol{X}_I^{-1} \boldsymbol{J}_I \right) \dot{\boldsymbol{q}}^{-}. \tag{3.15}$$

According to the expression (3.15), when after each collision for leg exchange, the status of the stance and swing leg will be switched. We should reset each velocity $\dot{\boldsymbol{q}}^{+}$ as

$$\dot{\boldsymbol{q}}^{+} = \begin{bmatrix} \dot{x}^{+} + L\dot{\theta}_1^{+}\cos\theta_1^{-} - L\dot{\theta}_2^{+}\cos\theta_2^{-} \\ \dot{z}^{+} - L\dot{\theta}_1^{+}\sin\theta_1^{-} + L\dot{\theta}_2^{+}\sin\theta_2^{-} \\ \dot{\theta}_2^{+} \\ \dot{\theta}_1^{+} \end{bmatrix}. \tag{3.16}$$

On the other hand, each position $\boldsymbol{q}^{+}$ is reset as

$$\boldsymbol{q}^{+} = \begin{bmatrix} x^{-} + L\sin\theta_1^{-} - L\sin\theta_2^{-} \\ z^{-} + L\cos\theta_1^{-} - L\cos\theta_2^{-} \\ \theta_2^{-} \\ \theta_1^{-} \end{bmatrix}. \tag{3.17}$$

3.2.3 Control methods

In this study, a gait model with a minimum number of degrees of freedom is introduced, and the simplest periodic waveform (sine wave) is used to generate a gait with a minimum periodic input, which is applied to the hip joint. In order to affect the dynamics of the robot itself as little as possible, the control waveform has to be applied using a smaller torque control instead of real-time angular feedback, where a feed-forward torque input waveform is shown below.

$$u(t) = A_m \sin(2\pi f_c t) \tag{3.18}$$

where A_m [N·m] and f_c [Hz] are the amplitude and frequency of the sine wave, respectively. When the input is applied to the robot, the amplitude determines the maximum torque given, and the frequency is the number of times the torque is repeated per unit of time. The onset of the entrainment phenomenon is determined as the convergence of the robot's walking frequency to the input frequency after the robot has reached a stable state over time.

3.3 Quasi-passive Dynamic Walking Based on the First Signal System

Numerical simulation needs to use the physical and control parameters shown in Table 3.1. Here it should be noted that the location of the grounding point of the foot is not the generalized coordinate system in x, z but x_c and z_c, so the need to calculate the actual role of the arc foot through the geometric relationship to the initial conditions of the ground, as shown below.

$$\begin{aligned} \boldsymbol{q}(0) &= \begin{bmatrix} -0.0149 & 0.0019 & 0.2 & -0.25 \end{bmatrix}^{\mathrm{T}} \\ \dot{\boldsymbol{q}}(0) &= \begin{bmatrix} 0 & 0 & 1 & -0.2 \end{bmatrix}^{\mathrm{T}} \end{aligned} \tag{3.19}$$

Since the initial state gives the right angle as well as sufficient speed, the robot can walk along the slope successfully.

3.3.1 Gait generation test

Figure 3.2 shows the simulation results for the first 10 seconds when the hip input torque follows a generally sinusoidal waveform. Fig. 3.2(a) is the center position (x, z) of the semicircular foot of the support leg, and the coordinate position z is enlarged in the figure for a total

Table 3.1: Physical and Control Parameters

Symbol	Value	Unit
m_H	10	kg
$m_1 = m_2$	5	kg
L	1	m
$a = b$	0.5	m
R	0.1	m
ϕ	0.05	rad
g	9.81	m/s^2
A_m	0.5	N·m
f_c	1.4	Hz

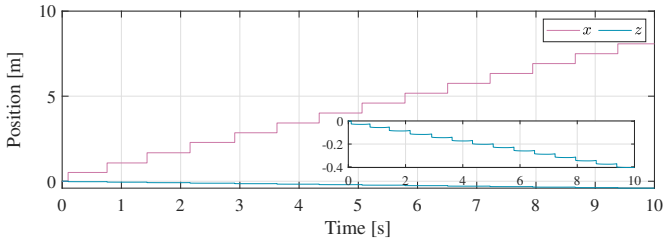

(a) Position

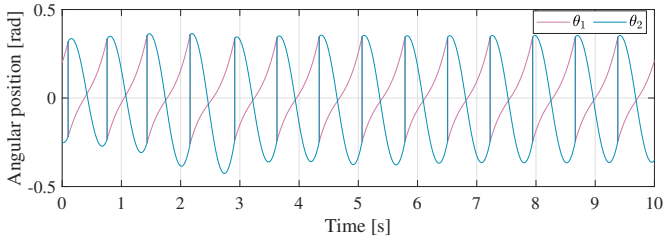

(b) Angular position

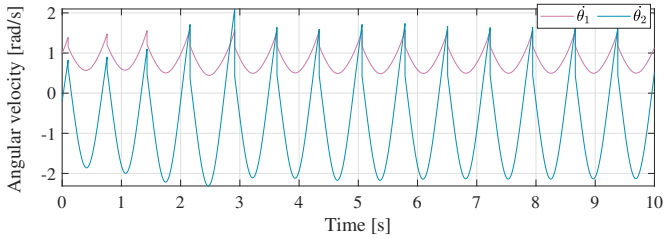

(c) Angular velocity

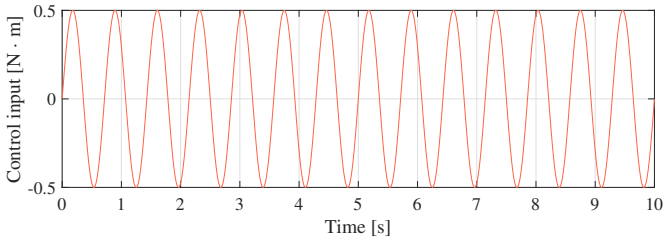

(d) Control input

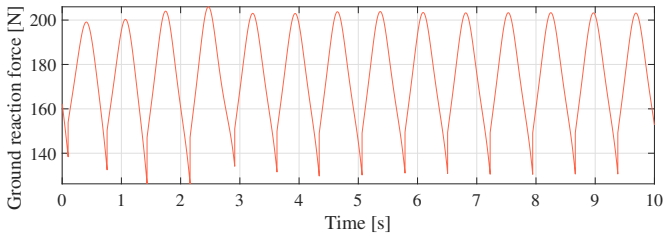

(e) Vertical ground reaction force

Figure 3.2: Simulation results of typical gait generation

descent of 0.4 m along the ramp for 10 seconds. Fig. 3.2(b) and Fig. 3.2(c) show the angular variation of the two legs and the angular velocity over time. It can be seen that the robot moves

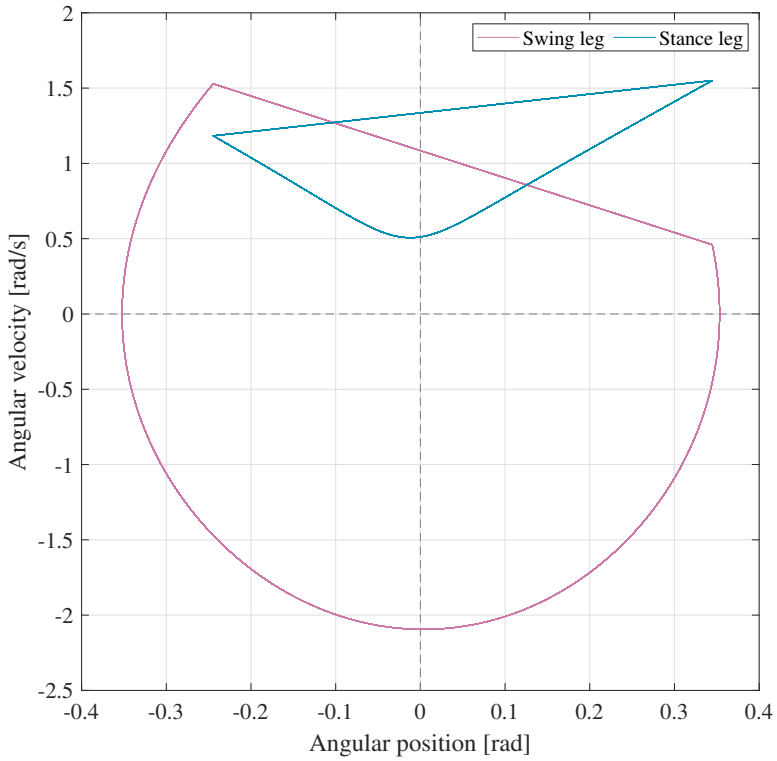

Figure 3.3: Phase plane plot of steady period-1 gait

forward at a relatively constant speed, even in the first few steps. Here the input torque magnitude is only 0.5 [N·m] and the oscillation of both legs increases slightly with time and finally stabilizes gradually. Figure 3.2(d) shows the variation of the torque given by the input. The last Fig. 3.2(e) shows the time variation of the vertical ground reaction force. It varies drastically due to the larger effect of the gravitational potential energy of walking on the slope. However, the value of the vertical ground reaction force is always positive, indicating that the stance leg does not leave the ground.

Without input from the hip, the robot will passively walk along a suitable ramp angle and will eventually generate a limit-cycle gait or a chaotic gait. To confirm whether the robot can converge to a stable limit-cycle gait after applying entrainment control, a phase plane plot of the gait after the sufficient time (after 100 [s]) is shown in Fig. 3.3. It can be seen that the robot is able to generate a period-1 limit-cycle gait on a downhill slope with a sinusoidal torque applied.

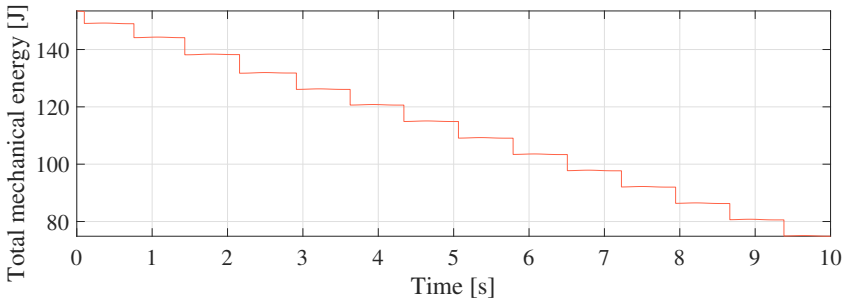

(a) Total mechanical energy

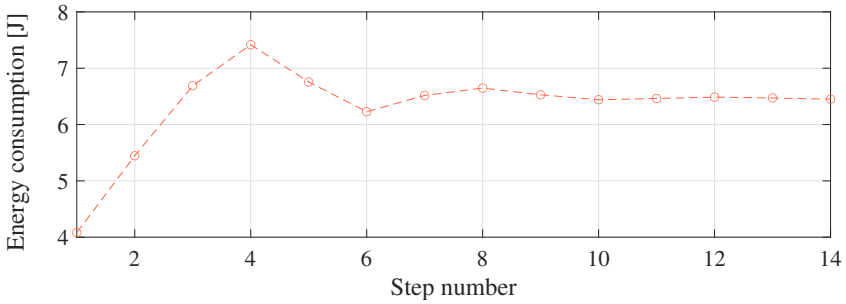

(b) Energy loss

Figure 3.4: Simulation results of energy change with feed-forward control

3.3.2 Energy change observation

We can observe the actual energy shift by calculating the mechanical energy of the robot. Moreover, the total mechanical energy of the robot is determined by the sum of its kinetic and potential energy and hence is solved by the following equation.

$$E_{total} = \frac{1}{2}\dot{\boldsymbol{q}}^{\mathrm{T}}\boldsymbol{M}\dot{\boldsymbol{q}} + P. \tag{3.20}$$

Note that P is the potential energy. In this numerical simulation, the mechanical energy of the robot is only lost when the legs hit the ground because external influences such as air resistance are neglected. Therefore, the missing mechanical energy can be calculated by the following condition.

$$E_{loss} = \frac{1}{2}\dot{\boldsymbol{q}}^{+\mathrm{T}}\boldsymbol{M}\dot{\boldsymbol{q}}^{+} - \frac{1}{2}\dot{\boldsymbol{q}}^{-\mathrm{T}}\boldsymbol{M}\dot{\boldsymbol{q}}^{-}. \tag{3.21}$$

Figure 3.4 shows the energy changes that occur in the robot walk with entrainment control induced. Figure 3.4(a) shows the change in the overall mechanical energy. Since the applied input torque is very small, only 0.5 [N·m], the mechanical energy change is not significant during each walking cycle. In Fig. 3.4(b), it is possible to observe the kinetic energy that is

consumed after the foot strikes the ground. Depending on the initial conditions, the energy consumed thereafter is almost constant except for the first few steps. This is due to the gradual transition of the robot to a stable walking condition.

3.3.3 Feasibility analysis of entrainment control

The previous simulation results demonstrate that the robot can walk into a limit-cycle gait with smaller feed-forward period input conditions. In order to verify the feasibility of the entrainment theory and to investigate whether the robot's walking frequency can be forcibly entrained by the input frequency under varying input frequency and input torque, simulations were performed according to the following Algorithm 2. Two ramp angles, smaller and general, are tried here, with ϕ set to 0.02 and 0.05 [rad], respectively. The input frequency and torque were adjusted at each angle, and the results of each simulation were analyzed by taking 20 steps after the robot had successfully walked for 100 seconds, and recording the frequency of these 20 steps. To systematically analyze this forced entrainment property, the Arnold tongue is used to quantify the overall entrainment range of the system. In nonlinear dynamics, Arnold tongue is used to evaluate the relationship between two oscillatory systems whose phases are affected by each other [54, 55].

The measured Arnold tongue is shown in Fig. 3.5. The generation of entrainment is identified when $|f_w - f_c| < 0.01$ [Hz]. The robot exhibits a typical Arnold tongue at both slopes, where the walking frequency is forced to be entrained by the input frequency as it approaches the robot's natural walking frequency, and the range of successful entrainment is marked by the pentagon. Figure 3.5(a) shows an Arnold tongue at a slope angle of $\phi = 0.02$ [rad]; the entrainment range increases as the torque increases, but the robot begins to move out of the entrainment range when the torque exceeds 0.45 [N·m]. In Fig. 3.5(b), roughly the same trend exists when the slope angle ϕ is set to 0.05 [rad]. However, the entrainment range at the same torque becomes significantly smaller, presumably because the compensation for the conversion of the robot's gravitational potential energy into kinetic energy becomes larger as the slope angle becomes larger, and a smaller torque can hardly affect the dynamics of the whole system.

Algorithm 2 Calculate walking frequency f_w

Require: The walking frequency f_w of the bipedal robot when it gets stabilized

Input: Initial state $\boldsymbol{q}(0)$, $\dot{\boldsymbol{q}}(0)$, ϕ, A_m and f_c

Output: Walking frequency f_w of the next 20 steps after 100 seconds

Initialization $f_w[l][m][20] = 0$, $f_c = 1$, $A_m = 0.1$
for $i = 1; i <= l : i++$ **do**
  for $j = 1; j <= m : j++$ **do**
    Run simulation for 100 seconds.
    Save the next 20 walking frequency to f
    $f_w[i][j] = f$
    $f_c = f_c + 0.01$
  end
  $A_\mathrm{m} = A_\mathrm{m} + 0.05$
end
Return f_w

3.4 Summary and Discussions

In this chapter, a nonlinear analysis is performed on a compass liked bipedal robot with semicircular feet in order to understand the motion mechanism of a passive walking robot under entrainment control. It was found that a minimal periodic torque input was able to influence the dynamics of the robot's passive walk successfully. It successfully entrains the robot from natural walking frequencies to input frequencies. From the analysis of Arnold tongue, it was found that the entrainment range is positively correlated with the magnitude of the input amplitude. The results of walking on different slopes show that the range of entrainment is considerably wider at smaller slopes. To make the robot workable in practice, passive walking on downhill slopes alone is not sufficient, and it is not known whether the method can be successfully followed on horizontal surfaces, so extending this controlling method to more general road conditions is necessary. The next chapter is devoted to the question of whether this method can be used to produce a stable and controllable gait when the robot walks on a horizontal surface.

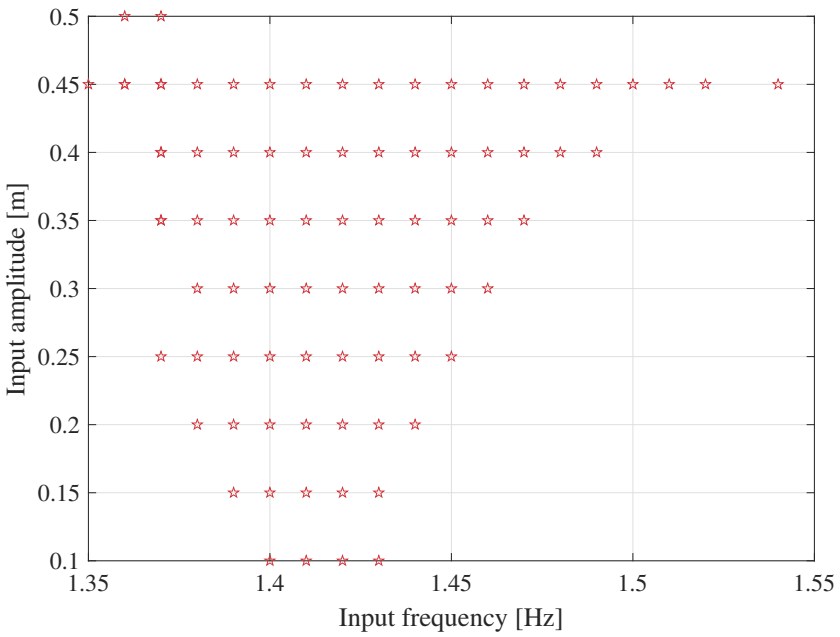

(a) Arnold tongue with small slope angle

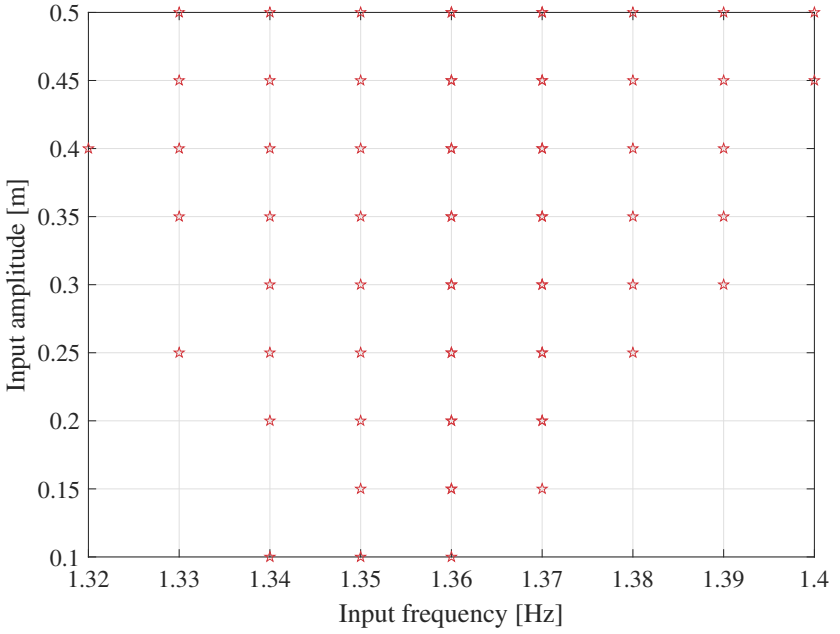

(b) Arnold tongue with large slope angle

Figure 3.5: Arnold tongues concerning frequency and amplitude of input

Chapter 4

Nonlinear Analysis of Semicircular-footed Bipedal Robot Walking on Horizontal Road Surface with Entrainment Effect

4.1 Overview

In Chap. 3, a simple and efficient method is successfully used to make the walking cycle of a biped robot controllable on a downhill slope. In this chapter, still based on the first signal system, a single feed-forward waveform is used to issue a minimal forward walk command to the robot to explore whether the robot can successfully combine the idea of entrainment to come out with a reasonable gait on a horizontal road surface. This requires the robot to continuously overcome potential barriers in the gravity field to achieve a gait similar to that of a human. Based on this, the nonlinear nature of the method needs to be further elucidated. The nonlinear analysis performed in this chapter helps to deepen the understanding of the dynamics of the entrainment-controlled bipedal robotic system, which is beneficial for further optimization and extension to follow.

This chapter is organized as follows. Section 2 presents the simplified equations of motion and velocity constraints under the horizontal road surface, based on the control method in Chap. 3 with the addition of a sinusoidal basis with singular subdivisions to make the torque at the input more prominent. Section 3 begins with a numerical simulation to demonstrate the feasibility of this control method. After successfully stepping out of the limit cycle gait, the size of the

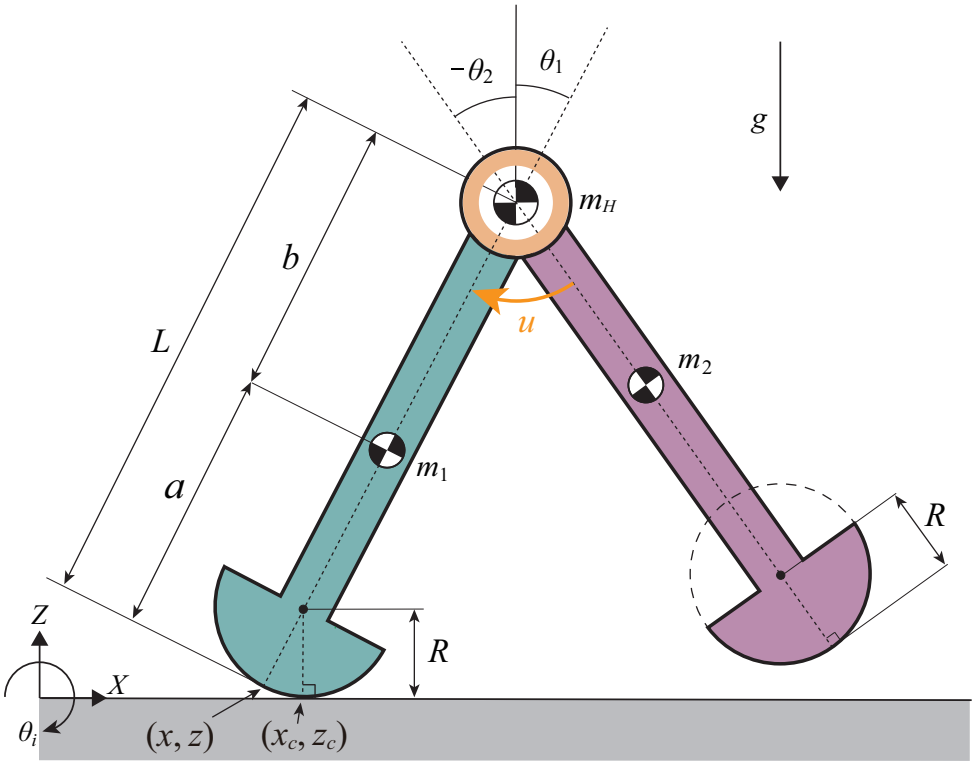

Figure 4.1: Mathematical model of a biped robot with semicircular feet walking on the horizontal road surface.

entrainment range is tested by adjusting the input parameters and analyzing the robot's walking performance in this state. Finally, the stability of the system is analyzed using the Poincaré map.

4.2 Simplified Modeling and Control Method

The model of the compass-like biped robot with semicircular feet walking on the horizontal road surface with single feed-forward control is illustrated in Fig. 4.1. The specific model details are the same as in Chap. 2.

4.2.1 Equation of motion

Let $\boldsymbol{q} = \begin{bmatrix} x & z & \theta_1 & \theta_2 \end{bmatrix}^{\mathrm{T}}$ be the generalized coordinate vectors. The equation of motion about the robot then becomes

$$\boldsymbol{M}\ddot{\boldsymbol{q}} + \boldsymbol{h} = \boldsymbol{J}^{\mathrm{T}}\boldsymbol{\lambda} + \boldsymbol{S}u, \tag{4.1}$$

$$\boldsymbol{J}\dot{\boldsymbol{q}} = \boldsymbol{0}_{2\times 1}. \tag{4.2}$$

Assuming that this model is on a horizontal road surface without sliding, the stance foot is rolling along the semi-circular arc during the walking cycle. Therefore, The velocity constraint at the position where the robot stance leg is in contact with the ground point is

$$\dot{x_c} = R\dot{\theta}_1, \quad \dot{z_c} = 0. \tag{4.3}$$

Therefore, Jacobians $\boldsymbol{J}$ are determined as

$$\boldsymbol{J} = \begin{bmatrix} 1 & 0 & R\cos\theta_1 - R & 0 \\ 0 & 1 & -R\sin\theta_1 & 0 \end{bmatrix}. \tag{4.4}$$

4.2.2 Equation of collision

In this model, the author still assumes that the swinging leg neither slides nor bounces when it hits the ground. When the swinging leg neglects contact with the ground during the swing, and when the final swinging leg forms an isosceles triangle with the stance leg based on the ground, the states of the two legs are immediately interchanged. Since the two legs are the same, the zero crossing of the following functions:

$$f(\theta_1, \theta_2) := \theta_1 + \theta_2, \tag{4.5}$$

starting from negative number, it requires $\frac{d}{dt}f(\theta_1, \theta_2) := \dot{\theta}_1 + \dot{\theta}_2 > 0$ to detect collision. The equation of collision is as follows:

$$\boldsymbol{M}\dot{\boldsymbol{q}}^{+} = \boldsymbol{M}\dot{\boldsymbol{q}}^{-} + \boldsymbol{J}_I^{\mathrm{T}}\boldsymbol{\lambda}_I, \tag{4.6}$$

$$\boldsymbol{J}_I\dot{\boldsymbol{q}}^{+} = \boldsymbol{0}_{2\times 1}. \tag{4.7}$$

Here, the superscripts "−" and "+" mean immediately before and after immediately a collision. Due to the robot has one pair of half-semicircular feet, when each time the leg is changed, the

fore leg is grounded at the point $(\bar{x_c}, \bar{z_c})$ of the foot. The velocity constraint condition for the landing point of the forefoot is determined as

$$\dot{\bar{x}_c}^+ = R\dot{\theta_2}^+, \quad \dot{\bar{z}_c}^+ = 0. \tag{4.8}$$

These are detailed as

$$\begin{aligned} \frac{\mathrm{d}}{\mathrm{d}t}\begin{bmatrix} \bar{x}_c \\ \bar{z}_c \end{bmatrix}^+ &= \frac{\mathrm{d}}{\mathrm{d}t}\begin{bmatrix} x+L\sin\theta_1-(L-R)\sin\theta_2 \\ z+L\cos\theta_1-(L-R)\cos\theta_2 \end{bmatrix}^+ \\ &= \begin{bmatrix} 1 & 0 & L\cos\theta_1^- & (R-L)\cos\theta_2^- \\ 0 & 1 & -L\sin\theta_1^- & (L-R)\sin\theta_2^- \end{bmatrix}\dot{\boldsymbol{q}}^+. \end{aligned} \tag{4.9}$$

Therefore, we can obtain the velocity constraint $\boldsymbol{J}_I^{\mathrm{T}}$ as

$$\boldsymbol{J}_I^{\mathrm{T}} = \begin{bmatrix} 1 & 0 \\ 0 & 1 \\ L\cos\theta_1^- & -L\sin\theta_1^- \\ -R-(L-R)\cos\theta_2^- & (L-R)\sin\theta_2^- \end{bmatrix}. \tag{4.10}$$

4.2.3 Control method

In this section, although there is no constant conversion of gravitational potential energy into kinetic energy as in passive walking, the author still wants to take advantage of the dynamics of the model itself as much as possible, so the author cannot use any angle tracking to control the motion of the robot and only apply minimal torque control. To smoothly affect the robot dynamics, the torque waveform acting on the hip input is still set to a sinusoidal trajectory as follows.

$$u(t) = A_m \sin^{\gamma}(2\pi f_c t). \tag{4.11}$$

where A_m [N·m] and f_c [Hz] represent the magnitude and frequency of the input, respectively. Furthermore, sinusoidal and square waves are often used as typical waveforms in nonlinear dynamics. However, the torque control of servo motors is difficult to track square waves directly in the real world. Based on previous results on indirect entrainment [52], the fastest indirect entrainment waveforms derived by mathematical means are similar to excitation waves. In this paper, the author uses a sine wave and adjusts the odd power of the sine wave to simulate the excitation wave, where γ is the odd power of the sine wave. The larger this value, the stronger the tendency of the waveform to approximate a discrete imposed input waveform.

4.3 Numerical Simulation Results

4.3.1 Motion generation

Table 4.1 shows the control and physical parameters to conduct the following process. It should be noted here that the size of the input torque is generally determined based on the size and weight of the model, but due to the wind resistance in the real environment, the mechanical vibration caused when the support leg hits the ground and other effects are neglected in the simulation environment. Thus, the minimum input torque required for the simulation is much smaller than that of the real environment, and the initial conditions are set as

$$\begin{aligned} \boldsymbol{q}(0) &= \begin{bmatrix} 0 & 0.0015 & 0.1745 & -0.1745 \end{bmatrix}^{\mathrm{T}}, \\ \dot{\boldsymbol{q}}(0) &= \begin{bmatrix} 0 & 0 & 0.75 & 0 \end{bmatrix}^{\mathrm{T}}. \end{aligned} \tag{4.12}$$

Since there is only one feed-forward input, the initial conditions are chosen relatively harshly. Here, when the applied input torque is extremely small, the angles between the stance and swing legs in the initial conditions are set to 10 and -10 degrees, so that the robot triggers collision detection at the beginning of the simulation. And since it is a semicircular leg, when the z_c of the contact point is 0, the z coordinate needs to be calculated based on the current angle.

Figure 4.2 shows the gait generated according to the appropriate initial state as well as the control parameters. Fig. 4.2(a) is the position of the centroid of the semicircular foot of the stance leg (x, z). Since the angular velocity given by the initial conditions is large enough, the robot starts with a slightly larger stride for the first few steps, but gradually converges over the next few seconds to move forward with a relatively constant stride. The figure zooms in to show

Table 4.1: Physical and control parameters

Symbol	Value	Unit
m_H	10	kg
m_1	5	kg
m_2	5	kg
a	0.5	m
b	0.5	m

Symbol	Value	Unit
L	1	m
R	0.1	m
g	9.81	$\mathrm{m/s^2}$
A_m	0.5	N·m
f_c	1.5	Hz

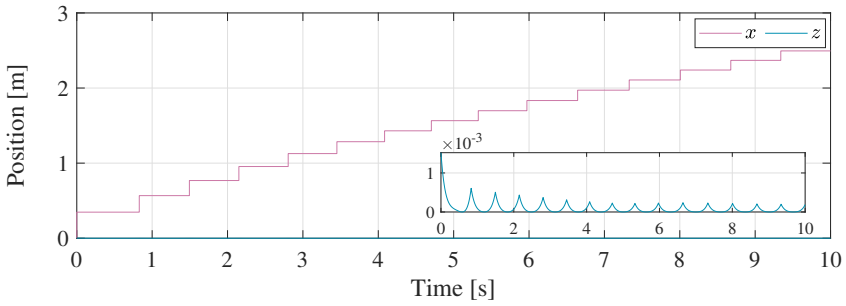

(a) Position

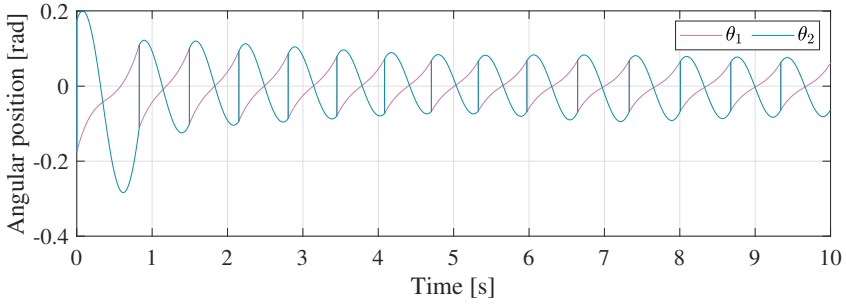

(b) Angular position

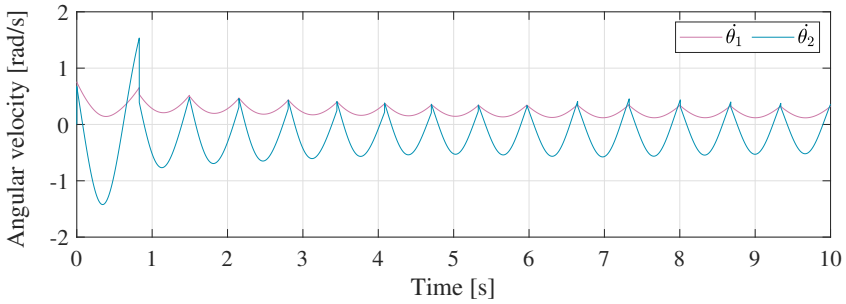

(c) Angular velocity

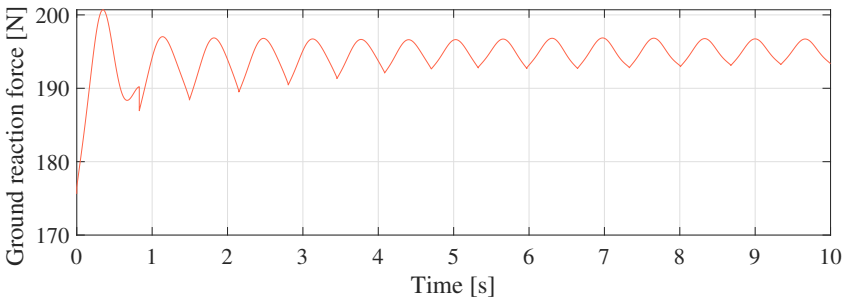

(d) Vertical ground reaction force

Figure 4.2: Simulation results of motion generation with feed-forward control

the variation of z coordinates, and it is found that the robot rolls nicely along the circular foot during walking, and the larger the stride length, the longer the rolling distance. In Fig. 4.2(b) and Fig. 4.2(c), the angular position and angular velocity of the two legs are shown as a function

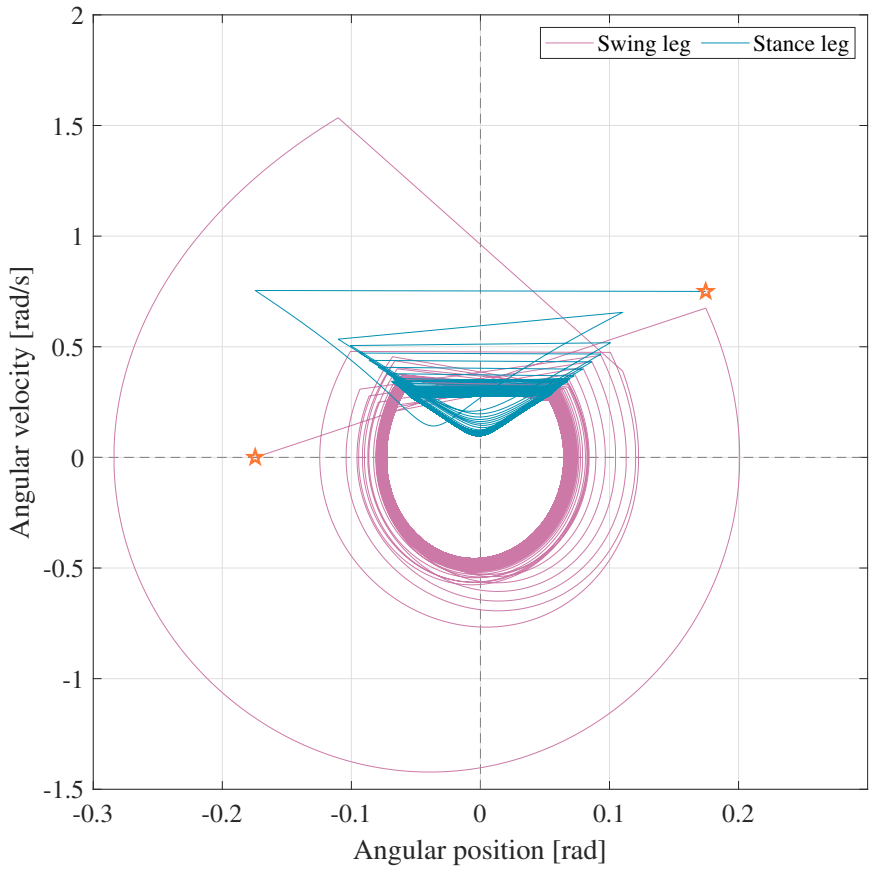

Figure 4.3: Phase plane plot of generated motion where A_m=0.5 [N·m] and f_c=1.5 [Hz]

of time. Because the input torque is really slight relative to the overall mass of the robot, after the first few collisions with the ground, we can see that the swing of the legs becomes extremely slight, only about 0.2 [rad]. Fig. 4.2(d) shows the time variation of the vertical ground reaction force. In contrast to the passive walk in Chap. 2, where the effect of the gravitational potential is reduced, the variation of the reaction force of the bed is not intense and the value is always approximately equal to the full mass of the robot. Moreover, we can see that these values remain continuously positive. This may be justified by the fact that the supporting foot never leaves the ground, and the resulting gait is reasonable.

To observe the state of the robot's long-term motion, a phase plane plot of the gait generated over 100 seconds is shown in Fig. 4.3. The initial state is marked with a firestar. The results show that although the limit loop of the robot keeps shrinking due to the minor applied torque, the robot can gradually converge to a relatively stable limit loop gait while walking on flat

ground without relying on any posture feedback by applying only a sinusoidal torque input to the robot's hips.

Figure 4.4 shows the input as well as the energy variation of the robot while walking. Fig. 4.4(a) is the torque variation with time. The torque magnitude is 0.5 [N·m] and the frequency is 1.5 [Hz]. Fig. 4.4(b) represents the total mechanical energy, which initially increases when the swing leg collides with the ground until the next collision, then decreases in order to overcome the potential energy barrier, and increases again after breaking the potential energy barrier because of gravitational potential energy. This illustrates that the idea of torque control based on entrainment allows for smooth transitions in the dynamics of the robot itself. After each collision of the swing leg, we can see the consumption of kinetic energy as shown in Fig. 4.4(c). After waiting for the kinetic energy given by the initial state to be offset by several collisions, the energy consumption afterward is extremely low. It is not difficult to find that at 10 seconds, the robot has taken exactly 15 steps, which is consistent with the input frequency of 1.5 [Hz] in the control parameters. It can be assumed that the entrainment control still has an effect on the horizontal road surface, which paves the way for additional analysis of nonlinear phenomena to follow.

4.3.2 Influence of A_m and f_c on gait

This subsection uses A_m [N·m] and f_c [Hz], which control the input sine wave, as variables to study their effects on the robot gait, such as walking frequency, step length, walking speed, and energy efficiency. In the following Algorithm 3, only f_c [Hz] is used as an example. Each time, the 30 steps that could successfully generate a gait after 100 seconds were taken for numerical analysis.

The SR (Specific Resistance) is a dimensionless quantity used to evaluate the efficiency of walking. It expresses the energy consumption required to move a 1 [kg] mass by 1 [m], and the lower this value is, the more efficient it is to move, defined as

$$SR := \frac{p}{m_{all} g \, |V_x|}. \tag{4.13}$$

Here, m_{all} [kg] is the mass of the whole robot, g [m/s^2] is the gravitational acceleration, and p [J/s] is the average input power, defined as

$$p := f_w \int_{100}^{100+\frac{1}{f_w}} \left|(\dot{\theta_1} - \dot{\theta_2})u\right| \mathrm{d}t. \tag{4.14}$$

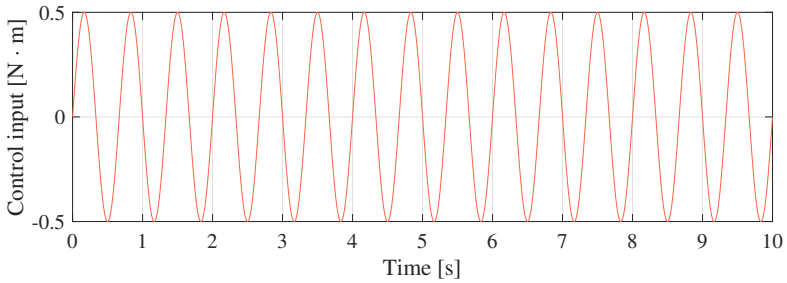

(a) Control input

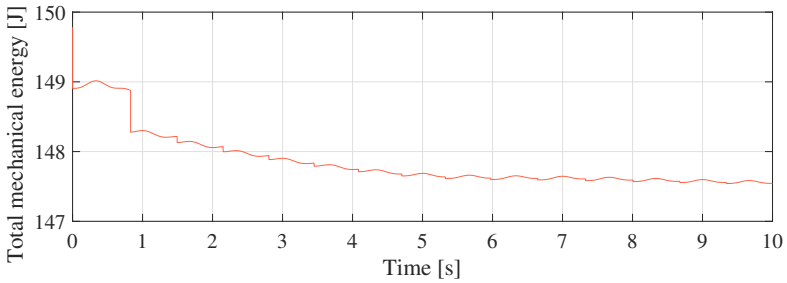

(b) Total mechanical energy

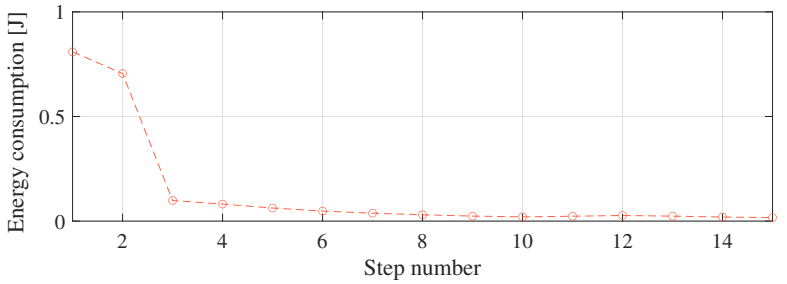

(c) Energy loss

Figure 4.4: Simulation results of energy change with feed-forward control

f_w represents the walking frequency. $|V_x|$ is the absolute value of the average walking speed, is then defined as

$$V_x := f_w \times S_l. \tag{4.15}$$

Here, S_l [m] represents the step length of the biped robot. Since the robots collide in an isosceles triangle, we can easily compute the step size at each step.

First, by fixing the remaining parameters and changing only the input frequency, the simulation results for f_c from 0.1 to 10 [Hz] are shown in Fig. 4.5 and Fig. 4.6, where the robot can successfully walk to keep from falling down for input frequencies f_c starting at 0.72 [Hz]. Because the author intercepted 30 steps of the gait after 100 seconds each time for analysis, there are really 30 hollow circles on each vertical axis in the figure to represent the magnitude of

Algorithm 3 Calculate f_w and SL

Require: The walking frequency f_w and step length SL of the Robot when they get stabilized

Input: Initial state $\boldsymbol{q}(0)$, $\dot{\boldsymbol{q}}(0)$, A_m and f_c

Output: The walking frequency f_w and step length SL of the next 30 steps after 100 steps

1: **Initialization** $f_w[l][30] = 0$, $SL[l][30] = 0$, $f_c = 0.1$
2: **for** $i = 1; i <= l : i++$ **do**
3: Run simulation for 130 steps.
4: Save the last 30 step walking frequency to f and the last 30 step length to L
5: $f_w[i] = f$
6: $SL[i] = L$
7: $f_c = f_c + 0.02$
8: **end**
9: **Return** f_w and SL

the 30-step values. Moreover, when the gait converges into a single limit ring, these 30 hollow circles overlap. In addition, the author uses solid points to indicate the mean values.

Fig. 4.5 (a) shows the shift of walking frequency when changing the input frequency. It can be noticed that, for example, from 1.28 to 1.56 [Hz], from 2.72 to 3.16 [Hz], and other ranges marked with light yellow intervals, the walking frequency invariably coincides with a multiple of the frequency of the input sine wave, which indicates that it is completely entrained in this interval. Setting the relationship between f_c:f_w to n:1 (n is a positive integer) yields entrainment ranges from 1:1 all the way up to 7:1. It is worth noting, however, that the input frequency following the 1:1 and 2:1 entrainment frequencies does not allow the robot to successfully generate a gait. Instead, as shown in Fig. 4.5 (b), we can see that for each n:1 entrainment range, the step length first becomes progressively longer and then continuously shorter as the frequency increases, and a local maximum is generated.

The results for walking speed and walking efficiency are shown in Fig. 4.6, Fig. 4.6(c) showing the effect of varying the frequency on walking speed. The walking speed, on the other hand, is proportional to the product of stride width and walking frequency, which also yields a local maximum walking speed in each entrainment range. The results for the walking efficiency in Fig. 4.6(d) show that when the input torque is kept constant, there is a minor shift in the walking efficiency with increasing input frequency only. Because the A_m set is extremely

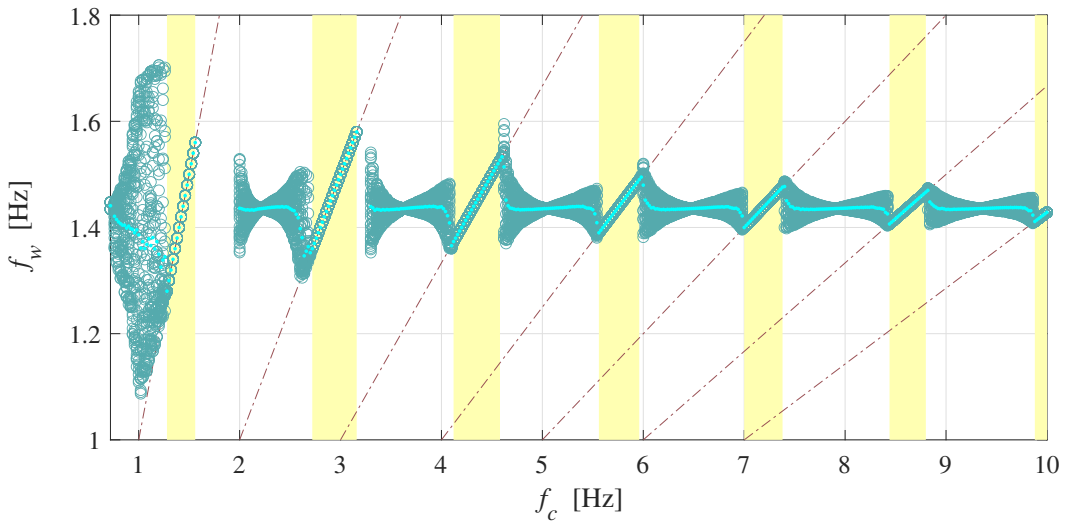

(a) Walking frequency

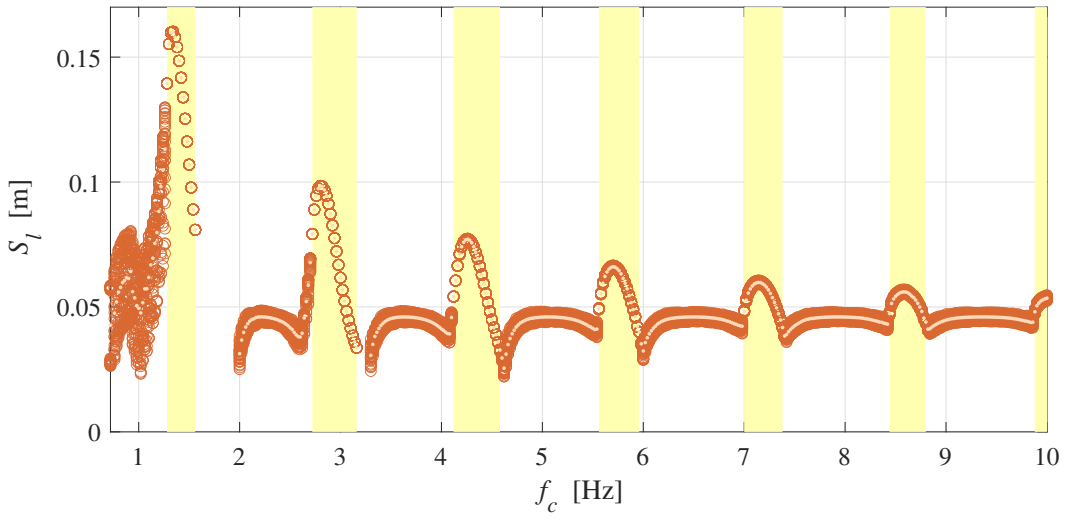

(b) Step length

Figure 4.5: Gait performance versus frequency of the sine wave

modest compared to the weight of the robot, SR is always stabilized at an extremely modest value.

The effect of the input torque magnitude A_m on the gait performance is shown in Fig. 4.7 and Fig. 4.8. Since the simulation conditions ignore much of the energy that needs to be consumed in real situations, it is possible to generate a stable gait with A_m while keeping highly modest values. Moreover, when the torque exceeds 18.2 [N·m], an attractive phenomenon of multi-cycle divergence is generated, which typically only occurs in passive bipedal walking. It is when the applied torque exceeds 20.5 [N·m] that the robot falls.

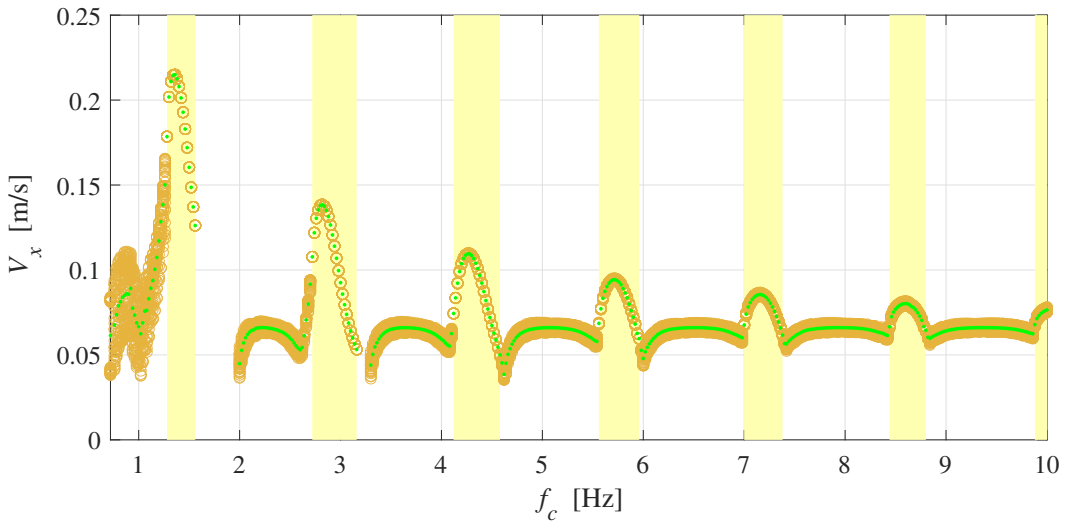

(c) Walking speed

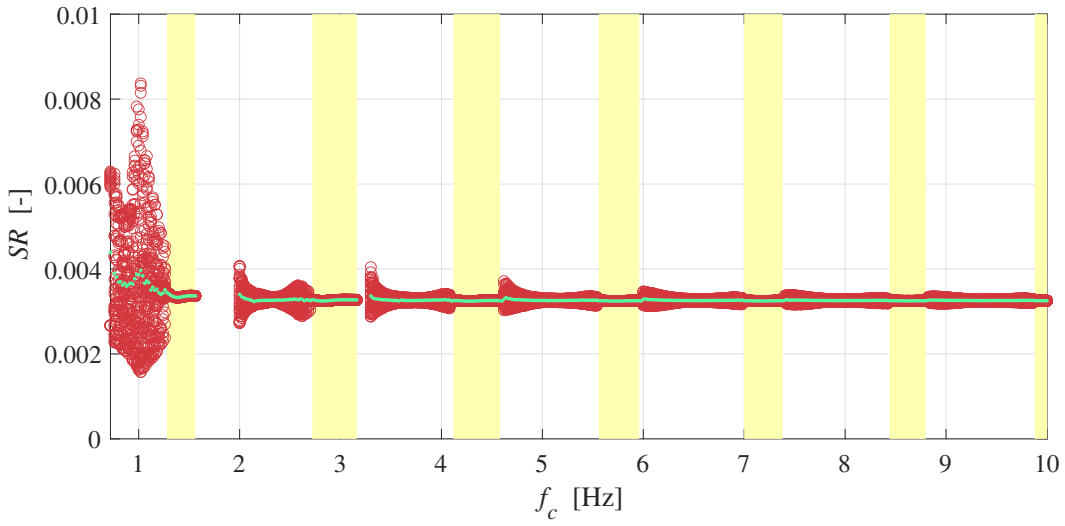

(d) Specific resistance

Figure 4.6: Gait performance versus frequency of the sine wave

Figure 4.7 (a) represents the variation of the walking frequency. When the input frequency is kept constant, entrainment is maintained except for values with too slight or too large an amplitude due to entrainment effects. Figure 4.7(b) shows the variation of the stride length, which makes the stride amplitude follow as the input torque increases when the swing leg is swinging. It is worth noting that the growth rate of the step size with torque is not linear, but instead resembles a logarithmic function of the curve.

In Fig. 4.8 (c), it is observed that the walking speed increases approximately monotonically as the torque becomes larger. However, there is an upper bound on the walking speed based on

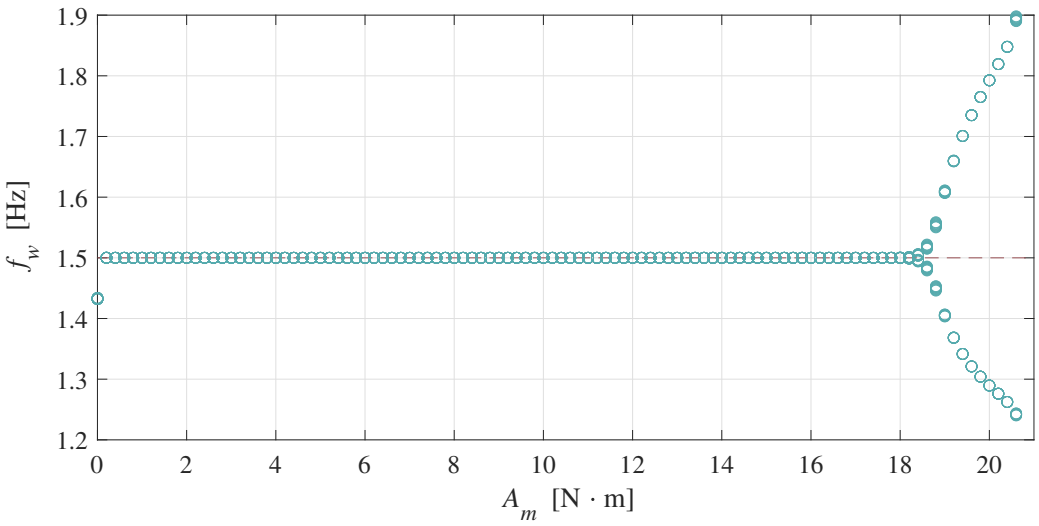

(a) Walking frequency

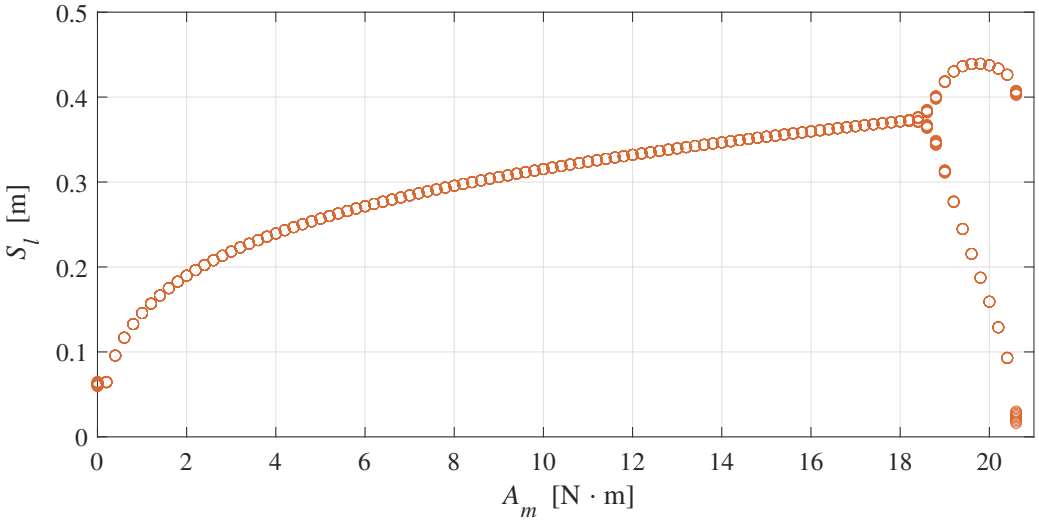

(b) Step length

Figure 4.7: Gait performance versus amplitude of the sine wave

a fixed input frequency. In Fig. 4.8(d), we can observe that as A_m increases, the value of SR also becomes progressively larger. However, until the torque increases until the robot falls, the value of SR is also much below 1. It indicates that the robot's walking efficiency is excellent with this method.

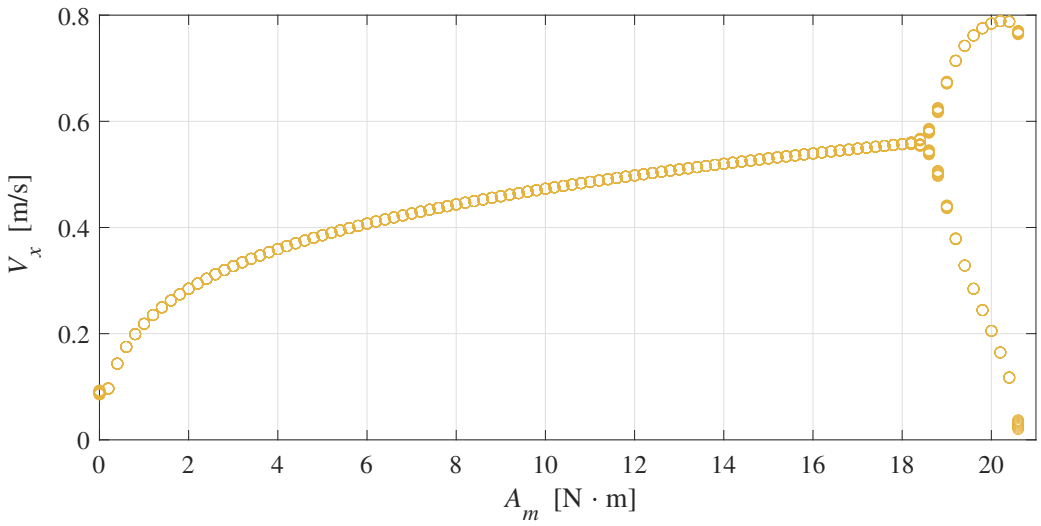

(c) Walking speed

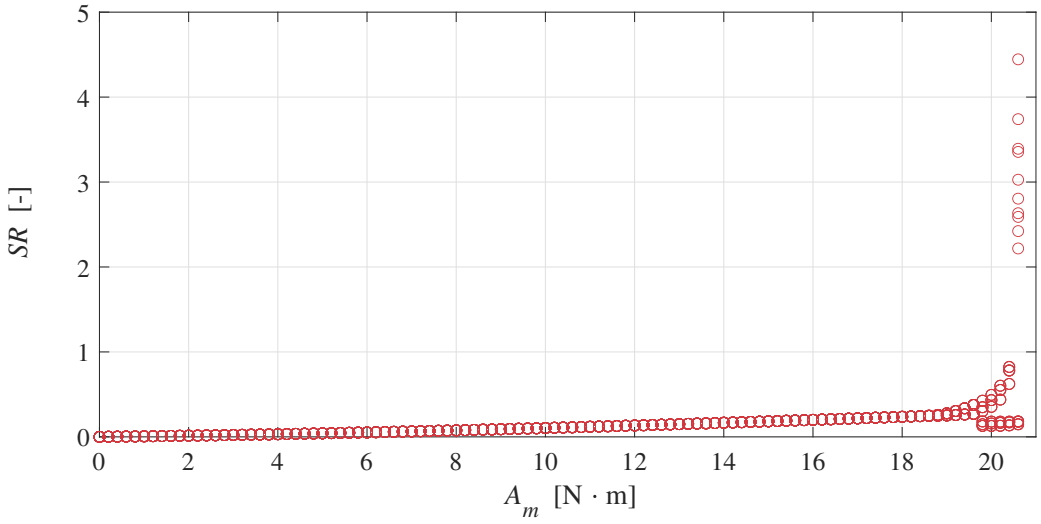

(d) Specific resistance

Figure 4.8: Gait performance versus amplitude of the sine wave

4.3.3 Effect of excitation wave

Figure 4.9 shows the excitation wave simulated by adjusting the sine wave to the singular power. As the value of the singular quadrature becomes larger, the input waveform becomes closer to the shock and the input torque appears to be applied discretely within each input period.

In Fig. 4.10 and Fig. 4.11, the author also investigates the effect of the excitation waveform on the gait pattern. Without changing the input frequency beyond the torque, the walking frequency remains the same as the input frequency. Although the walking efficiency becomes

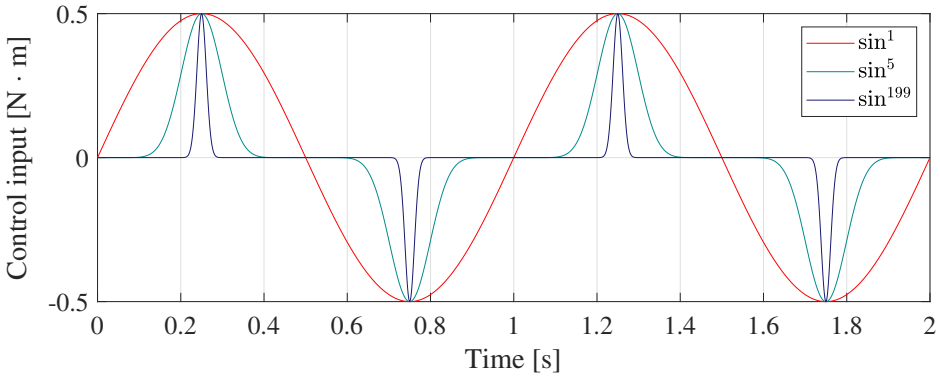

Figure 4.9: Control input by adjusting sinusoidal trajectory

better as the odd power γ increases, this also sacrifices part of the walking speed. Specifically, because the applied input torque, as well as the frequency, do not alter, the greater the γ, the less kinetic energy is input to the robot per unit cycle, and thus the efficiency becomes better.

This subsection uses an entrainment control approach to stabilize the robot's walk. When the given torque is within a reasonable range and remains constant, the control frequency only affects the speed of the leg swing, and overly quick or too low control frequency will cause the robot legs to touch the ground earlier or later, resulting in errors between the walking frequency and the input frequency, and the resulting gait then becomes multi-cycle or chaotic. In contrast, in the entrainment interval, the robot can be controlled to achieve a periodically forgotten gait by changing only the parameters of the feedforward input. It requires prior modeling and nonlinear analysis of the robot.

4.3.4 Poincaré map

Although the robot can converge to a periodic-1 limit cycle gait with the same input frequency under the approach of entrainment control, the robustness of the system has not been explored. The existence of steady-state phases in passive dynamic walking has been thoroughly investigated in some past studies [8, 9]. Moreover, limit cycle gait is normally checked by the following Poincaré map [56, 57]:

$$\boldsymbol{Q}_{n+1} = \boldsymbol{P}(\boldsymbol{Q}_n). \tag{4.16}$$

Here, $\boldsymbol{Q}_n$ is the state vector at the beginning of the n^{th} step. This is because the Poincaré section of the Poincaré map of the leg motion is usually defined as the instant immediately after the leg

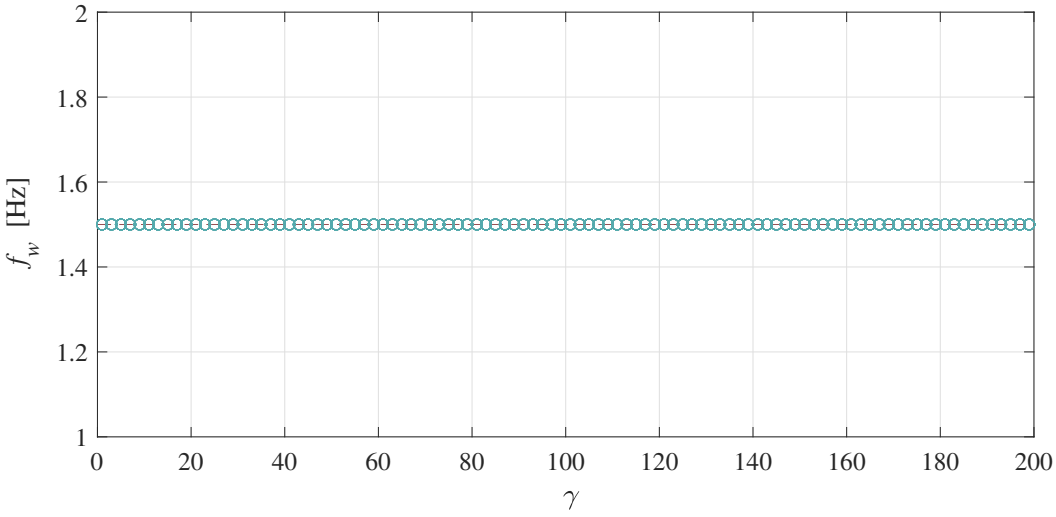

(a) Walking frequency

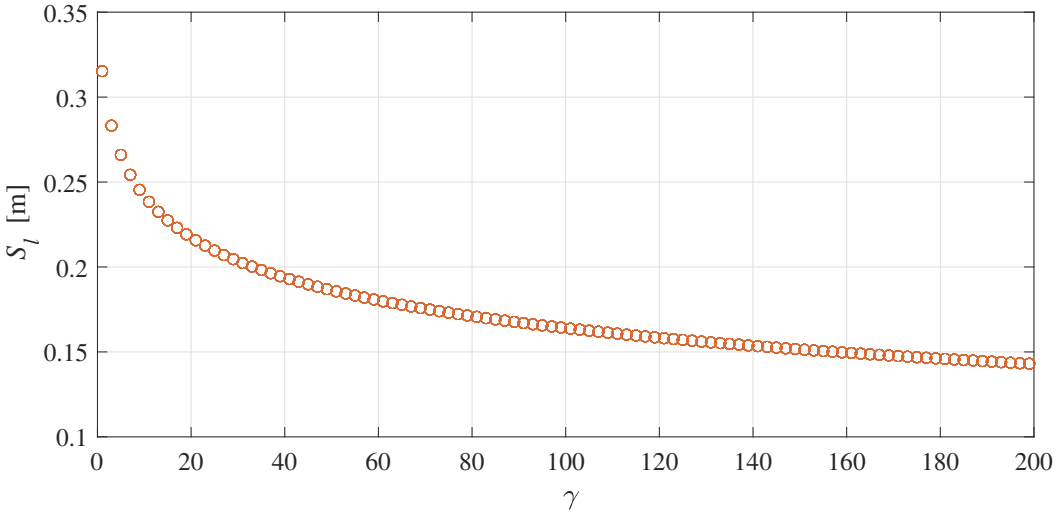

(b) Step length

Figure 4.10: Gait performance versus the excitation wave

collision. In addition, $\boldsymbol{P}$ is the Poincaré map of the state vector $\boldsymbol{Q}$ from the current step n to the next step $n+1$, and the state vectors are chosen as follows.

$$\boldsymbol{Q}^* = \boldsymbol{P}(\boldsymbol{Q}^*). \tag{4.17}$$

For periodic motion, the states are mapped to themselves and the number of steps is neglected. When a slight disturbance is applied to the steady-state dimension i^{th}, the output of the Poincaré map is determined as follows

$$\boldsymbol{Q}^* + \boldsymbol{\delta}_1^i \;=\; \boldsymbol{P}(\boldsymbol{Q}^* + \boldsymbol{\delta}_0^i) \approx \boldsymbol{P}(\boldsymbol{Q}^*) + \left.\frac{\partial \boldsymbol{P}}{\partial \boldsymbol{Q}}\right|_{\boldsymbol{Q}^*} \boldsymbol{\delta}_0^i \tag{4.18}$$

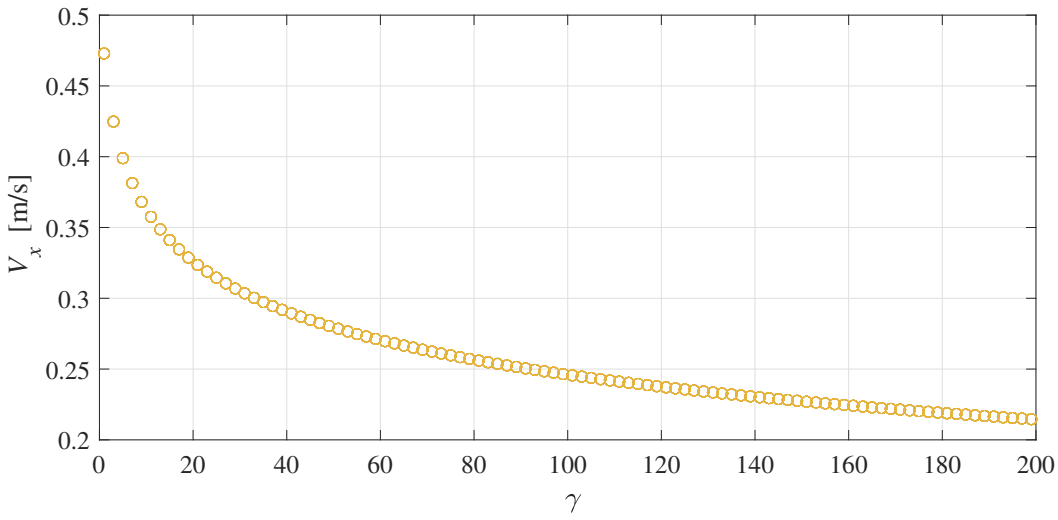

(c) Walking speed

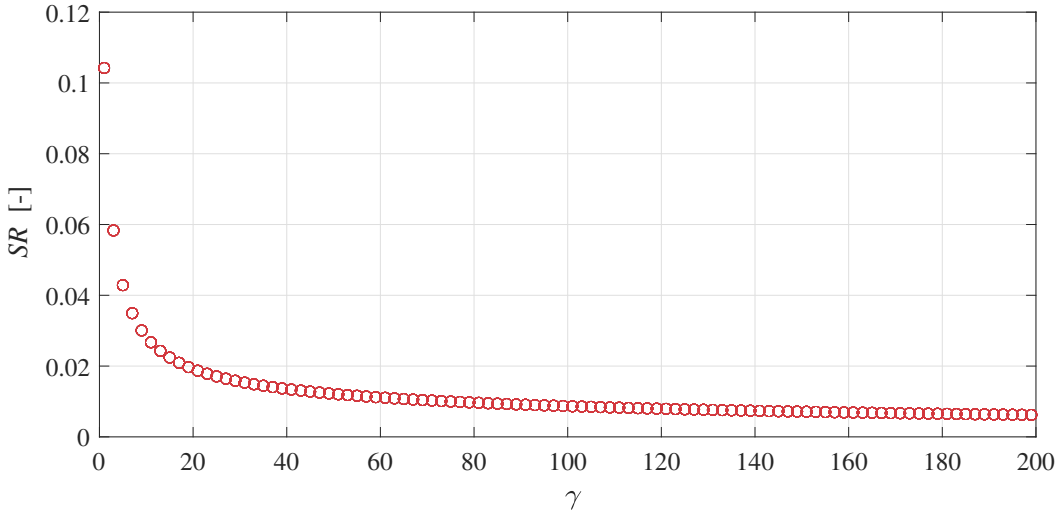

(d) Specific resistance

Figure 4.11: Gait performance versus the excitation wave

Here, the perturbations in the steady-state i^{th} dimension are represented by the vector $\boldsymbol{\delta}_0^i$ and the resulting deviation is defined as $\boldsymbol{\delta}_1^i$. Thus, the gradient matrix can be obtained by replacing the equation (4.17) with the equation (4.18) and then applying it to the perturbations in each dimension separately.

$$\left.\frac{\partial \boldsymbol{P}}{\partial \boldsymbol{Q}}\right|_{\boldsymbol{Q}^*} \approx \begin{bmatrix} \boldsymbol{\delta}_1^1 & \boldsymbol{\delta}_1^2 & \cdots & \boldsymbol{\delta}_1^n \end{bmatrix} \begin{bmatrix} \boldsymbol{\delta}_0^1 & \boldsymbol{\delta}_0^2 & \cdots & \boldsymbol{\delta}_0^n \end{bmatrix}^{-1} \tag{4.19}$$

For λ_i, which defines the eigenvalue of i^{th} in the matrix $\left.\frac{\partial \boldsymbol{P}}{\partial \boldsymbol{Q}}\right|_{\boldsymbol{Q}^*}$, the gait is locally stable if $\max |\lambda_i| < 1$. Therefore we can conclude that the gait of the robot under entrainment control

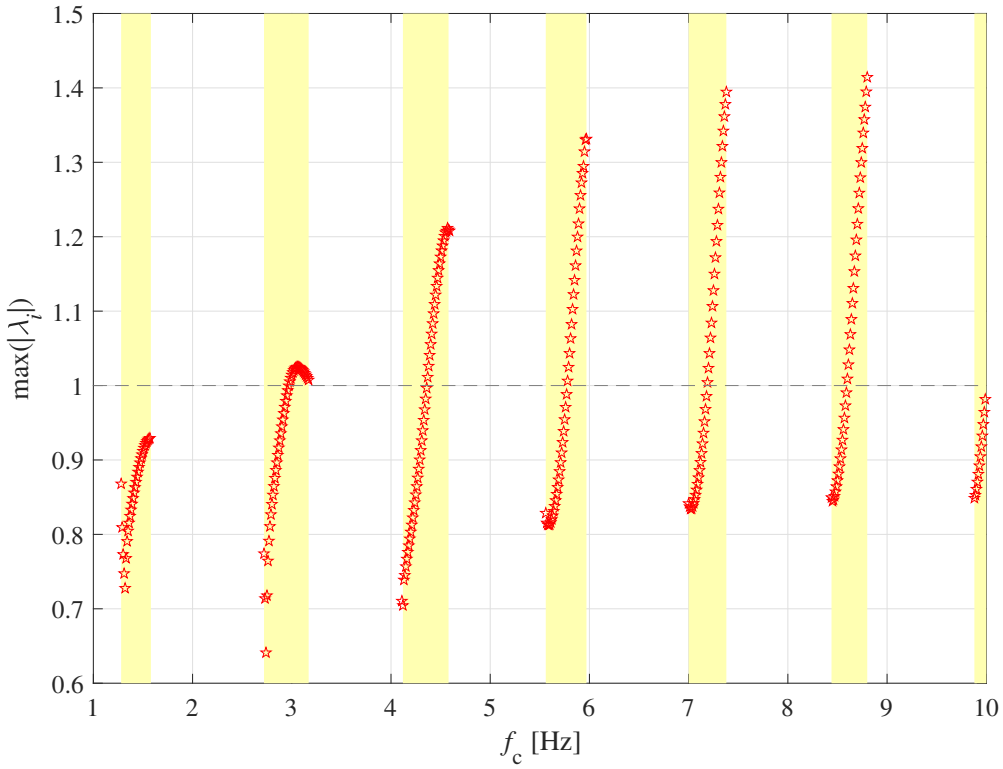

Figure 4.12: Stability versus frequency of the sine wave

is stable if max $|\lambda_i|$ is calculated to be smaller than one by applying a slight perturbation at the moment after the leg collision.

With entrainment control, it is particularly crucial to observe the shift in the stability of the robot system as the input frequency changes. Figure 4.12 shows the relationship between the input frequency and walking stability in the entrainment range (yellow region). In contrast, most gaits outside the entrainment region are chaotic gaits, so it is not possible to analyze them using the Poincaré map. From left to right, the entrainment ranges from 1:1 to n:1. The robot is constantly stable (max$|\lambda_\mathrm{i}|$ is less than 1) throughout the 1:1 entrainment region, and the value of max$|\lambda_\mathrm{i}|$ starts to decrease as the input frequency increases, reaching a minimum at 1.32 [Hz] and then gradually increasing again. It is extremely remarkable that in each entrainment range, the most stable place is precisely the input frequency applied when the robot has the largest stride and the fastest speed in that range. It can be assumed that in each isometric entrainment range, the robot has an optimal control parameter under which all performances are excellent. In contrast, in the entrainment range beyond 1:1, not all gaits are stable, especially when the multiplier n is increasing, and virtually more than half of the input frequencies are unstable.

Therefore, it can be assumed that for better control of the robot, it is better to use 1:1 or 2:1 control parameters.

4.3.5 Random uphill and downhill stability tests

From the point of view of practicality in realistic environments, the ability of a robot to penetrate mildly uneven terrain is an indispensable capability. Here, the author verifies whether current methods of entrainment control can help the robot to successfully walk by randomly generating the angle of the up and down slope every few steps.

Figure 4.13 shows the results of the robot successfully passing a randomly generated uneven surface in 50 seconds. Figure 4.13(a) represents the random shift in the tilt angle of the ground for every 5 steps taken by the robot, and each shift is set to within 0.3 [rad]. 15 changes are made in 50 seconds, and it should be noted that the simulation sets the robot's leg shift condition to be triggered when z_c is 0, thus the simulated surface is a potholed one. Figure 4.13(b) is the input waveform applied by the robot with a torque magnitude of 5 [N·m] and a frequency of 1.5 [Hz]. Figure 4.13(c) is the bed reaction force in the vertical direction of the stance leg, which varies with the terrain on the way. The total mechanical energy of the robot changes as shown in Fig. 4.13(d), and the energy consumed in each collision is shown in Fig. 4.13(e); it can be found that the bipedal robot walked 75 steps in 50 seconds at an input frequency of 1.5 [Hz], which can illustrate the robustness of the entrainment effect.

If walking on horizontal ground, the robot's gait can converge to a periodic-1 limit-cycle gait. However, the robot continuously changes its state inside the basin of attraction due to the ground angle shift every 5 steps. Fig. 4.14 shows the phase plane plot for all 50 seconds, and it can be observed that the robot forms a sizable basin of attraction during walking without changing the control parameters under the entrainment control approach. Within this basin of attraction, the robot can successfully continuously walk under the changing terrain.

4.4 Summary and Discussions

In this chapter, the author assumes that the bipedal robot has only one input at the hip joint, and instead of using the usual feedback control, a default waveform torque is applied as input. The author shows through numerical simulations that it is possible to generate a gait on a flat

surface. The adjustable range of frequencies and amplitudes for a given sine wave has also been explored under the assumption that gait generation is possible. Moreover, the effect of different frequencies, amplitudes, and excitation waves on gait performance is observed. With entrainment control, the robot can be adequately controlled to achieve the desired gait without posing feedback in an efficient and easy-to-implement situation.

In the next chapter, the author plans to verify on a real machine whether the proposed method can bring the gait period closer to the input frequency through the entrainment effect, and choose an optimal detection method to measure the gait data. Parameters for matching the numerical simulation will be set and observed on a real machine to confirm the difference between the real environment and the simulation. In addition, optimization is required for additional improvements in gait stability.

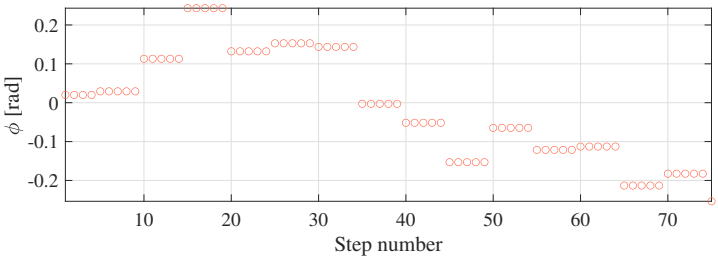

(a) Random slop angle ϕ

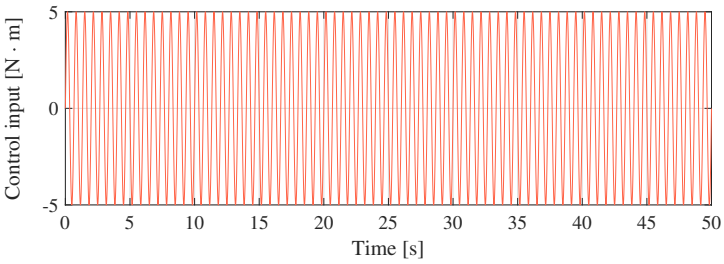

(b) Control input

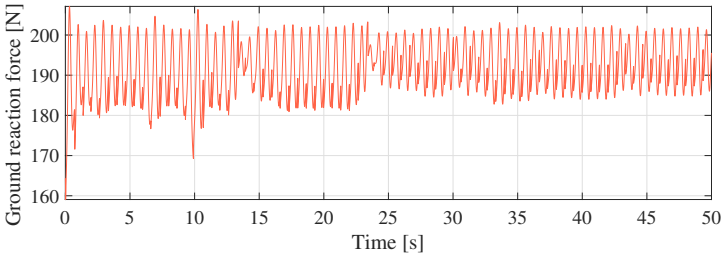

(c) Vertical ground reaction force

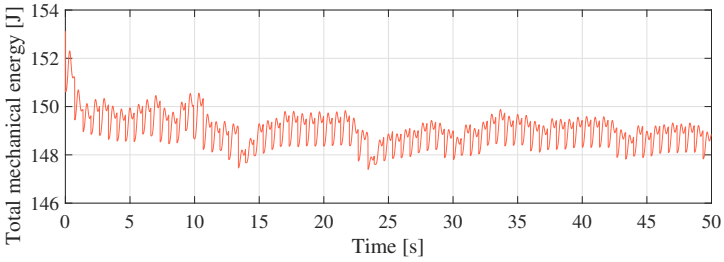

(d) Total mechanical energy

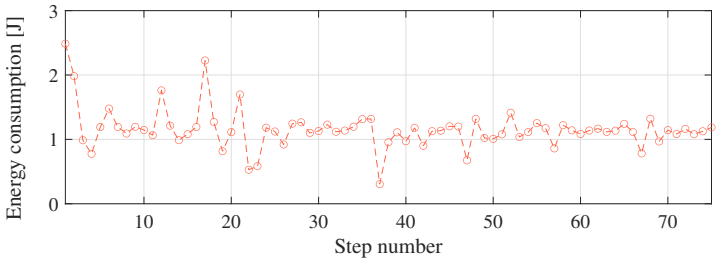

(e) Energy loss

Figure 4.13: Simulation results of biped robot walking on the random uphill and downhill based on entrainment effect

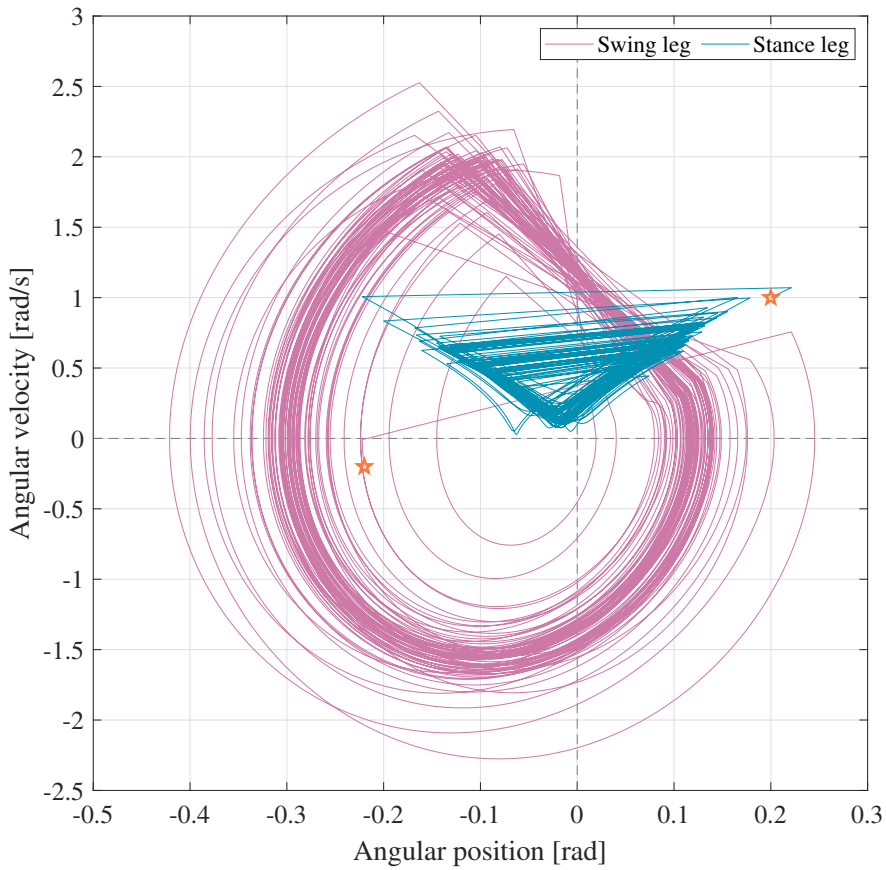

Figure 4.14: Phase portrait of generated motion by changing ϕ randomly where A_m=5 [N·m] and f_c=1.5 [Hz]

Chapter 5

Experimental Verification of Entrainment Effect for a Bipedal Robot with Half Semicircular Feet

5.1 Overview

To validate the results of the numerical analysis presented thus far. Therefore, it is necessary to develop an experimental machine that implements the ensemble specification. In this chapter, an underactuated bipedal robot is fabricated and an entrainment-based control method is sincerely introduced [58]: a unique input is used to simulate a predetermined waveform without any feedback control. Specifically, the bipedal walking robot is approximated as an oscillator that can be entrained by a periodic input from the input frequency. Since the model in the simulation does not have knees, the shape of the feet is modified to avoid foot scuffing during the swinging of the legs in a realistic environment. The designed individual experimental robot is shown in Fig. 5.1.

5.2 Dynamics for Real Machine

5.2.1 Model of robot

Compared with the previous simulation model, here only the shape of the foot is changed from a complete semicircular foot to half, which causes the velocity constraint and collision

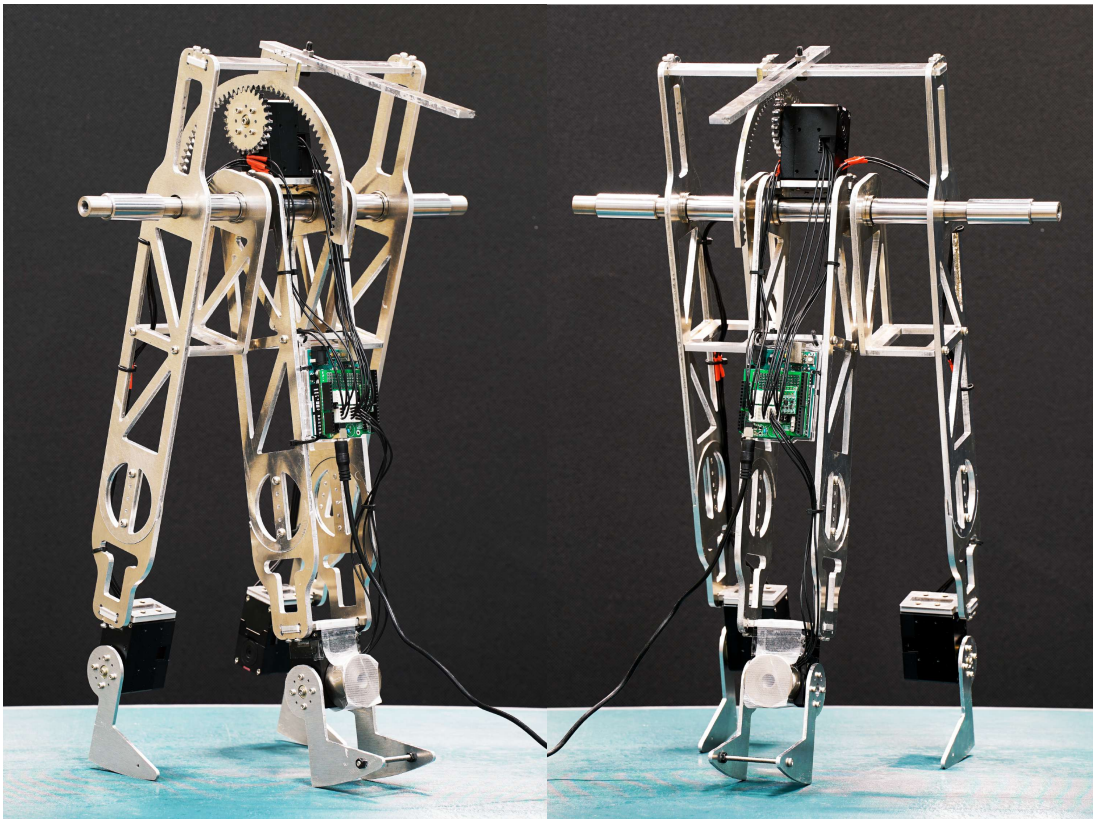

Figure 5.1: Model of an underactuated biped robot with half-semicircular feet

detection to modify, so it is necessary to re-model and simulate first. Fig. 5.2 illustrates the mathematical model of the underactuated biped walking robot.

5.2.2 Equation of motion

Let $\boldsymbol{q} = \begin{bmatrix} x & z & \theta_1 & \theta_2 \end{bmatrix}^{\mathrm{T}}$ be the generalized coordinate vector. The robot equation of motion then becomes

$$\boldsymbol{M}\ddot{\boldsymbol{q}} + \boldsymbol{h} = \boldsymbol{J}^{\mathrm{T}}\boldsymbol{\lambda} + \boldsymbol{S}u, \tag{5.1}$$

where $\boldsymbol{M}$ represents the inertia matrix, $\boldsymbol{h}$ is the combination of the central force, Coriolis force, and gravity terms. On the right side, $\boldsymbol{J}^{\mathrm{T}}\boldsymbol{\lambda}$ is the holonomic constraint. In addition, by letting u be the only control input applied to the hip joint, the driving vector becomes

$$\boldsymbol{S} = \begin{bmatrix} 0 & 0 & 1 & -1 \end{bmatrix}^{\mathrm{T}}. \tag{5.2}$$

The author assumes that the robot is in non-sliding contact with the ground. Due to the semi-circular feet, the velocity constraint at the contact point between the stance leg and the ground

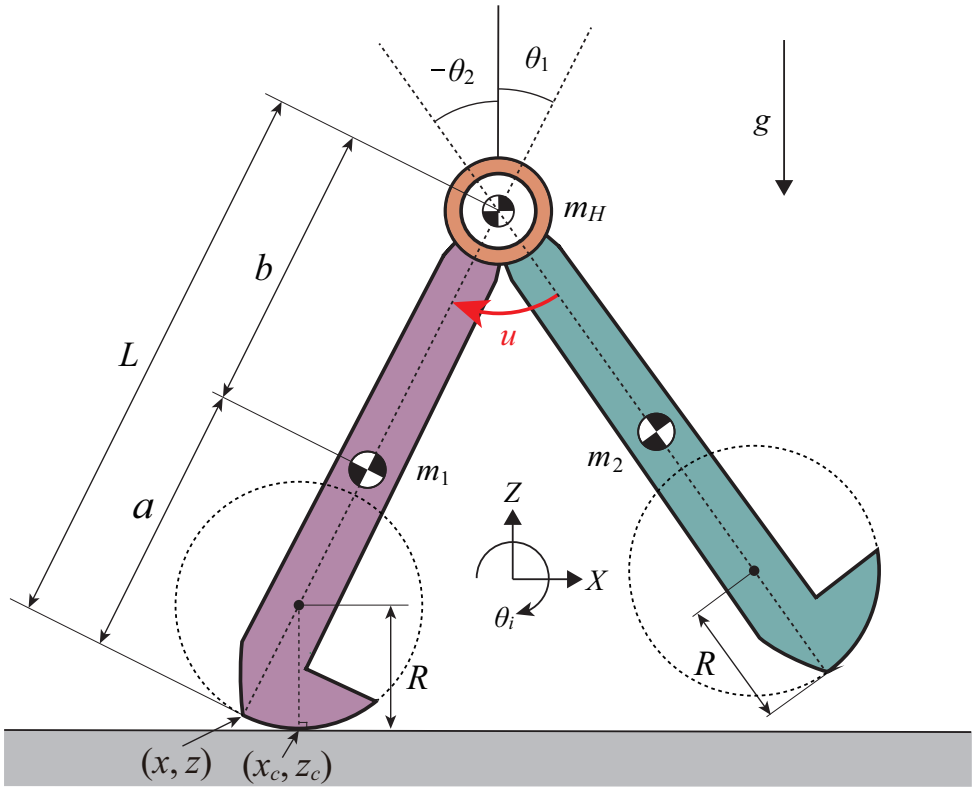

Figure 5.2: Mathematical model of an underactuated biped robot with half-semicircular feet

during the walking period should satisfy the following conditions: when the angle of stance leg θ_1 is larger than zero,

$$\dot{x}_c = R\dot{\theta}_1, \quad \dot{z}_c = 0. \tag{5.3}$$

Otherwise,

$$\dot{x_c} = \dot{x} = 0, \quad \dot{z_c} = \dot{z} = 0. \tag{5.4}$$

Therefore, Jacobians $\boldsymbol{J}$ are determined as:

$$\boldsymbol{J}_1 = \begin{bmatrix} 1 & 0 & R\cos\theta_1 - R & 0 \\ 0 & 1 & -R\sin\theta_1 & 0 \end{bmatrix}, \quad \text{or} \quad \boldsymbol{J}_2 = \begin{bmatrix} 1 & 0 & 0 & 0 \\ 0 & 1 & 0 & 0 \end{bmatrix}, \tag{5.5}$$

where the conditions of $\theta_1 > 0$ or $\theta_1 \leq 0$, respectively. Refer to the previous Chap. 2 for other details.

5.2.3 Equation of collision

According to the inelastic collision model, the swing leg neither slides nor bounces when it touches the ground. Therefore, the swing and stand legs are immediately exchanged at the moment of ground-contacting. Since the two legs are identical, the zero crossing of the following

function becomes:

$$f(\theta_1, \theta_2) := \bar{z}_c, \tag{5.6}$$

The transition that occurs before and after the collision is shown below:

$$\boldsymbol{M}\dot{\boldsymbol{q}}^{+} = \boldsymbol{M}\dot{\boldsymbol{q}}^{-} + \boldsymbol{J}_I^{\mathrm{T}}\boldsymbol{\lambda}_I, \tag{5.7}$$

where the superscripts "+" and "−" represent the instant immediately after and before the collision, respectively, and J_I and λ_I represent the constraint matrix and constraint forces vector at the landing instant. Due to the robot having one pair of half-semicircular feet, when each time the leg is changed, the foot is grounded at the center point $(\bar{x}, \bar{z})$. The velocity constraint condition for the landing point of the forefoot is determined as

$$\dot{\bar{x}}^{+} = 0, \quad \dot{\bar{z}}^{+} = 0. \tag{5.8}$$

The constraint equation at landing instant is therefore summarized as:

$$\boldsymbol{J}_I\dot{\boldsymbol{q}}^{+} = \begin{bmatrix} 1 & 0 & L\cos\theta_1^{-} & -L\cos\theta_2^{-} \\ 0 & 1 & -L\sin\theta_1^{-} & L\sin\theta_2^{-} \end{bmatrix} \dot{\boldsymbol{q}}^{+} = \boldsymbol{0}_{2\times 1}. \tag{5.9}$$

That is when the heel of the swinging leg touches the ground at the moment when the leg exchange occurs.

5.2.4 Entrainment control method

Since the control method does not change, see the previous chapter for details.

5.3 Numerical Simulation Results

Due to the changing shape of the foot, the model corresponds to a combination of a pointed foot and a semicircular foot, just in time to verify the generalizability of the proposed control method with the aid of the current model.

5.3.1 Typical gait generation

The physical and control parameters as listed in Table 5.1 to conduct the following process. Set the initial conditions as

$$\begin{aligned} \boldsymbol{q}(0) &= \begin{bmatrix} 0 & 0 & -0.209 & 0.209 \end{bmatrix}^{\mathrm{T}}, \\ \dot{\boldsymbol{q}}(0) &= \begin{bmatrix} 0 & 0 & 1 & -0.2 \end{bmatrix}^{\mathrm{T}}. \end{aligned} \tag{5.10}$$

Therefore, walking starts from the state immediately after the leg collides with sufficient kinetic energy.

Fig. 5.3 are the results of the simulation in which the input torque is set to a generally sinusoidal waveform. Figure 5.3(a) is the center point position (x, z) of the semicircular foot of the stance leg. We can see that the first few steps are slightly longer than the last, but they gradually converge over the course of a few seconds, moving forward at a relatively constant pace. In Fig. 5.3(b) and Fig. 5.3(c), the positions of the biped angles and the time variation of the angular velocity are shown. Since the input torque is only 0.5 [N·m], after a period of time, we can see that the swing of both feet is very small. Figure 5.3(d) shows the time variation of the vertical ground reaction force, which varies violently for the first step. This value is then approximately equal to the mass of the walker. In addition, we can notice that the values always remain positive. It can be assumed that the foot is not off the ground.

To verify that the robot motion can converge, the author shows in Fig. 5.4 the phase plane portrait of the gait that has passed (intercepting the data from the beginning of the walk to the 300 [s]). We can find that the robot shows a tendency to converge even after changing the foot reach shape.

Table 5.1: Physical and Control Parameters

Symbol	Value	Unit
m_H	10	kg
$m_1 = m_2$	5	kg
$a = b$	0.5	m
L	1	m

Symbol	Value	Unit
R	0.1	m
g	9.81	m/s^2
A_m	0.5	N·m
f_c	1.5	Hz

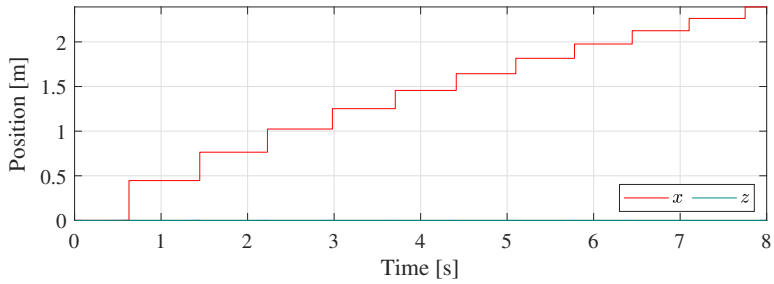

(a) Position

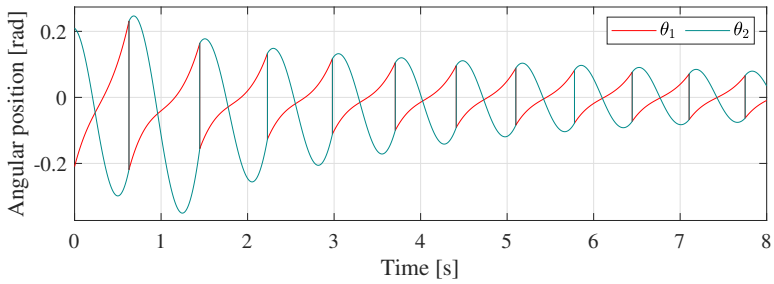

(b) Angular position

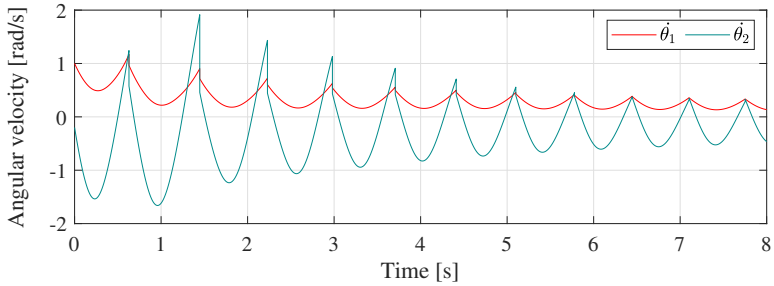

(c) Angular velocity

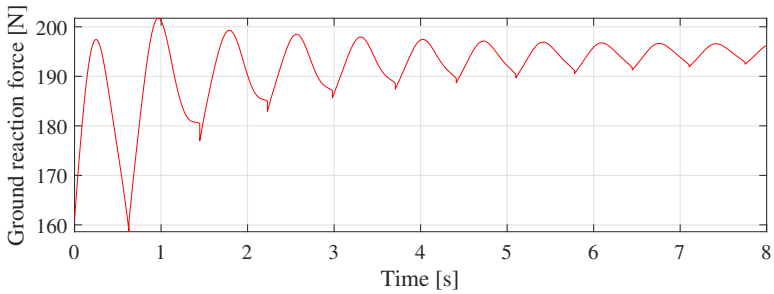

(d) Vertical ground reaction force

Figure 5.3: Simulation results of motion generation with half-semicircular feet

Figure 5.5 shows the shift of the robot energy with time. Figure 5.5(a) indicates the total mechanical energy shift, and at the moment after the foot collision, we can see the kinetic

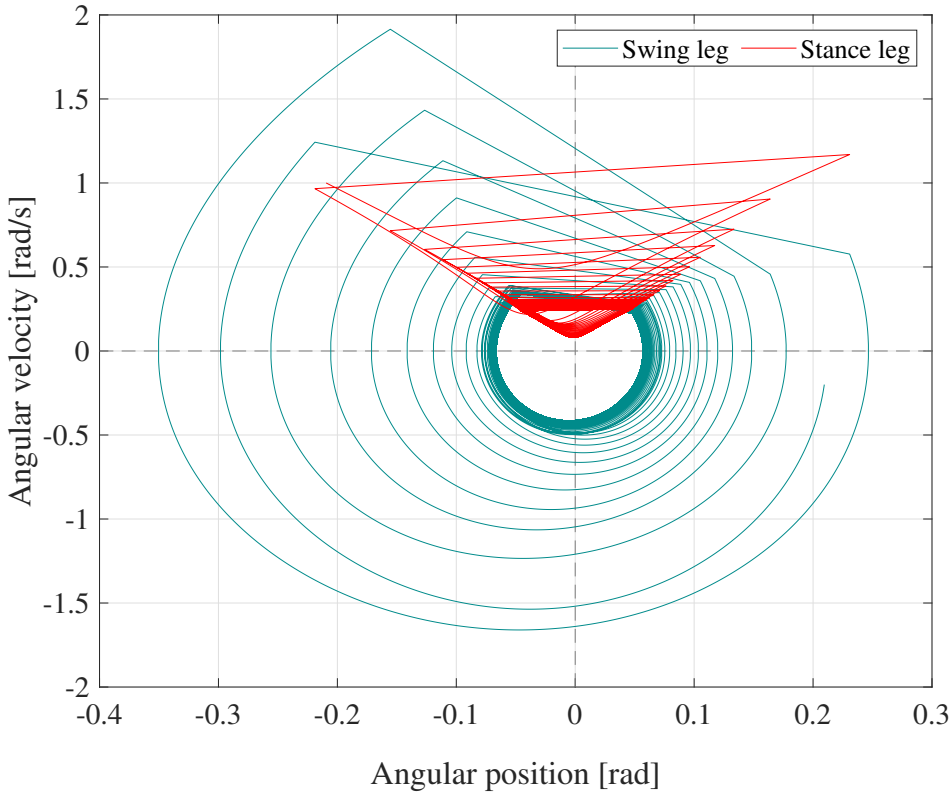

Figure 5.4: Phase portrait of limit-cycle walking gait

energy consumption as shown in Fig. 5.5(b). Compared with the complete semicircular foot in the previous chapter 4, this model has a higher energy loss than before because it is similar to the pointed foot at the time of the collision. This also confirms previous results that rounded corners are more conducive to producing efficient gaits [59].

5.3.2 Parametric study

The control input frequency f_c [Hz] is also simulated in the following procedure in order to investigate the entrainment effect on gait performance. In the following Algorithm 4, each time, the 20 steps that could successfully generate a gait after 100 seconds were taken for numerical analysis.

The simulation results in Fig. 5.6 show the walking frequency, walking speed, and specific resistance for this robot with respect to f_c. Gait generation is possible for the sinusoidal frequency f_c from 0.98[Hz]. It is obvious that not all subsequent frequencies can generate a stable gait, there are many breakpoints within these frequencies. Figure 5.6(a) shows the effect of

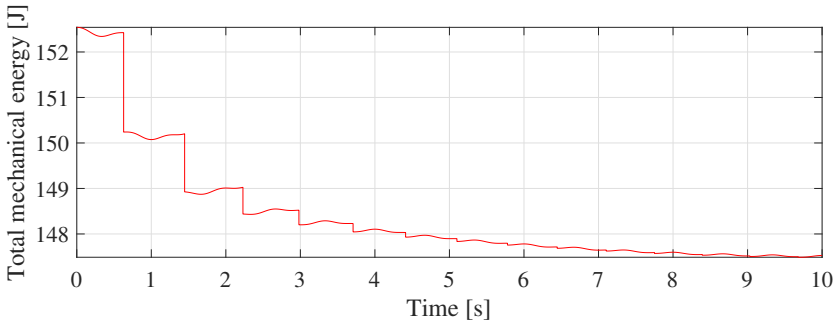

(a) Total mechanical energy

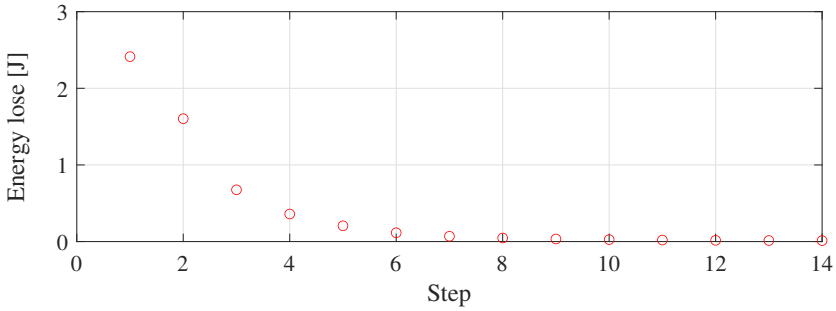

(b) Energy loss

Figure 5.5: Simulation results of energy change with feed-forward control

walking frequency and sine wave frequency. As the area marked in light yellow in Fig. 5.6, due to the effects of entrainment, within the range from 1.16 to 1.62 [Hz], the walking frequency is always in line with the frequency of the input sine wave. It is worth noting that entrainment effects occur not only at 1:1 input and walk frequencies, but also at n:1. As shown in Fig. 5.6(b), we can see the effect of input frequency on walking speed. One can observe that there exists local-maxima walking speed within each of the entrainment regions (light yellow), and reaches a global maximum value of 0.23 [m/s] at the input frequency of 1.34 [Hz]. From Fig. 5.6(c), we can see that the walking efficiency gradually is not strongly affected by the velocity since SR is small in the whole range.

Overall numerical simulation results show that an underactuated bipedal robot, which cannot stand in place, can achieve a stable walking state with feed-forward control combined with its own gravity and inertial effects. The parameters of the feed-forward control can be finitely tuned to achieve controlled walking performance. These results provide the feasibility of the next experiment.

Algorithm 4 Calculate T and SL

Require: The step period T and step length SL of the Robot when they get stabilized

Input: Initial state $\boldsymbol{q}(0)$, $\dot{\boldsymbol{q}}(0)$, A_m and f_c

Output: Step period T and step length SL of the next 20 steps after 100 seconds

1: **Initialization** $T[l][20] = 0$, $SL[l][20] = 0$, $f_c = 0.1$

2: **for** $i = 1; i <= l : i++$ **do**

3: Run simulation for 100 seconds.

4: Save the next 20 step periods to t and the next 20 step length to L

5: $T[i] = t$

6: $SL[i] = L$

7: $f_c = f_c + 0.02$

8: **end**

9: **Return** T and SL

5.4 Experimental Verification

5.4.1 Hardware and software

The designed experimental system is based on a compass-type biped, as shown in Fig. 5.7. Its total height is about 0.55 [m] (0.44 [m] for the legs) and its total mass, including the controller system, is 3.5 kg. Unlike most conventional real-world machines that use weights concentrated at the waist [60], this allows the overall weight of the robot to be distributed relatively evenly. All body frames are made from metal materials such as aluminum, resulting in superior machining accuracy and durability. The dark blue and red sections of the legs allow for easy adjustment of leg length.

Because all sensing and computation are performed on board, the robot does not require a boom or tether and only requires a 12V power adapter to power it [61]. The outer pair of legs move together as one leg, as does the inner leg. Each leg has one foot and one ankle joint (three in total). The inner legs move together through a servo motor connection; the outer leg moves together through two servo motors (set to follow mode with each other). The bipedal robot has three DOFs (hip and ankle pairs), and the three motors on the ankle joints are not directly involved in the forward motion of the robot, but merely to avoid the feet scuffing during walking. The motor acting on the hip joint is the most essential part, allowing the use of a

planetary gear mechanism to move the legs against each other, thus mimicking the control method in the Founder.

All servo motors are powered by servo motors (Robotis Dynamixel) with a gear ratio of 272.5:1. With the exception of the hip joint, which requires a slightly higher torque to drive the leg swing, the ankle joint requires only a slight torque. Regarding the mode of operation, the hip uses a current control mode to mimic the torque mode, while the ankle uses a position control mode.

To avoid foot scuffing, a deterministic program was written to enable the servo motor on each foot to turn the half-semicircular foot according to the angle of the servo motor at the hip joint, thus achieving the act of lifting the foot during walking. The main control loop runs on a microcontroller (Arduino Uno), using a pre-written program, and burned in, thus simulating full feed-forward control of the simulation. The controller for the servo motor is mounted on the microcontroller and the protocol type is RS485 (synchronous serial communication, 8-bit, 1-stop, no parity). The servo motor itself is equipped with various types of sensors, including a non-contact absolute encoder (12-bit), voltage sensors, and current sensors. It is able to sample data from the inner ankle motor, the outer ankle motor, and the hip motor at a rate of 20 per second, making it easy to calculate angular position, angular velocity, and power. Although the motor does not have torque sensors, the torque calculation formula allows us to calculate torque based on power as well as speed.

5.4.2 Experimental result

When all the preparations are completed, the validation is performed on the experimental robot based on the entrainment control method. Initially, the author found that the robot could not reliably walk in this open-loop mode and always fell after a few segments. By examining the data displayed on the sensor's output, it is found that the oscillations of the outer leg are smaller than those of the inner leg. Further physical measurements confirmed that this is because the outer leg is heavier and has a higher moment of inertia than the inner leg. To bring the experimental machine as close as possible to the simulation model, the asymmetry of the two-body oscillations was reduced by adjusting the counterweights. In Fig. 5.8, we can see that the bias in the hip angle can be reduced very effectively by increasing the counterweight. This is very important because once the center of gravity and the weight of the legs are not close

enough, the bipedal robot itself has a tiny basin of attraction and is even less likely to be able to walk stably. Another point to note is that the sine wave frequency is set to 1/2 of that of the simulated case due to the planetary gearing between the legs; for example, if the author sets the input frequency to 0.9 [Hz], it corresponds to 1.8 [Hz] in the simulation. Eventually, by tuning the input parameters, the robot is able to walk on horizontal ground.

First, the tracking performance of the motor to the input can be observed in Fig. 5.9. The author must recognize the difference between conditions in the real environment and the simulation; The observations here were made with the robot walking, and although there is a partial perturbation in the actual current, it is within acceptable limits. The cause of this perturbation is the small jitter in the signal from the servo motor whenever the leg collides with the ground during each input cycle. By using a current of only 0.48 [A] for the hip joint, the input frequency was 1.8 [Hz]. By looking at the video after the experiment, it can be seen that the robot took 24 steps in about 13.5 seconds, it illustrates the effective entrainment effect that can be produced at this input frequency, and the robot walks at a walking frequency equal to the input frequency, creating a limit cycle gait.

Unlike simulations where the phase planes of the supporting and swinging legs are described separately, in the experiments, the author uses the angles and angular velocities between the legs for approximate analysis since the absolute angles and angular velocities of each leg cannot be measured accurately in real time. Fig. 5.10 shows the phase plane of the generated walking gait. After the initial 6 steps (blue), the robot can converge to a relatively stable limit cycle (yellow).

Finally, in Fig. 5.11, it shows the variation of the foot-lifting action over two walking cycles, in order, with the inner foot touching the ground, the outer foot lifting, followed by the outer foot touching the ground, the inner foot lifting, and finally returning to the inner foot touching the ground.

5.4.3 More details

The shape of the foot has a great influence on the gait [62]. This robot is designed to be between a pointed foot and a semicircular foot because the pointed foot consumes part of the kinetic energy after a collision to reduce the instantaneous tendency to fall forward and stabilize the center of gravity, followed by the semicircular foot to smooth the gait, and here the radius of the semicircular foot is adjusted to achieve a smoother gait.

The reason why the author does not use SEA (Series Elastic Actuator) [63, 64], which is an elastic actuator with improved impact resistance, commonly used in legged robots, but since the control method in this study is to apply the output torque to an actuator mounted on the hip joint to execute the default torque waveform, this requires a high-frequency response servo motor combined with torque control to achieve this. The proprioceptive actuator [65] meets our requirements with elevated frequency response and more accurate torque feedback and will be tried in the future if available.

5.5 Summary and Discussions

In this chapter, the simulations are re-validated based on the model applied to the experiments, and the results show that bipedal walking robots are still feasible using the previously proposed approach. A tunable range of control input frequencies within the entrainment range has also been explored for this purpose, with observed performance in gait. In addition, to verify the feasibility of the proposed control method for the simulated model, a bipedal walking robot is designed and constructed to be as consistent as possible with the simulation, and the corresponding experiments are conducted. The experimental results show that the control method can also exhibit the same gait trend (convergence to limit cycle walking) in a real robot.

With these verifications, it is safe to believe that entrainment effects occur in this fully feedforward control system. In the following chapter, it is necessary to optimize based on this control approach to improve the overall performance.

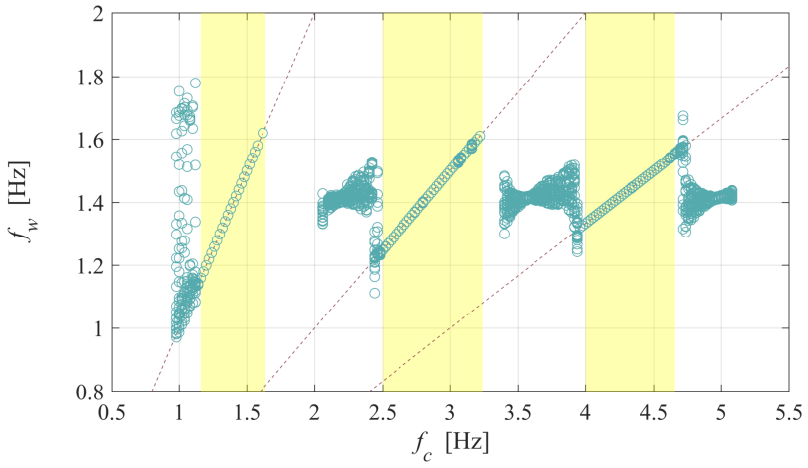

(a) Walking frequency

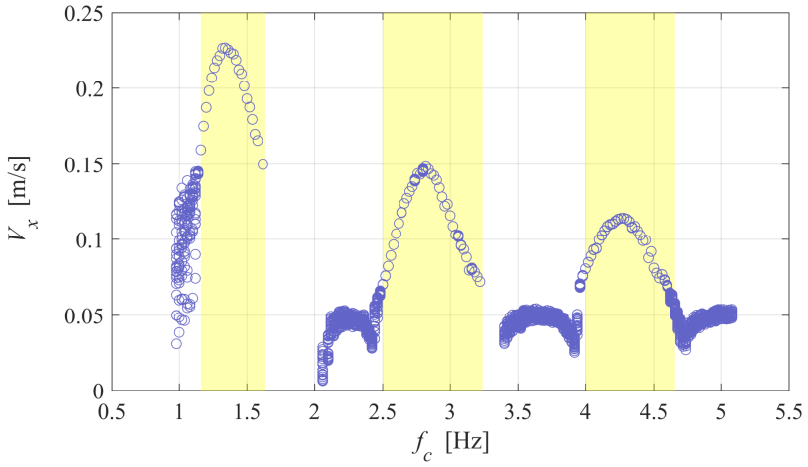

(b) Walking speed

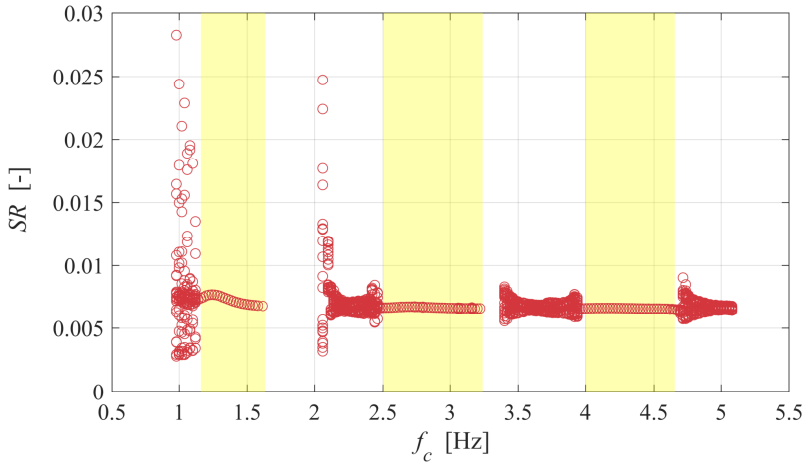

(c) Specific resistance

Figure 5.6: Gait performance versus frequency of the sine wave

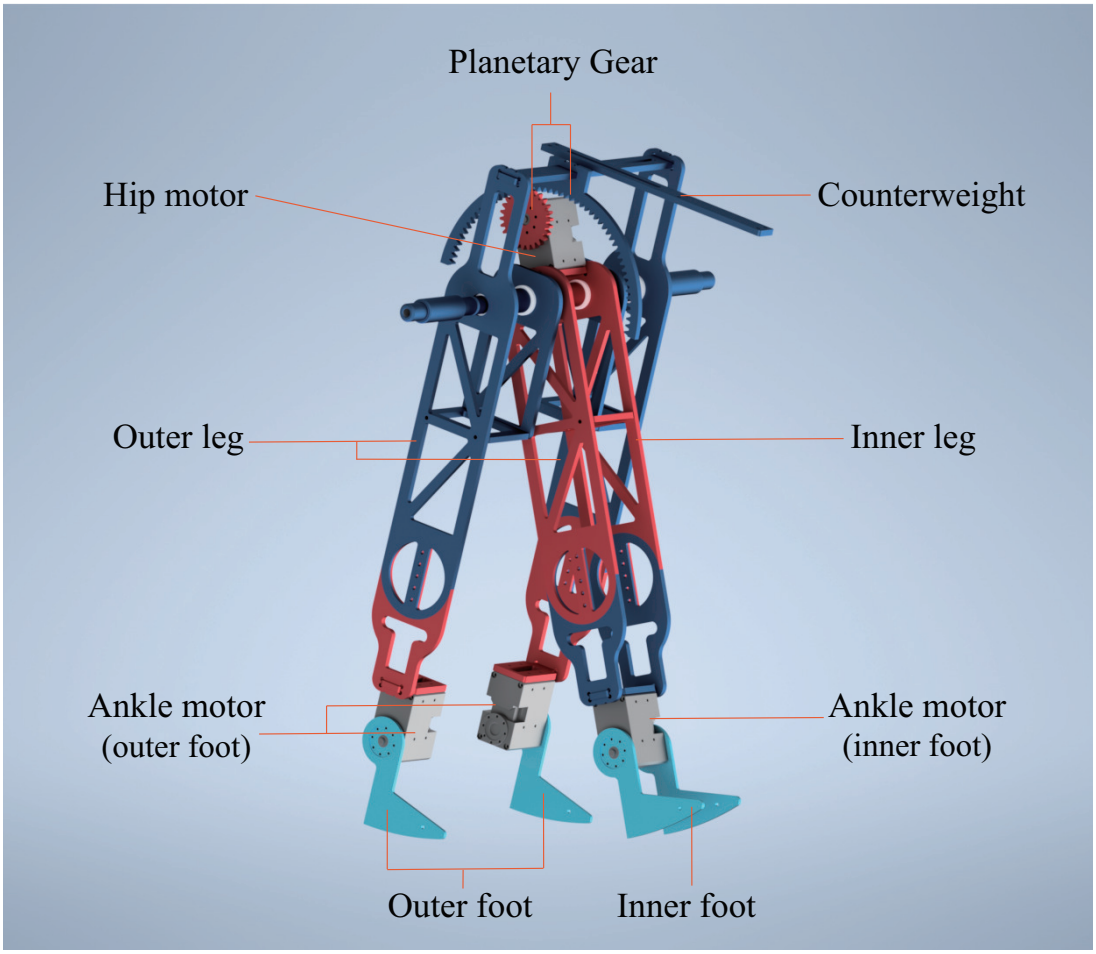

Figure 5.7: 3D model of an underactuated biped robot with half-semicircular feet

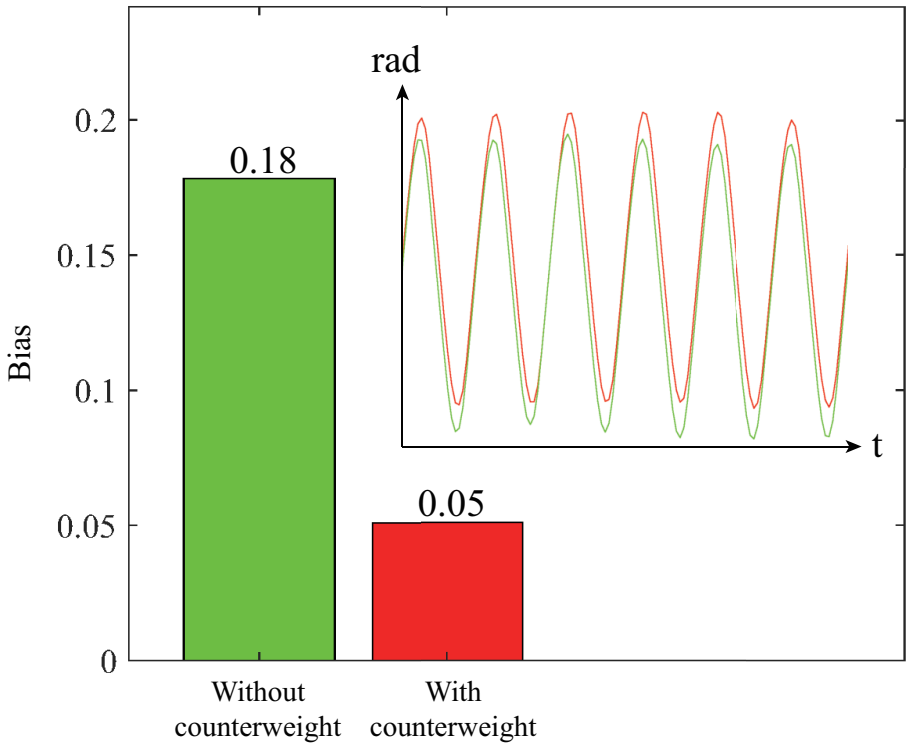

Figure 5.8: Symmetry optimization of both legs

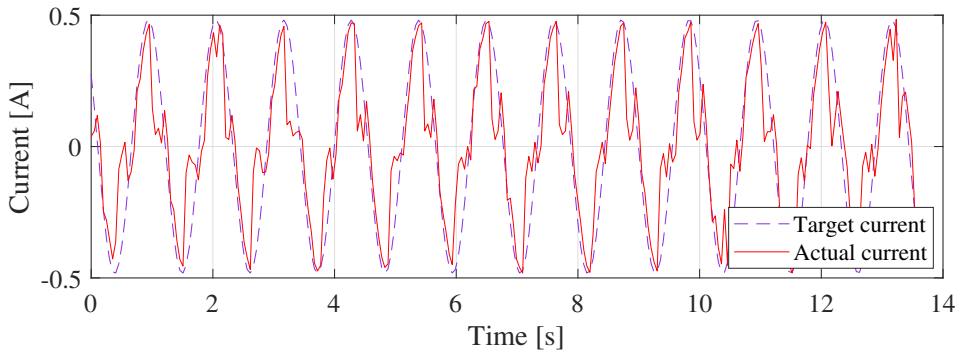

Figure 5.9: Current (proportional to torque) change in experiment

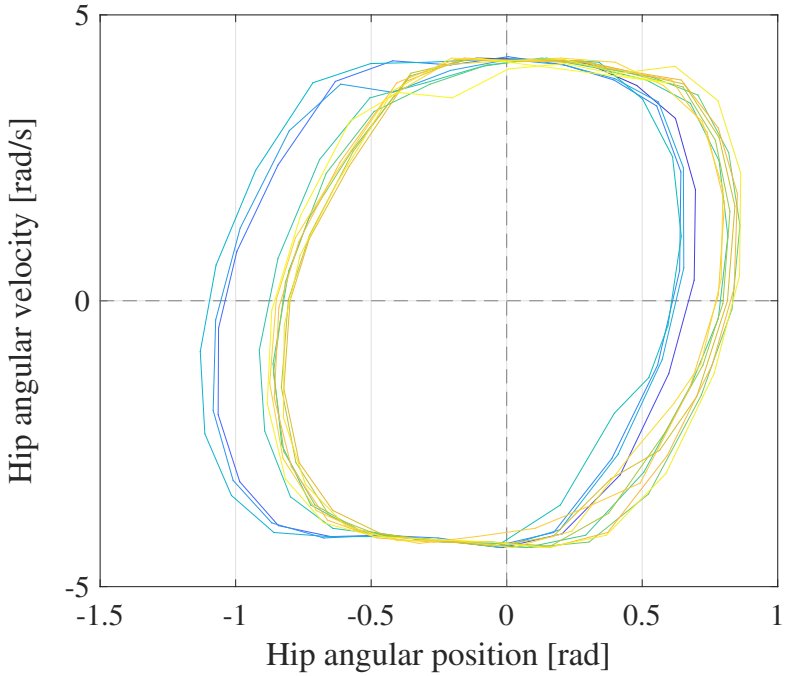

Figure 5.10: Experimental result about phase plane defined by hip angle and angular velocity

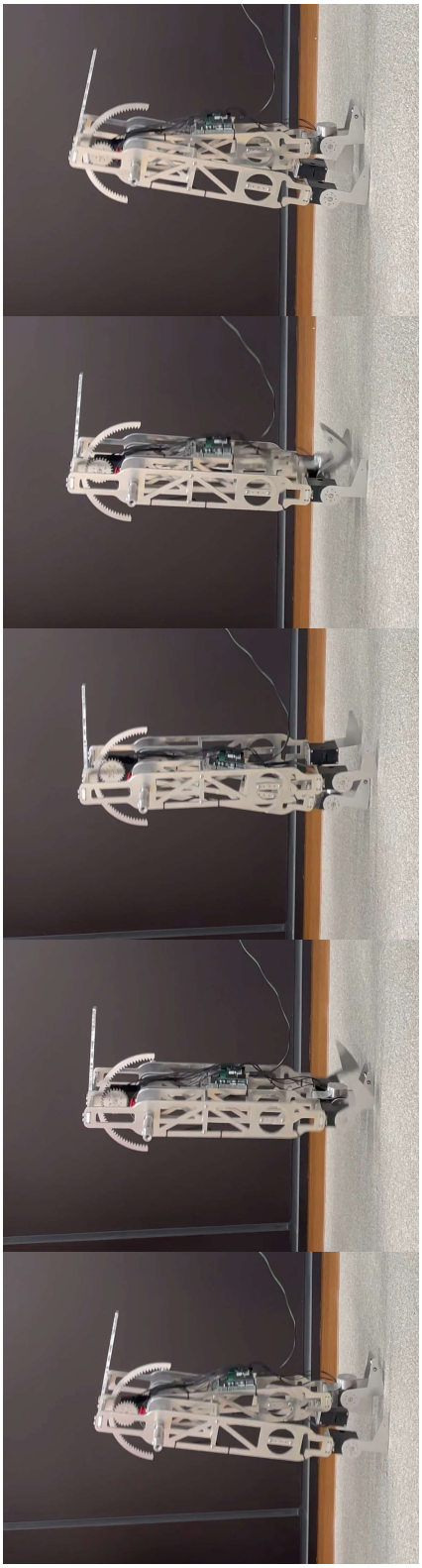

Figure 5.11: Diagram of the operation of each servo motor under walking

Chapter 6

Optimal Entrainment Input and Parameters of Robot by Bayesian Optimization

6.1 Overview

In the previous chapters, the effectiveness of the entrainment-based control has been validated by simulations and experiments. However, the optimization of the parameters using enumerative methods is extremely difficult due to the large number of physical parameters of the robot coupled with a large number of input parameters. It requires efficient alternatives to perform a deeper search for optimal parameters. The idea of Bayesian optimization is to first generate an initial set of candidate solutions, then find the next most likely extreme value point based on these points, add that point to the set, and repeat this step until the iteration terminates. Finally, the point with the largest value of the function from these points is found as the solution to the problem. Since the solution process uses information from previously searched points, it is more efficient than grid search and random search. This chapter explores the optimal performance of the proposed control method by using Bayesian optimization of the system's control parameters as well as physical parameters.

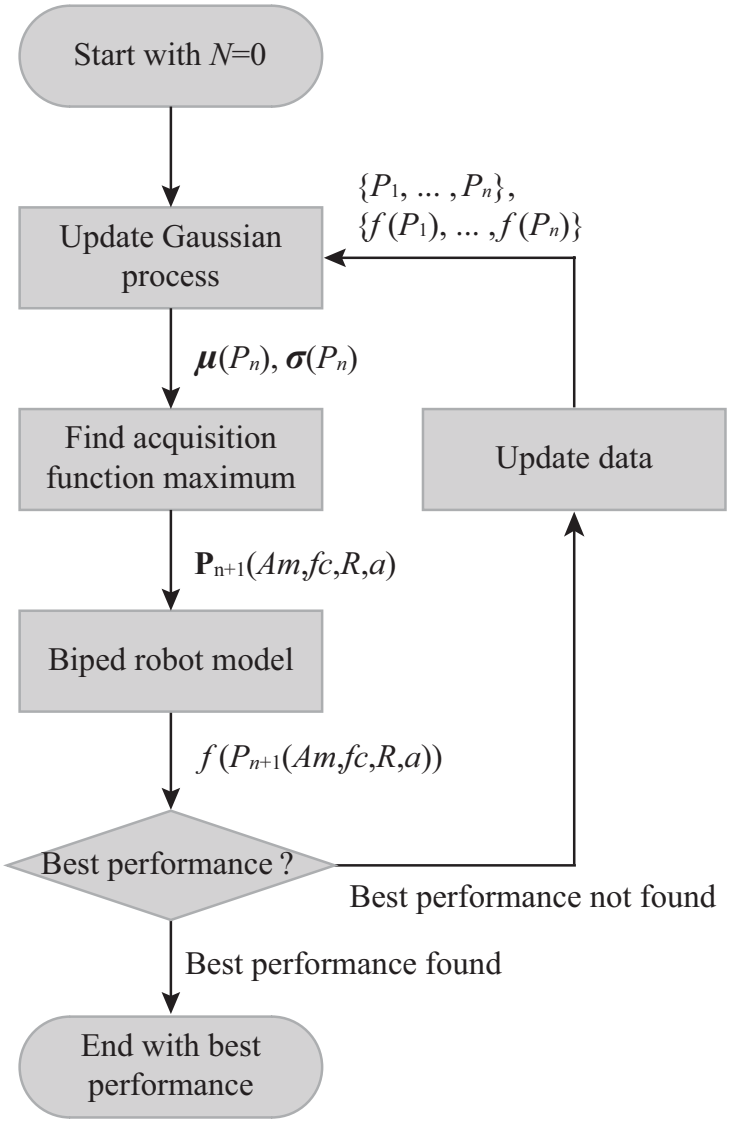

Figure 6.1: A Bayesian optimization process for bipedal robots

6.2 Parameter Setting and Optimization Process

6.2.1 Parameter setting

The object of Bayesian optimization is set to be the robot model of Chap. 4. When applying Bayesian optimization, it is necessary to give prior data in order to reduce the convergence time of the results and to bring the objective function closer to the true one. For the a priori given data set, the system parameters, and initial values are referred to in the previous Chap. 4.

6.2.2 Evaluation functions and constraints

Figure 6.1 illustrates the Bayesian optimization process for a bipedal robot. where the specific meaning is as follows.

- $\boldsymbol{P}$ denotes the set of parameters involved in the optimization, containing the A_m and f_c of the control inputs, the radius R of the semicircular foot of the robot, and the center-of-mass position a of the leg
- N denotes the number of iterations
- f denotes the optimization function
- μ and σ represent the expectation and standard deviation

This chapter addresses the optimization of the robot's movement speed and energy efficiency. The author refers the reader to Eq. 4.15 and 4.13 of Chap. 4 for the calculation of the walking velocity and energy efficiency of the motion. The evaluation functions regarding the optimization of both are shown below.

$$\hat{\boldsymbol{P}} = \arg\max_{\boldsymbol{P}^* \in \boldsymbol{P}} V_x(\boldsymbol{P}), \tag{6.1}$$

$$\hat{\boldsymbol{P}} = \arg\max_{\boldsymbol{P}^* \in \boldsymbol{P}} \frac{1}{SR}(\boldsymbol{P}). \tag{6.2}$$

$\hat{\boldsymbol{P}}$ denotes the set of parameters that have been optimized. Since the optimization is performed using the method of finding the maximum value, and the lower value of SR indicates more efficient robot motion, the inverse form is used. The following conditions must be satisfied in the optimization process.

- Each set of parameters was simulated for more than 100 seconds, and 20 steps after stabilization were taken for the calculation
- If the ground reaction force $\lambda < 0$, the data is directly judged invalid
- Only take the result that the input frequency f_c and walking frequency f_w are equal

It is also essential to note here that a certain minimum speed limit must be given when exploring the optimal energy efficiency, otherwise, in most cases, the system defaults to the minimum value of A_m in the custom input parameter range, and all the best energy efficiencies in the next result analysis are optimized based on a walking speed that minimally satisfies 0.5 [m/s].

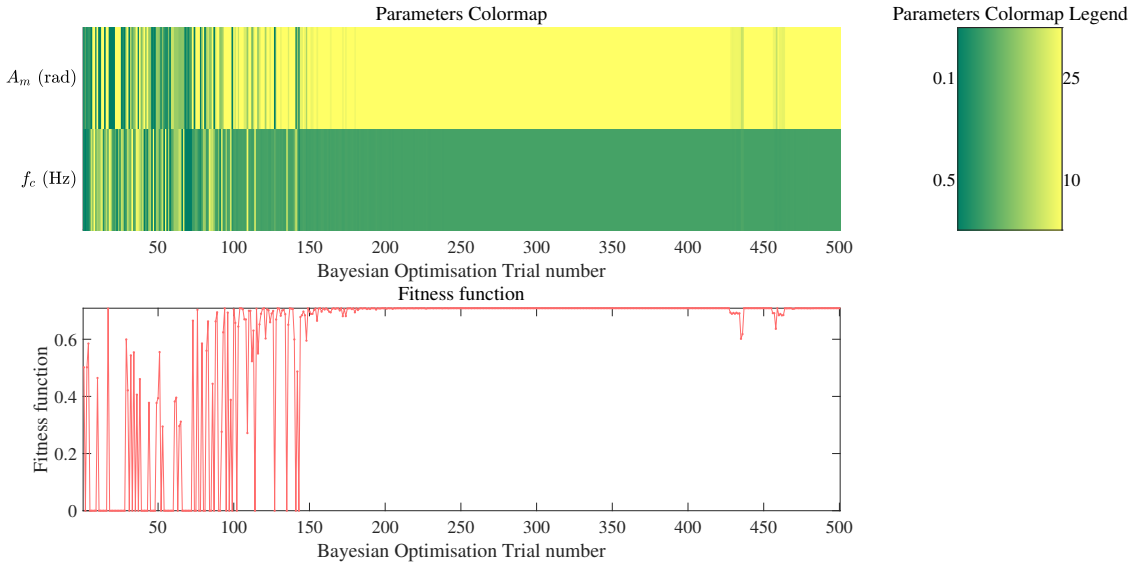

(a) Optimal walking speed

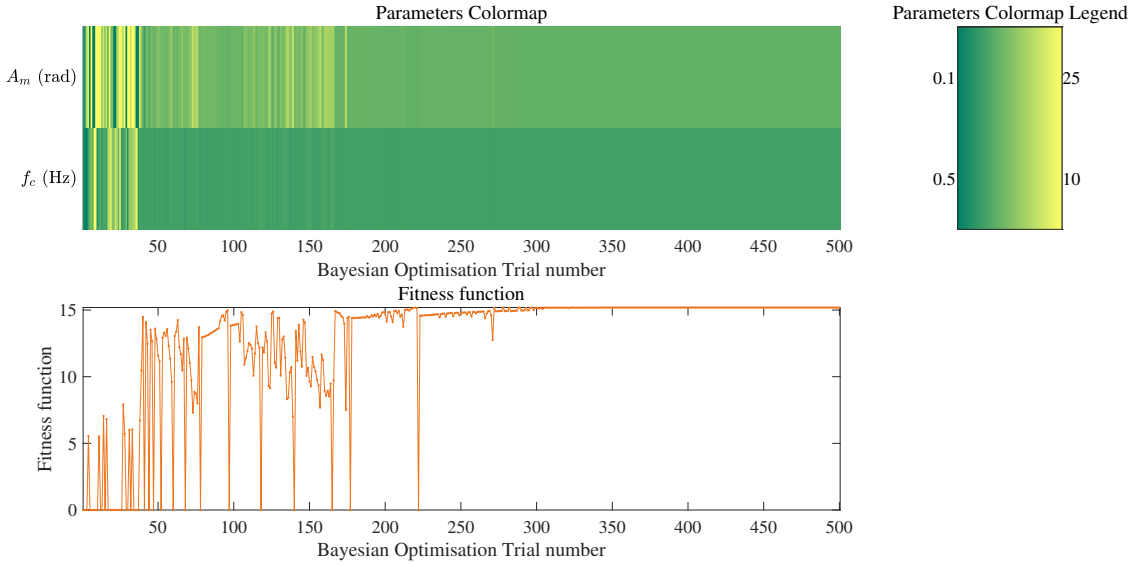

(b) Optimal energy efficiency (limit minimum speed)

Figure 6.2: Optimal gait performance versus the control input

6.3 Bayesian Optimization Results

Figure 6.2 shows the results of the Bayesian optimization for the control parameters. The upper parameters colormap shows the specific changes in the optimized parameters during the optimization process, with the right-hand side corresponding to the custom adjustable range. The fitness function at the bottom indicates the optimal point found at each iteration. The

values stabilize as the objective function converges to a solution close to the global optimum. The results of the optimization for the control inputs A_m and f_c only are shown in Table 6.1. Without optimizing the robot's own physical parameters, the fastest walking speed is desired and the input torque reaches a maximum value of 25 [N·m] in the pre-set parameter range, where the input frequency exhibits a 2:1 entrainment relation to the actual walking frequency. The optimal walking efficiency is 0.0658 while maintaining a walking speed of 0.5 [m/s] or more, which is already a low value.

Based on Fig. 6.2, an optimization parameter, i.e., the radius of the semicircular foot, is added. The exploration process is shown in Fig. 6.3, and the specific results are shown in Table 6.2. It can be found that when the radius of the semicircular foot becomes larger (initially set

Table 6.1: Bayesian optimization results versus the control input

A_m [N·m]	f_c [Hz]	Performance
25	3.0851	0.7087 [m/s] (V_x)
9.7566	2.9286	0.0658 [-] (SR)

Table 6.2: Bayesian optimization results versus the control input and radius of the semicircular foot

A_m [N·m]	f_c [Hz]	R [m]	Performance
22.1769	1.4263	0.5	1.046 [m/s] (V_x)
1.6356	1.3077	0.4682	0.011 [-] (SR)

Table 6.3: Bayesian optimization results versus the control input, radius of the semicircular foot, and center of mass distribution

A_m [N·m]	f_c [Hz]	R [m]	a [m]	Performance
19.4667	1.6728	0.5	0.6037	1.0569 [m/s] (V_x)
1.0122	1.5426	0.4998	0.6602	0.007 [-] (SR)

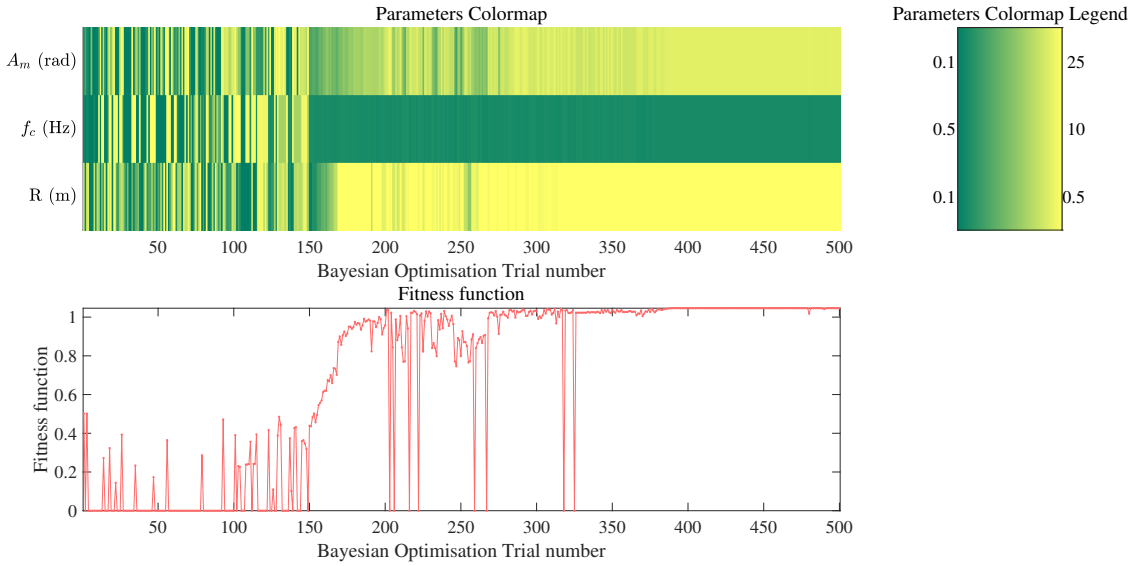

(a) Optimal walking speed

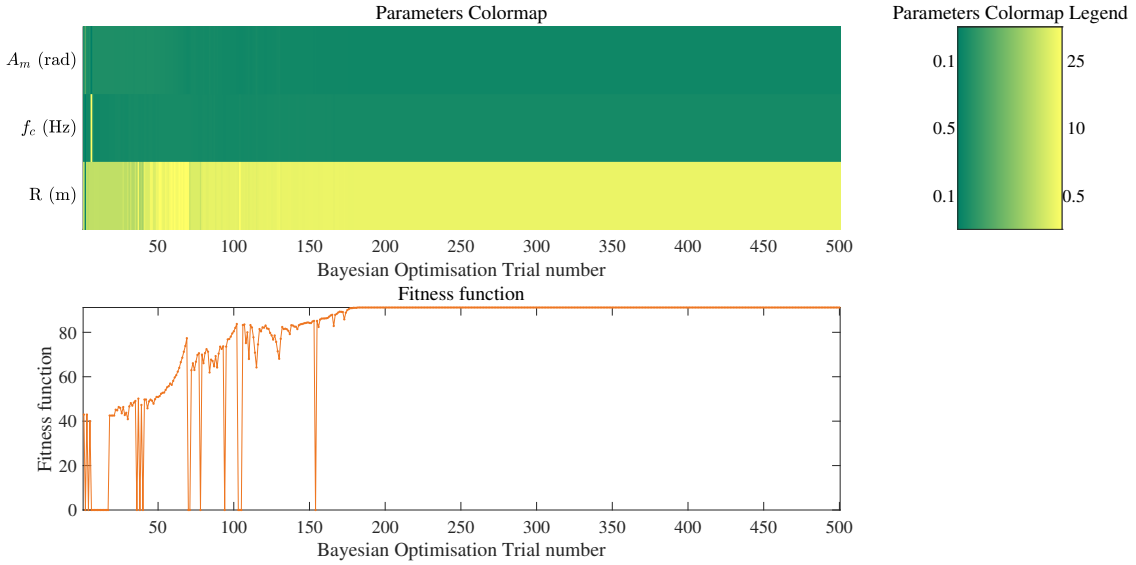

(b) Optimal energy efficiency (limit minimum speed)

Figure 6.3: Optimal gait performance versus the control input and radius of the semicircular foot

to 0.1m), only a smaller input torque is required to reach a faster walking speed, and the entrainment relationship between the input frequency and walking frequency becomes 1:1. When looking at the walking efficiency, it can also be found that an additional optimization of the foot radius improves the energy efficiency by a factor of 6 when maintaining the same speed of 0.5 [m/s] or more.

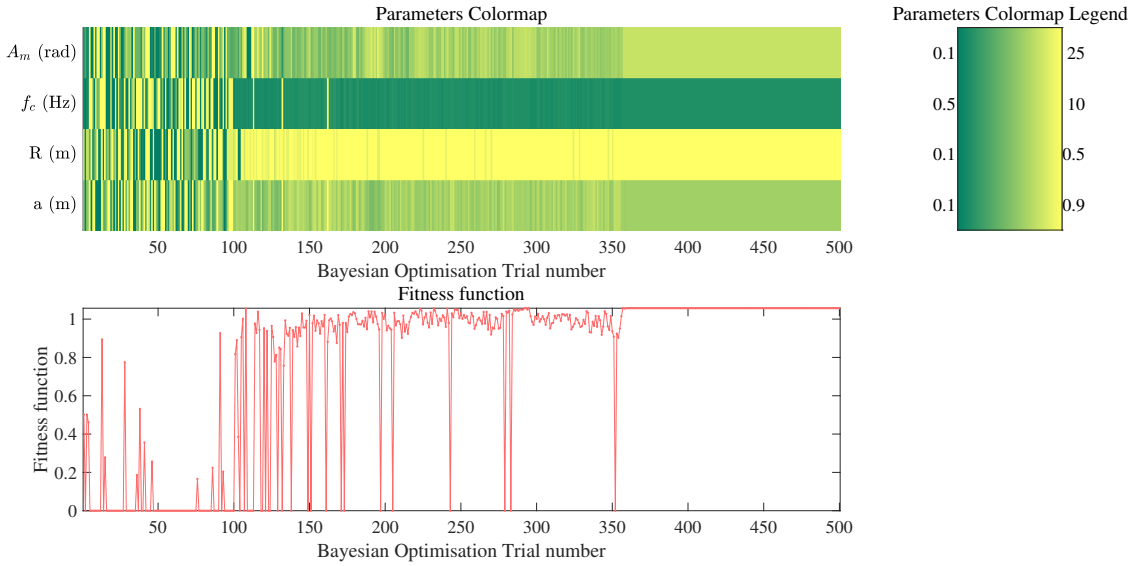

(a) Optimal walking speed

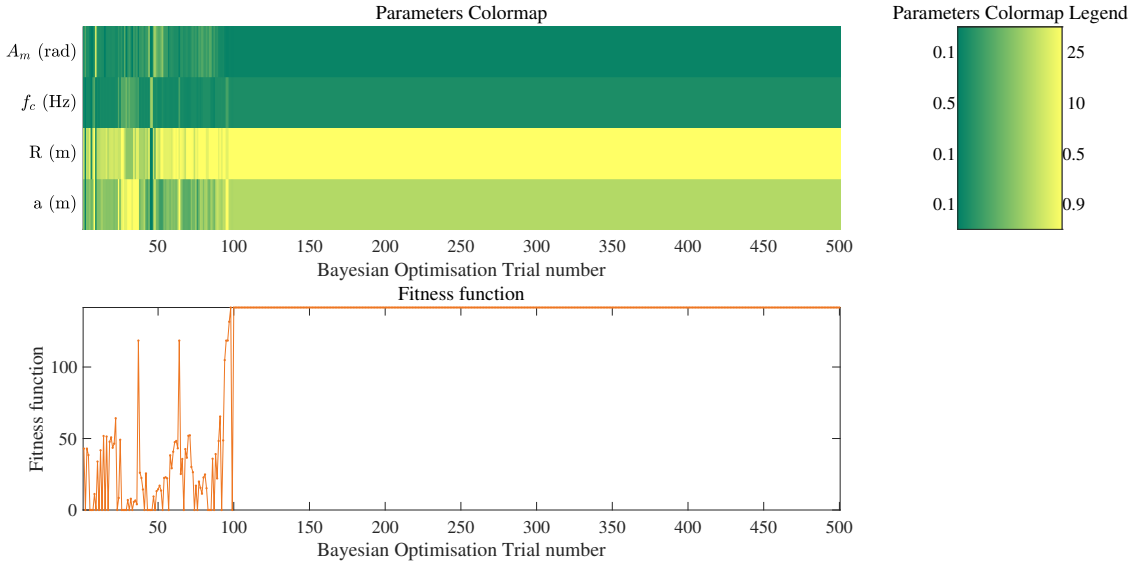

(b) Optimal energy efficiency (limit minimum speed)

Figure 6.4: Optimal gait performance versus the control input, Radius of the semicircular foot, and center of mass distribution

Finally, Fig. 6.4 shows the optimization process of the parameter a for the additional adjustment of the center of gravity position of the legs, and the results are shown in Table 6.3. It can be found that the results of the exploration of the radius of the feet have been the same as Fig. 6.3, and the maximum walking speed becomes slightly faster when the center of gravity position of the legs is shifted slightly upward, but the required input torque becomes smaller

again, and the entrainment relationship between the input frequency and the walking frequency is also 1:1 at this time. When both the control parameters and the physical parameters of the robot are optimized, the walking efficiency reaches 0.007.

6.4 Summary and Discussions

In this chapter, a Bayesian optimization approach is used to optimize the control parameters and physical parameters of the robot, and all the results are based on the successful entrainment of the gait. The optimized results are excellent. The energy efficiency, in particular, is considerably higher than for robots using conventional control methods. Thus far, qualitative and quantitative analysis of the limit cycle gait that can be entrained has been performed, but in addition to the limit cycle gait, there is also a chaotic gait based on this control method, which needs to be analyzed and discussed further.

Chapter 7

Gait Generation and Analysis of Chaotic Biped Walking Based on Rössler Attractor

7.1 Overview

It is difficult to maintain its walking stability due to the fact that the bipedal robots are nonlinear dynamical systems containing both continuous and discrete states [66], making its basin of attraction extremely limited. In addition to periodic limit-cycle gait [67], it has been found that the gait becomes fractal and eventually leads to chaotic gait when the slope increases to a certain level [68]. At the present, there is a unanimous agreement that chaotic phenomena bring only negative effects to bipedal walking. Therefore, several works have been conducted to avoid chaotic gait generation or directly control chaotic gait to limit-cycle walking [35] [34]. However, from another point of view, the most fundamental requirement for bipedal walking is the ability to keep walking, and therefore a larger basin of attraction is required to tolerate external perturbations. In this sense, chaotic oscillators tend to have larger basins of attraction compared to limit cycles. Moreover, the human walking process indeed shows chaotic behavior, as observed in previous works [69]. Considering these factors, the author hypothesizes that a reasonably generated chaotic bipedal gait is likely to be more robust to perturbations.

In order to study the performance of chaotic gait, in this chapter, the author adopts a convenient control idea based on a compass-like bipedal walker. First, the author exploits the Rössler attractor [36] to generate chaotic control waveforms suitable as input torque to the robot. Accordingly, chaotic gait is generated via entrained to the input waveform, and the stability domain

is explored by tuning the control parameters. The observed phenomena suggest that chaotic input waveforms bring large stability domains with pure open-loop control. Finally, the author puts this chaotic walking on uneven terrain. Unlike typical works which actively resist disturbances, our results show that the walker passively tolerates disturbance, thanks to its chaotic behavior. The proposed control concept paves the way for additional understanding of the properties of chaotic gait. The findings not only confirm the positive role of chaotic gait but may also help to design more stable bipedal control systems.

7.2 Chaotic Input Design

Previous studies have pointed out that for a continuous nonlinear dynamical system to generate chaotic attractors, there must be at least two nonlinear modes of motion and non-strictly periodic transitions between the two modes of motion. Over time, the gradual separation of neighboring states moving in the same mode of motion and the non-simultaneous transitions between different modes of motion lead to a sensitive dependence of the motion of the chaotic system on the initial value. Therefore, it is not easy to find a suitable chaotic waveform as input. In this paper, the author adopts the Rössler attractor [36], one of the well-known attractors, to model chaotic input waveforms with the following equations:

$$\begin{cases} \frac{\mathrm{d}}{\mathrm{d}t}R_x = -R_y - R_z, \\ \frac{\mathrm{d}}{\mathrm{d}t}R_y = R_x + \alpha R_y, \\ \frac{\mathrm{d}}{\mathrm{d}t}R_z = \beta + R_z(R_x - \gamma). \end{cases} \tag{7.1}$$

Here, the author designed chaotic input based on the Rössler attractor using predetermined constant parameters. Subsequently, by observing the trajectory of $u := R_x$, a suitable initial value is found and the generated chaotic waveform is directly used as the torque input to the robot crotch joint (it is necessary to ensure that the initial torque is approximately half of the overall size so that the point can be set as the origin). Based on the entrainment theory in which two interacting oscillating systems exhibit the same period, the author attempts to generate chaotic gaits with the same period by chaotic input waveforms, more details will be mentioned in the next section.

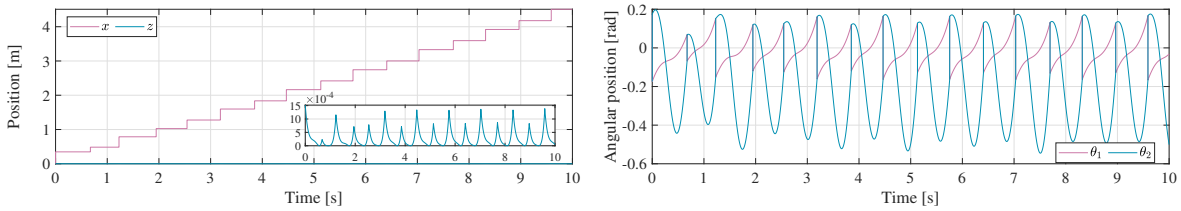

(a) Position

(b) Angular position

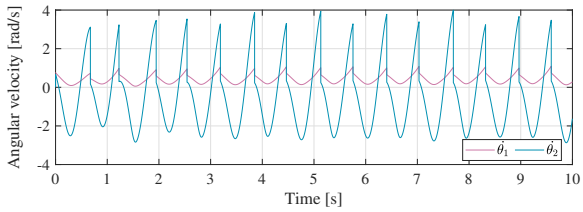

(c) Angular velocity

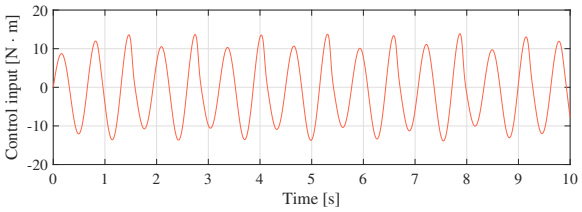

(d) Control input by Rössler attractor

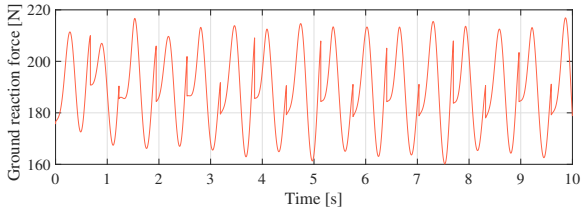

(e) Vertical ground reaction force

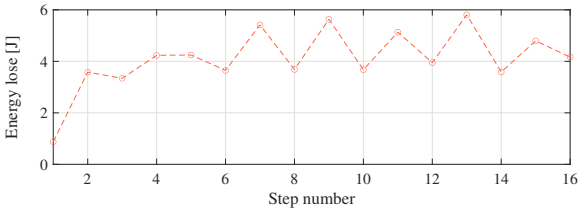

(f) Energy consumption

Figure 7.1: Simulation results of typical gait generation by a chaotic control input

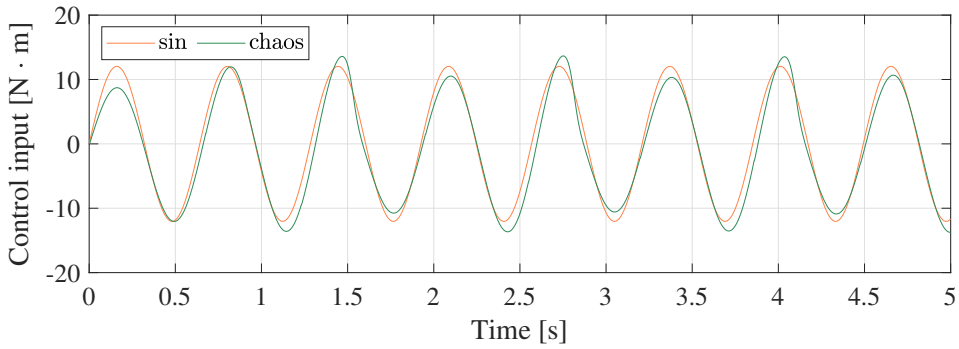

Figure 7.2: Normalization of sinusoidal and chaotic input waveforms

7.3 Numerical Simulation Results

This section describes the driving method used to generate a stable chaotic walking gait. Chaotic input waveforms are generated based on the characteristics of the Rössler attractor, and the input is directly used as a torque waveform for the hip motor drive using an open-loop control method. The advantage of torque control is that it potentially exploits the inherent dynamics of the robot. In addition, the walking performance can be controlled by appropriately

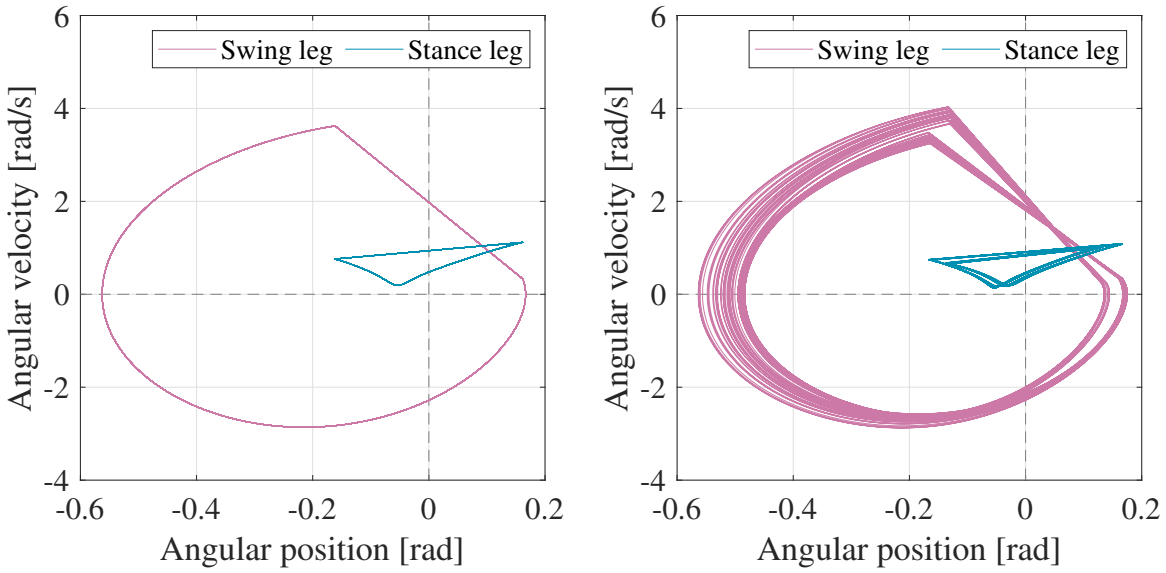

(a) Walking with periodic input

(b) Walking with chaotic input

Figure 7.3: Phase-plane plots of the robot on a horizontal surface by comparing periodic input with chaotic input

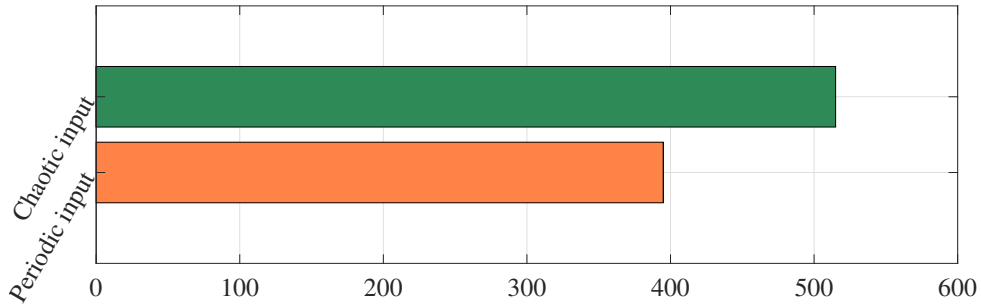

Figure 7.4: Basin of attraction (Number of initial conditions that can be successfully walked)

tuning the parameters of the chaotic waveform.

7.3.1 Typical gait generation

Table 7.1 shows the physical and control parameters to conduct the following process. It should be noted here that since the chaotic waveform generated by the time-dependent Rössler attractor cannot change the frequency, the coefficients ζ and δ used here compress the frequency

and the amplitude. The author sets the initial conditions as

$$\begin{aligned} \boldsymbol{q}(0) &= \begin{bmatrix} 0 & 0.0015 & 0.1745 & -0.1745 \end{bmatrix}^{\mathrm{T}}, \\ \dot{\boldsymbol{q}}(0) &= \begin{bmatrix} 0 & 0 & 0.75 & 0 \end{bmatrix}^{\mathrm{T}}. \end{aligned} \tag{7.2}$$

Here, since the robot with a semicircular foot, the z coordinate needs to be calculated based on the angle of the stance leg when the height of contact point z_c is 0 [m]. The initial condition has the same angle as the stance leg and the swing leg. Thus, the walking is simply initialized at the collision condition.

Figure 7.1 shows a typical gait generated by the biped walker based on chaotic inputs. The centroid position (x, z) of the semicircular foot of the stan leg is shown in Fig. 7.1(a), because the frequency and torque of the chaotic input are not fixed, it cannot converge to the same step length and step frequency. The author zooms in on the variation in z-coordinate to distinctly see the circular foot rolling on the ground. In Fig. 7.1(b) and (c), we can see the angular position and angular velocity of the two legs. Because of the chaotic input, the legs swing asymmetrically, and so is the angular velocity. The input waveform generated based on the parameters listed in Table 7.1 is shown in Fig. 7.1(d), where the frequency and amplitude are not fixed, but vary in a certain range. Figure 7.1(e) shows the variation of the vertical ground reaction force with an average value approximately equal to the entire robot mass. Moreover, these values constantly remain positive. It can be shown that the stance leg never leaves the ground and the resulting gait is reasonable. Figure 7.1(f) shows the energy consumed by the robot at each step when a collision occurs, and since the swing leg does not smash into the ground at the same speed each time, the kinetic energy consumed is therefore continuously changing.

Table 7.1: Physical and Control Parameters

Symbol	Value	Unit	Symbol	Value	Unit
m_H	10	kg	g	9.81	m/s^2
m_1=m_2	5	kg	α=β	0.1	
a=b	0.5	m	γ	9	
L	1	m	δ	1	
R	0.1	m	ζ	9.5	

7.3.2 Compare with limit cycle gait

Previous results [70] have shown that a bipedal walking robot can converge to a limit-cycle gait while walking horizontally on the ground, even without any feedback control, provided a sinusoidal torque input is given. To verify the stability of the generated chaotic gait, the author compares it with the limit-cycle gait. In Fig. 7.3, the author compares the phase planes of the same robot for the conditions of periodic and chaotic inputs, respectively, and it is essential to note that for a fair comparison, we need to normalize the waveforms of both, as shown in Fig. 7.2, where the sinusoidal input has the same total input energy as the chaotic one. The author uniformly lets the robot walk for 100 [s]. In Fig. 7.3 (a) and (b), the sine wave input and the chaotic input are used respectively, and the robot intercepts the phase plane from the 50th to the 100th second after walking for 50 [s]. We can see that the robot in 7.3(a) generates a period-1 limit-cycle gait, while 7.3(b) has a chaotic gait. Figure 7.4 shows a comparison of the explored BOA sizes. The author divided the angles of the feet and the angular velocities of the combined four initial conditions into nine equal parts, and they range from θ_1 from -0.5 to 0.5 [rad], $\dot{\theta}_1$ from -1 to 2 [rad/s], θ_2 from -0.7 to 0.3 [rad], and $\dot{\theta}_2$ from -5 to 6 [rad/s]. This implies that there are 10^4 combinations of initial conditions. It was shown that 395 initial states can be successfully walked for more than 50 seconds when periodic inputs are used. It was expanded to 515 groups when chaotic wave input was used.

7.3.3 Effect of chaotic control input

The author initially explained the chaotic gait based on the Rössler attractor. However, the range of inputs that can provide stable walks remains to be examined, and thus the goal of this subsection is to explore the effect of chaotic input waveform parameters and explore the possible walk dynamics induced by the proposed control method. The method for exploring the stability domain is as Algorithm 5.

The explored stability domains are shown in Fig. 7.5 and Fig. 7.6, with two non-connected size stability domains present. In general, as open-loop control, the domain is sufficiently broad. In contrast, the gait generated by the chaotic controller is essentially influenced not only by the frequency coefficient ζ but also by the amplitude coefficient δ. Fig. 7.5(a) represents the variation of the walking frequency, a performance metric that is roughly linearly related to the frequency coefficients in the input, with a gradual increase in walking frequency as the input

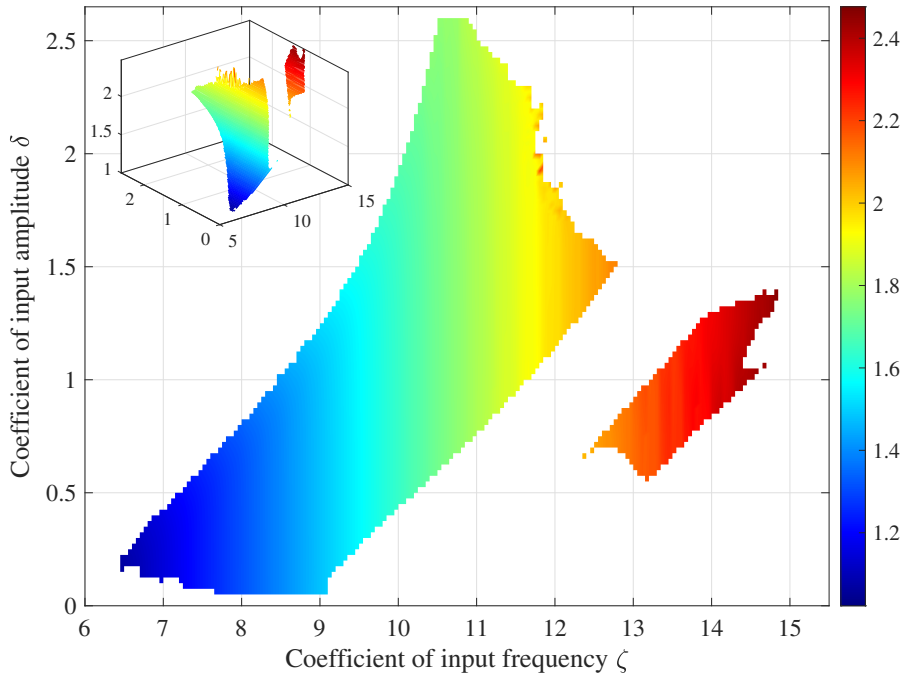

(a) Walking frequency

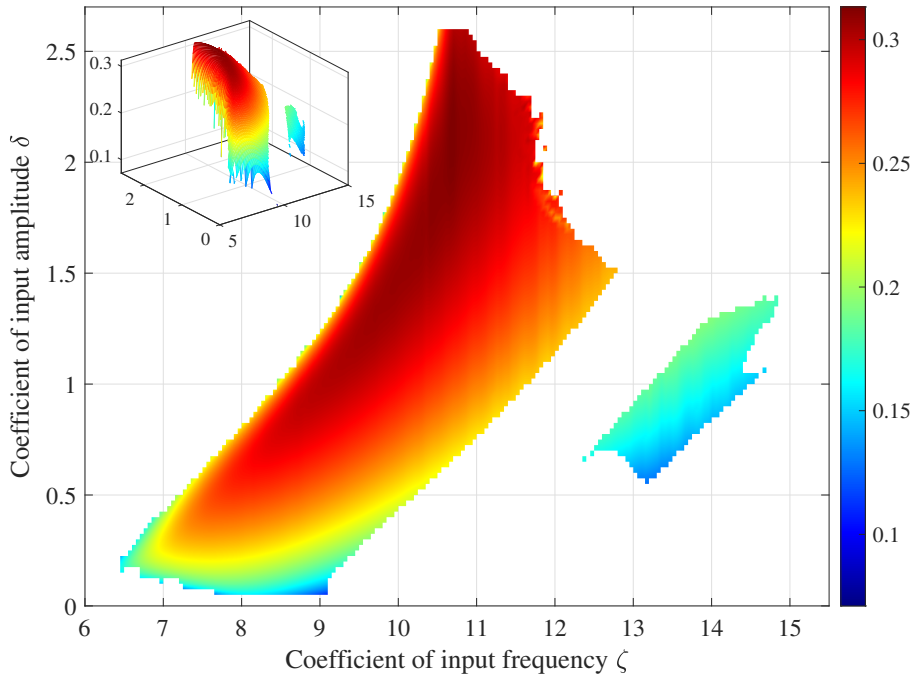

(b) Step length

Figure 7.5: Gait performance versus the chaotic control input

frequency increases. Although the chaotic input does not have a fixed frequency, it invariably approximates the walking frequency. The variation of the step length is shown in Fig. 7.5(b). Compared with the walking frequency, the step length is more influenced by the input ampli-

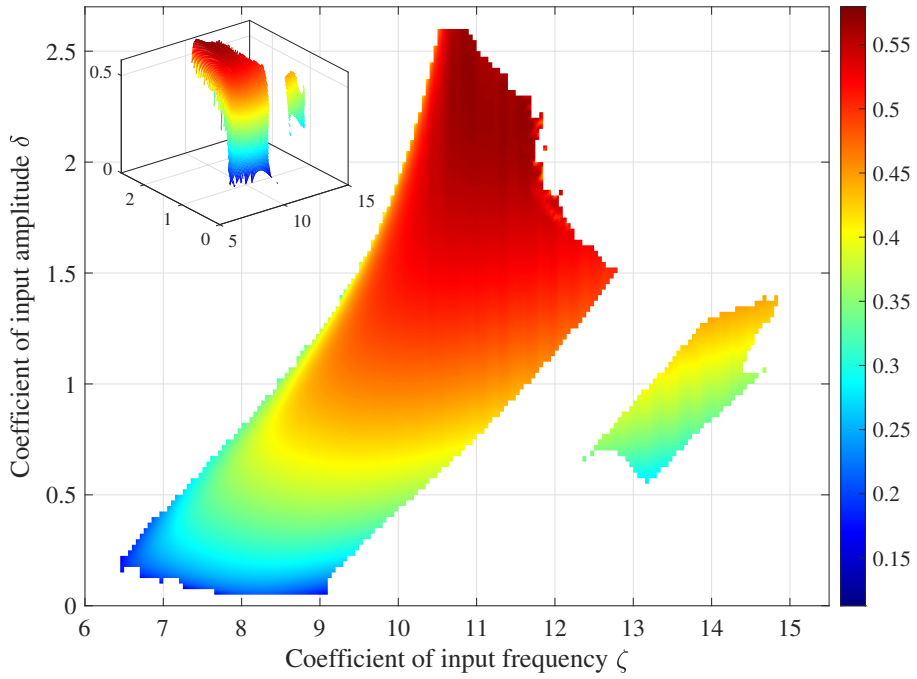

(a) Walking speed

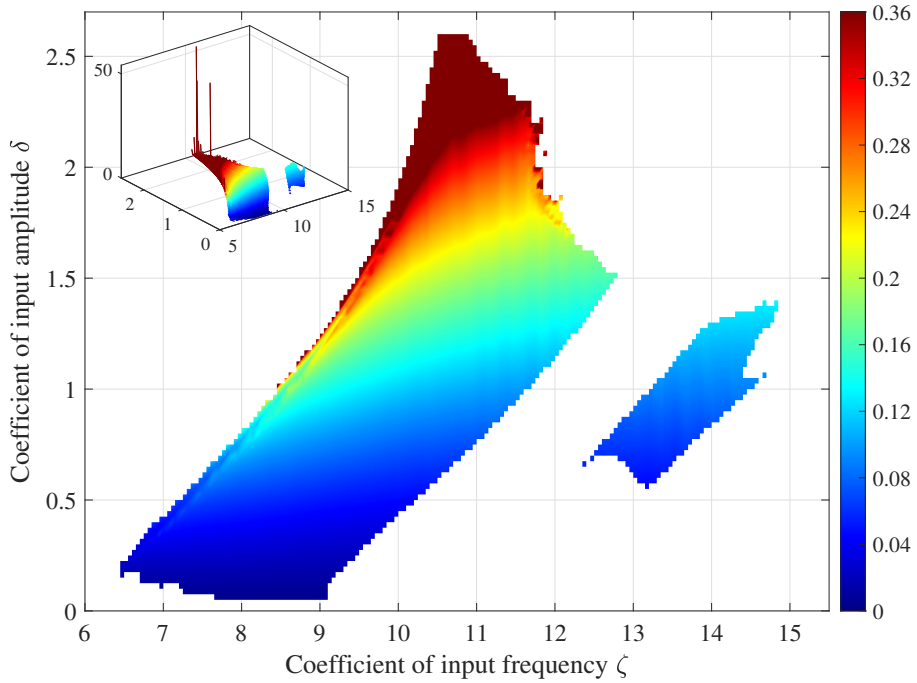

(b) Specific resistance

Figure 7.6: Gait performance versus the chaotic control input

tude coefficient, and the longest step length comes to approximately 0.32 [m] at larger torques. However, even though the amplitude parameter varies considerably, it is around 0.25 [m] most of the time. The walking speed is obtained by multiplying the walking frequency by the step

Algorithm 5 Calculate T and SL

Require: The step period T and step length SL of the Robot when they get stabilized

Input: Initial state $\boldsymbol{q}(0)$, $\dot{\boldsymbol{q}}(0)$, ζ and δ

Output: Step period T and step length SL of the next 20 steps after 50 seconds

Initialization $T[l][m][20] = 0$, $SL[l][m][20] = 0$, $\zeta = 0.1$, $\delta = 0.1$
for $i = 1; i <= l : i++$ **do**
  for $j = 1; j <= m : j++$ **do**
    Run simulation for 50 seconds.
    Save the next 20 step periods to t and the next 20 step length to L
    $L[i][j] = t$
    $SL[i][j] = SL$
    $\zeta = \zeta + 0.05$
  end
  $\delta = \delta + 0.025$
end
Return T and SL

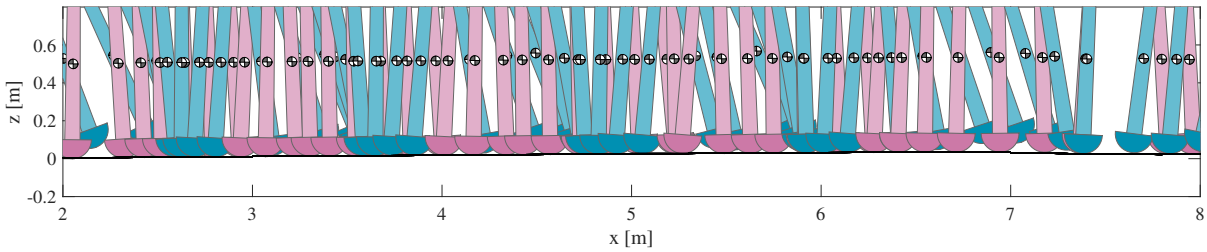

Figure 7.7: Biped robot walking on uneven terrain with chaotic input

length. In Fig. 7.6, it is easy to see from Fig. 7.6(c) that a larger torque complemented by a larger input frequency gives the fastest walking speed. Finally, Fig. 7.6(d) as an important indicator of bipedal walking, the walking efficiency stays below 0.3 most of the time, which is better than the vast majority of walking robots and is closer to human walking efficiency.

Finally, the author generated a section of uneven terrain to verify the stability of the proposed method, and the walk results are shown in Fig. 7.7, and it illustrates a screenshot from the walk animation, intercepted at intervals according to the input period because the walking frequency is known to converge with the input frequency. The initial 2 [m] is a horizontal surface, and

Figure 7.8: CAD of a compass bipedal walking robot designed to conform to the simulation style

when the robot is faced with an uphill slope, the step length and walking frequency become significantly smaller due to the fact that the semicircular foot is more difficult to cross the potential energy barrier during the uphill slope. Eventually, the robot walked the entire distance. Based on these results, the author conjectures that the proposed approach helps one to more easily study chaotic gait in passive walking.

7.4 Summary and Discussions

In this chapter, the author hypothesizes that a reasonably generated chaotic bipedal gait is potentially more robust to perturbations than a limit-cycle gait under equivalent road conditions. Numerical simulations have shown that it is possible to generate gaits on the horizontal ground using chaotic input waveforms generated based on Rössler attractors. Although the simple

control method is open-loop, the author explores a relatively large stability domain, and by comparing periodic gaits, our method provides a larger basin of attraction. In addition, the author observed the effect of different control parameters on gait performance and successfully applied the method to uneven terrain. Our results confirm that there are positive aspects of chaos in bipedal walking, and the proposed concept of chaotic control may offer new possibilities for understanding bipedal dynamic walking. While only constructive results are available, the author plan to delve into the logic behind chaotic gaits. Moreover, for future work, the author will use an improved bipedal robot based on the one that has been made so far, Fig. 7.8 shows the design of the improved robot and will be validated in a real-world environment.

Chapter 8

Conclusion and Future Works

8.1 Summary

From the perspective of making full use of the robot's inherent dynamics, traditional control means relying solely on feedback is discarded. In order to achieve efficient and stable motion of bipedal robots using the entrainment control mechanism on level ground as well as on uneven ground, the following work is carried out in this dissertation:

- The advantages of the compass robot are analyzed and demonstrated by RW under time-symmetric and asymmetric input signals.
- The nonlinear characteristics of a passive bipedal robot based on entrainment control are analyzed and the range of successful entrainment is observed by Arnold tongue.
- The entrainment principle was successfully applied to pavements other than downhill, and a large number of observations on walking speed, efficiency, and entrainment range were made by varying the control parameters, and the system stability was analyzed by means of the Poincaré map.
- Based on the entrainment control theory, an experimental machine was designed and built, and the experimental results successfully verified the feasibility of the theory.
- Using Bayesian optimization theory, the optimal control parameters and physical parameters of the robot under entrainment control are optimized for walking speed and walking efficiency.

- In addition to the periodic limit cycle gait, the chaotic gait is designed by using the characteristics of the chaotic attractor with a large attraction basin, and the above results are combined to successfully expand the basin of attraction of the gait.

8.2 Conclusion

Conventional robots generally require precise real-time feedback control to achieve stable walking, which leads to significant energy losses that cannot be sustained for long periods of time in realistic environments. In this paper, the aim is to explore further intrinsic mechanisms of walking and to realize a simpler and more efficient method of motion control for bipedal robots. Two signaling systems, the first and the second, acquired by humans during evolution are borrowed. A similar classification of signal systems can be done for robot motion generation. The former is used to reliably generate and maintain basic motions, while the latter is used to adapt flexibly to complex environments, where each system operates in a shared and coordinated manner.

In the case of a compass bipedal robot, for example, the use of a reasonable feedforward input waveform, based on the entrainment effect, allows the bipedal robot to walk efficiently and stably on downhill as well as horizontal surfaces. It can be viewed as the motion generation of control signals (first signal system) generated at the level of human reflexes without any feedback control, which considerably reduces the cost of control. At the same time, step length, walking frequency, and walking speed, which are critical indicators of walking within the entrainment range, can be simply tuned by the control parameters. To verify whether the entrainment control method can successfully control a robot to generate dynamic walking in a realistic environment, a bipedal walker was designed and fabricated. Although only a 1:1 entrainment between the input waveform frequency and the actual walking frequency can be achieved due to hardware conditions, the experimental results demonstrate the feasibility of the proposed method.

In order to pursue higher walking performance, such as superior walking speed, and to obtain the highest energy utilization while limiting the walking speed, the control parameters as well as the physical parameters of the robot itself are globally optimized by Bayesian optimization. The results show that the fastest walking speed occurs in a 2:1 entrainment waveform when only the control parameters are changed, while the fastest walking speed can be achieved

in a 1:1 entrainment waveform after optimizing the foot shape, which indicates that the structural design of the robot itself is also significant. The results of walking efficiency show that SR can be as low as 0.007 (better than human) with the proposed control method while maintaining a walking speed of 0.5 [m/s] or more.

Moreover, in bipedal dynamic walking, it is common to expect the gait to converge to a limit cycle gait. However, from another point of view, the most essential requirement to achieve stable bipedal walking is not to fall, which requires a large BOA to tolerate disturbances. Chaotic oscillators tend to have large basins of attraction compared to the limit cycle. Accordingly, it is hypothesized in this paper that a chaotic bipedal gait correctly generated due to entrainment effects may be more robust to perturbations (e.g., walking on uneven ground). Based on this consideration, chaotic gaits are generated by employing a Rossler attractor, which is typical of chaotic oscillators. It was shown that chaotic bipedal gait has a larger BOA than restricted periodic walking for the same input strength, and the domain of stable walking was further explored by varying the control parameters of chaotic bipedal gait.

8.3 Contribution

This dissertation presents a theoretical analysis of the control of entrainment-based bipedal walking robots from a nonlinear dynamics perspective. It was initially found that limit cycle gaits can be generated on both RW and compass-like bipedal robots using time-symmetric input waveforms, but RW requires extremely large semicircular feet and entrainment is difficult to occur. Compass-like bipedal robots, on the other hand, are also applicable and have a larger range of entrainment due to the presence of a swinging leg, which can effectively improve walking performance when entrained. When time-asymmetric input waveforms are used, RW can produce an entrainment effect, but the improvement in walking performance is not sufficiently obvious, so the control method is more appropriate for compass-like bipedal robots.

Moreover, its applicability in realistic environments is verified by designed experimental machines. In addition, global optimization of the system is performed based on theoretical analysis. More importantly, the positive aspects of the chaotic gait are revealed. Thus, the control theory advocated in this dissertation can significantly improve the energy efficiency of realistic robots. Moreover, the proposed concept of chaotic control may provide different possibilities for understanding bipedal dynamic walking.

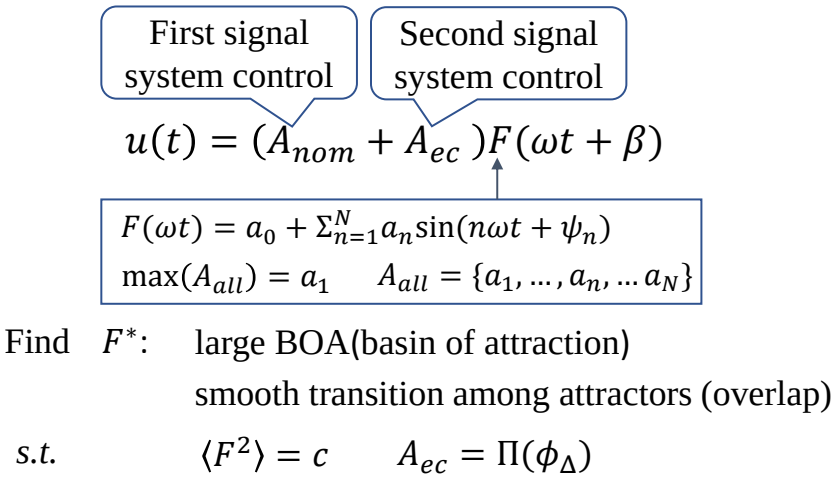

Figure 8.1: Migration of attractors through fusion and optimization of signal systems

8.4 Future Works

Currently, the control method proposed in the paper is only applicable to the first signal system, and although it can substantially improve walking efficiency, its adaptability to different road environments still needs to be improved. Here it is necessary to use a second signal system, based on the feed-forward ground state, for partial compensation. As shown in Fig. 8.1, keeping the system with only a single input $u(t)$ and without adding additional degrees of freedom, F (based on Fourier transform) achieves the maximum area of the attraction basin when walking on a horizontal road surface is first found by Bayesian optimization. Then, error compensation is introduced to ensure the stability of the system in the case of complex pavements. Here, A_{nom} denotes the parameter that determines the input size when walking on a horizontal pavement, A_{ec} denotes the error compensation parameter, and β denotes the phase change parameter. In terms of phase space, both A_{ec} and β are zero when it is not out of the initial area of the BOA, which means that the robot moves forward only under the control of the first signal system; once the ground conditions change and the system is out of the initial BOA, the A_{ec} and β, which act as the control of the second signal system, is introduced to make the robot stabilize in the new BOA and gradually migrate to the initial BOA. In this way, a higher walking performance is expected to be achieved with the combination of the first and second signal systems.

Bibliography

[1] S. Kuindersma, R. Deits, M. Fallon, A. Valenzuela, H. Dai, F. Permenter, T. Koolen, P. Marion, and R. Tedrake, "Optimization-based locomotion planning, estimation, and control design for the atlas humanoid robot," *Autonomous robots*, vol. 40, no. 3, pp. 429–455, 2016.

[2] M. Vukobratović and B. Borovac, "Zero-moment point—thirty five years of its life," *International journal of humanoid robotics*, vol. 1, no. 01, pp. 157–173, 2004.

[3] Y. Sakagami, R. Watanabe, C. Aoyama, S. Matsunaga, N. Higaki, and K. Fujimura, "The intelligent asimo: System overview and integration," *IEEE/RSJ international conference on intelligent robots and systems*, vol. 3, pp. 2478–2483, 2002.

[4] F. Iida, G. Gomez, and R. Pfeifer, "Exploiting body dynamics for controlling a running quadruped robot," *ICAR '05. Proceedings., 12th International Conference on Advanced Robotics, 2005.*, pp. 229–235, 2005.

[5] F. Iida and R. Tedrake, "Minimalistic control of biped walking in rough terrain," *Autonomous Robots*, vol. 28, no. 3, pp. 355–368, 2010.

[6] T. McGeer, "Passive dynamic walking," *The International Journal of Robotics Research*, vol. 9, no. 2, pp. 62–82, 1990.

[7] A. Goswami, B. Espiau, and A. Keramane, "Limit cycles and their stability in a passive bipedal gait," vol. 1, pp. 246–251, IEEE, 1996.

[8] A. Goswami, B. Thuilot, and B. Espiau, "Compass-like biped robot part i: Stability and bifurcation of passive gaits," tech. rep., INRIA, 1996.

[9] A. Goswami, B. Espiau, and A. Keramane, "Limit cycles in a passive compass gait biped and passivity-mimicking control laws," *Autonomous Robots*, vol. 4, no. 3, pp. 273–286, 1997.

[10] S. Collins, A. Ruina, R. Tedrake, and M. Wisse, "Efficient bipedal robots based on passive-dynamic walkers," *Science*, vol. 307, no. 5712, pp. 1082–1085, 2005.

[11] S. Collins and A. Ruina, "A bipedal walking robot with efficient and human-like gait," pp. 1983–1988, IEEE, 2005.

[12] M. W. Spong, "Energy based control of a class of underactuated mechanical systems," *Proceedings of the 1996 IFAC World Congress*, pp. 431–435, 1996.

[13] M. W. Spong and F. Bullo, "Controlled symmetries and passive walking," *IEEE Transactions on Automatic Control*, vol. 50, no. 7, pp. 1025–1031, 2005.

[14] F. Asano, M. Yamakita, N. Kamamichi, and Z. Luo, "A novel gait generation for biped walking robots based on mechanical energy constraint," *IEEE Transactions on Robotics and Automation*, vol. 20, no. 3, pp. 565–573, 2004.

[15] F. Asano, M. Yamakita, N. Kamamichi, and Z. Luo, "A novel gait generation for biped walking robots based on mechanical energy constraint," *IEEE/RSJ International Conference on Intelligent Robots and Systems*, vol. 3, pp. 2637–2644 vol.3, 2002.

[16] Y. Harata, F. Asano, Z. Luo, K. Taji, and Y. Uno, "Biped gait generation based on parametric excitation by knee-joint actuation," *Robotica*, vol. 27, no. 7, pp. 1063–1073, 2009.

[17] Y. Harata, F. Asano, K. Taji, and Y. Uno, "Efficient parametric excitation walking with delayed feedback control," *Nonlinear Dynamics*, vol. 67, no. 2, pp. 1327–1335, 2012.

[18] G. Taga, Y. Yamaguchi, and H. Shimizu, "Self-organized control of bipedal locomotion by neural oscillators in unpredictable environment," *Biological Cybernetics*, vol. 65, no. 3, pp. 147–159, 1991.

[19] S. Miyakoshi, G. Taga, Y. Kuniyoshi, and A. Nagakubo, "Three dimensional bipedal stepping motion using neural oscillators—towards humanoid motion in the real world—," *Journal of the Robotics Society of Japan*, vol. 18, no. 1, pp. 87–93, 2000.

[20] R. Altendorfer, D. E. Koditschek, and P. Holmes, "Stability analysis of a clock-driven rigid-body slip model for rhex," *The International Journal of Robotics Research*, vol. 23, no. 10-11, pp. 1001–1012, 2004.

[21] K. D. Mombaur, R. W. Longman, H. G. Bock, and J. P. Schlöder, "Open-loop stable running," *Robotica*, vol. 23, no. 1, pp. 21–33, 2005.

[22] I. Obayashi, S. Aoi, K. Tsuchiya, and H. Kokubu, "Common formation mechanism of basin of attraction for bipedal walking models by saddle hyperbolicity and hybrid dynamics," *Japan Journal of Industrial and Applied Mathematics*, vol. 32, no. 2, pp. 315–332, 2015.

[23] M. W. Oppenheimer, D. B. Doman, and M. A. Bolender, "Control allocation for over-actuated systems," in *2006 14th Mediterranean Conference on Control and Automation*, pp. 1–6, IEEE, 2006.

[24] S. Gupta and A. Kumar, "A brief review of dynamics and control of underactuated biped robots," *Advanced Robotics*, vol. 31, no. 12, pp. 607–623, 2017.

[25] C. Chevallereau, J. W. Grizzle, and C.-L. Shih, "Asymptotically stable walking of a five-link underactuated 3-d bipedal robot," *IEEE Transactions on Robotics*, vol. 25, no. 1, pp. 37–50, 2009.

[26] A. Hereid, E. A. Cousineau, C. M. Hubicki, and A. D. Ames, "3d dynamic walking with underactuated humanoid robots: A direct collocation framework for optimizing hybrid zero dynamics," in *2016 IEEE International Conference on Robotics and Automation*, pp. 1447–1454, IEEE, 2016.

[27] O. Matsumoto, S. Kajita, M. Saigo, and K. Tani, "Dynamic trajectory control of passing over stairs by a biped type leg-wheeled robot with nominal reference of static gait," *Journal of the Robotics Society of Japan*, vol. 16, no. 6, pp. 868–875, 1998.

[28] M. Wisse, "Essentials of dynamic walking; analysis and design of two-legged robots," 2004.

[29] S. Kajita, F. Kanehiro, K. Kaneko, K. Fujiwara, K. Harada, K. Yokoi, and H. Hirukawa, "Biped walking pattern generation by using preview control of zero-moment point," in

2003 IEEE International Conference on Robotics and Automation, vol. 2, pp. 1620–1626, IEEE, 2003.

[30] A. Pikovsky, M. Rosenblum, and J. Kurths, *Synchronization: a universal concept in nonlinear sciences*, vol. 12. Cambridge, U.K.: Cambridge university press, 2003.

[31] T. Roenneberg, S. Daan, and M. Merrow, "The art of entrainment," *Journal of Biological Rhythms*, vol. 18, no. 3, pp. 183–194, 2003.

[32] J. Snoek, H. Larochelle, and R. P. Adams, "Practical bayesian optimization of machine learning algorithms," *Advances in Neural Information Processing Systems*, vol. 25, 2012.

[33] K. A. Saar, A. Rosendo, and F. Llda, "Bayesian optimization of gaits on a bipedal slip model," in *2017 IEEE International Conference on Robotics and Biomimetics*, pp. 1812–1817, IEEE, 2017.

[34] H. Gritli, N. Khraief, and S. Belghith, "Chaos control in passive walking dynamics of a compass-gait model," *Communications in Nonlinear Science and Numerical Simulation*, vol. 18, no. 8, pp. 2048–2065, 2013.

[35] Y. Huang, Q. Huang, and Q. Wang, "Chaos and bifurcation control of torque-stiffness-controlled dynamic bipedal walking," *IEEE Transactions on Systems, Man, and Cybernetics: Systems*, vol. 47, no. 7, pp. 1229–1240, 2016.

[36] O. Rossler, "An equation for hyperchaos," *Physics Letters A*, vol. 71, no. 2-3, pp. 155–157, 1979.

[37] Q. Huang, S. Kajita, N. Koyachi, K. Kaneko, K. Yokoi, H. Arai, K. Komoriya, and K. Tanie, "A high stability, smooth walking pattern for a biped robot," in *Proceedings 1999 IEEE International Conference on Robotics and Automation*, vol. 1, pp. 65–71, IEEE, 1999.

[38] Q. Huang, K. Yokoi, S. Kajita, K. Kaneko, H. Arai, N. Koyachi, and K. Tanie, "Planning walking patterns for a biped robot," *IEEE Transactions on Robotics and Automation*, vol. 17, no. 3, pp. 280–289, 2001.

[39] P. Sardain and G. Bessonnet, "Forces acting on a biped robot. center of pressure-zero moment point," *IEEE Transactions on Systems, Man, and Cybernetics-Part A: Systems and Humans*, vol. 34, no. 5, pp. 630–637, 2004.

[40] M. Raibert, K. Blankespoor, G. Nelson, and R. Playter, "Bigdog, the rough-terrain quadruped robot," *IFAC Proceedings Volumes*, vol. 41, no. 2, pp. 10822–10825, 2008.

[41] M. Fujita and H. Kitano, "Development of an autonomous quadruped robot for robot entertainment," *Autonomous Robots*, vol. 5, no. 1, pp. 7–18, 1998.

[42] H. Kimura, Y. Fukuoka, and A. H. Cohen, "Adaptive dynamic walking of a quadruped robot on natural ground based on biological concepts," *The International Journal of Robotics Research*, vol. 26, no. 5, pp. 475–490, 2007.

[43] R. B. McGhee and G. I. Iswandhi, "Adaptive locomotion of a multilegged robot over rough terrain," *IEEE Transactions on Systems, Man, and Cybernetics*, vol. 9, no. 4, pp. 176–182, 1979.

[44] S. Inagaki, H. Yuasa, T. Suzuki, and T. Arai, "Wave cpg model for autonomous decentralized multi-legged robot: Gait generation and walking speed control," *Robotics and Autonomous Systems*, vol. 54, no. 2, pp. 118–126, 2006.

[45] S. H. Collins and A. Ruina, "A bipedal walking robot with efficient and human-like gait," in *Proceedings of the 2005 IEEE International Conference on Robotics and Automation*, pp. 1983–1988, 2005.

[46] M. J. Coleman, A. Chatterjee, and A. Ruina, "Motions of a rimless spoked wheel: a simple three-dimensional system with impacts," *Dynamics and Stability of Systems*, vol. 12, no. 3, pp. 139–159, 1997.

[47] F. Asano, "Stability principle underlying passive dynamic walking of rimless wheel," in *2012 IEEE International Conference on Control Applications*, pp. 1039–1044, 2012.

[48] F. Asano, "Efficiency and optimality of two-period limit cycle walking," *Advanced Robotics*, vol. 26, no. 1-2, pp. 155–176, 2012.

[49] Y. Harata, K. Iwano, F. Asano, and T. Ikeda, "Efficiency analysis of two-period asymmetric gaits," *International Journal of Dynamics and Control*, vol. 2, no. 3, pp. 304–313, 2014.

[50] F. Asano and I. Tokuda, "Indirectly controlled limit cycle walking of combined rimless wheel based on entrainment to active wobbling motion," *Multibody System Dynamics*, vol. 34, no. 2, pp. 191–210, 2015.

[51] L. Li, F. Asano, and I. Tokuda, "Nonlinear analysis of an indirectly controlled sliding locomotion robot," in *2018 IEEE/RSJ International Conference on Intelligent Robots and Systems*, pp. 1–9, 2018.

[52] L. Li, I. Tokuda, and F. Asano, "Optimal fast entrainment waveform for indirectly controlled limit cycle walker against external disturbances," in *2020 IEEE International Conference on Robotics and Automation*, pp. 3458–3463, 2020.

[53] L. Li, I. Tokuda, and F. Asano, "Optimal input waveform for an indirectly controlled limit cycle walker," *2018 IEEE/RSJ International Conference on Intelligent Robots and Systems*, pp. 7454–7459, 2018.

[54] P. L. Boyland, "Bifurcations of circle maps: Arnol'd tongues, bistability and rotation intervals," *Communications in Mathematical Physics*, vol. 106, no. 3, pp. 353–381, 1986.

[55] C. Reichhardt and F. Nori, "Phase locking, devil's staircases, farey trees, and arnold tongues in driven vortex lattices with periodic pinning," *Physical Review Letters*, vol. 82, no. 2, p. 414, 1999.

[56] Y. Hurmuzlu and C. Basdogan, "On the measurement of dynamic stability of human locomotion," *Journal of Biomechanical Engineering*, vol. 116, no. 1, pp. 30–36, 1994.

[57] B. Morris and J. W. Grizzle, "A restricted poincaré map for determining exponentially stable periodic orbits in systems with impulse effects: Application to bipedal robots," in *Proceedings of the 44th IEEE Conference on Decision and Control*, pp. 4199–4206, 2005.

[58] A. Pikovsky, M. Rosenblum, and J. Kurths, *Synchronization: a universal concept in nonlinear science*. American Association of Physics Teachers, 2002.

[59] F. Asano and Z. Luo, "Efficient dynamic bipedal walking using effects of semicircular feet," *Robotica*, vol. 29, no. 3, pp. 351–365, 2011.

[60] P. A. Bhounsule, J. Cortell, A. Grewal, B. Hendriksen, J. G. D. Karssen, C. Paul, and A. Ruina, "Low-bandwidth reflex-based control for lower power walking: 65 km on a single battery charge," *The International Journal of Robotics Research*, vol. 33, no. 10, pp. 1305–1321, 2014.

[61] C. Hubicki, J. Grimes, M. Jones, D. Renjewski, A. Spröwitz, A. Abate, and J. Hurst, "Atrias: Design and validation of a tether-free 3d-capable spring-mass bipedal robot," *The International Journal of Robotics Research*, vol. 35, no. 12, pp. 1497–1521, 2016.

[62] A. Smyrli and E. Papadopoulos, "A methodology for the incorporation of arbitrarily-shaped feet in passive bipedal walking dynamics," *2020 IEEE International Conference on Robotics and Automation*, pp. 8719–8725, 2020.

[63] G. A. Pratt and M. M. Williamson, "Series elastic actuators," *Proceedings 1995 IEEE/RSJ International Conference on Intelligent Robots and Systems. Human Robot Interaction and Cooperative Robots*, vol. 1, pp. 399–406, 1995.

[64] D. W. Robinson, J. E. Pratt, D. J. Paluska, and G. A. Pratt, "Series elastic actuator development for a biomimetic walking robot," *1999 IEEE/ASME International Conference on Advanced Intelligent Mechatronics (Cat. No. 99TH8399)*, pp. 561–568, 1999.

[65] P. M. Wensing, A. Wang, S. Seok, D. Otten, J. Lang, and S. Kim, "Proprioceptive actuator design in the mit cheetah: Impact mitigation and high-bandwidth physical interaction for dynamic legged robots," *IEEE Transactions on Robotics*, vol. 33, no. 3, pp. 509–522, 2017.

[66] B. J. West and N. Scafetta, "Nonlinear dynamical model of human gait," *Physical Review E*, vol. 67, no. 5, p. 051917, 2003.

[67] D. G. Hobbelen and M. Wisse, *Limit cycle walking*. Citeseer, 2007.

[68] B. Thuilot, A. Goswami, and B. Espiau, "Bifurcation and chaos in a simple passive bipedal gait," in *Proceedings of International Conference on Robotics and Automation*, vol. 1, pp. 792–798, 1997.

[69] J. M. Hausdorff, C.-K. Peng, Z. Ladin, J. Y. Wei, and A. L. Goldberger, "Is walking a random walk? evidence for long-range correlations in stride interval of human gait," *Journal of Applied Physiology*, vol. 78, no. 1, pp. 349–358, 1995.

[70] F. Iida and R. Tedrake, "Minimalistic control of biped walking in rough terrain," *Autonomous Robots*, vol. 28, no. 3, pp. 355–368, 2010.

Publications

Book Chapter

[1] Longchuan Li, Isao T Tokuda, Fumihiko Asano and Cong Yan, "Nonlinear analysis and control of quasi-passive dynamic walker based on entrainment effect," *Recent Trends in Chaotic, Nonlinear and Complex Dynamics*, pp. 514-530, 2021.

Journal Paper

[2] Cong Yan, Fumihiko Asano and Longchuan Li, "Modeling, control and analysis of semicircular-footed bipedal robot with entrainment effect," *Artificial Life and Robotics* , vol. 27, pp. 384-392, 2022.

International Conference

[3] Cong Yan, Yanqiu Zheng, Fumihiko Asano and Longchuan Li, "Modeling and analysis of bipedal robot walking uphill by hybrid control," *Proceedings of the Fifth International Symposium on Swarm Behavior and Bio-Inspired Robotics*, pp. 1709-1713, 2022.

[4] Runyu Liu, Cong Yan and Fumihiko Asano, "Analysis of synchronization between active and passive bipedal walkers on tilted vibrating stage," *Proceedings of the Fifth International Symposium on Swarm Behavior and Bio-Inspired Robotics*, pp. 1735-1740, 2022.

[5] Cong Yan, Haosong Chen, Yanqiu Zheng, Longchuan Li, Isao Tokuda and Fumihiko Asano, "Entrainment-based control for underactuated compass-like biped robot," *Proceedings of the 20th International Conference on Advanced Robotics*, pp. 404-409, 2021.

[6] Cong Yan, Fumihiko Asano, Yanqiu Zheng and Longchuan Li, Xindi Zhao and Haosong Chen, "Analysis of biped robot on uneven terrain based on feed-forward control," *Proceedings of the 24th issue of the International Conference Series on Climbing and Walking Robots and the Support Technologies for Mobile Machines*, pp. 37-39, 2021.

[7] Haosong Chen, Cong Yan, Fumihiko Asano and Longchuan Li, "Quasi-passive dynamic biped walking based on entrainment effect," *Proceedings of the SWARM2021: The 4th International Symposium on Swarm Behavior and Bio-inspired Robotics*, pp. 441-450, 2021.

[8] Cong Yan, Longchuan Li and Fumihiko Asano, "Modeling and analysis of semicircular-footed compass-like biped robot with entrainment-based control," *Proceedings of the SWARM2021: The 4th International Symposium on Swarm Behavior and Bio-inspired Robotics*, pp. 451-462, 2021.

[9] Cong Yan, Haosong Chen, Yanqiu Zheng and Fumihiko Asano, "Gait analysis of biped robot with semicircular feet only on front side driven by sinusoidal hip torque," *Proceedings of the SWARM2021: The 4th International Symposium on Swarm Behavior and Bio-inspired Robotics*, pp. 486-497, 2021.

Domestic Conference

[10] Cong Yan, Longchuan Li, Yanqiu Zheng and Fumihiko Asano "Gait Generation and Motion Analysis of Quasi-passive Walking Robot Based on Entrainment Effect," *Proceedings of the 33rd symposium on Robotics and Mechatronics*, pp. 2P3-G15(1)-2P3-G15(4), 2021. (In Japanese)

[11] Cong Yan, Longchuan Li, Haosong Chen and Fumihiko Asano "Stable Gait Generation Based on Entrainment Effect Considering Natural Dynamics of Underactuated Biped Robot," *Proceedings of the 21st SICE Symposium on System Integration*, 1D3-04, pp. 455-459, 2020. (In Japanese)

[12] Cong Yan, Fumihiko Asano and Longchuan Li, "Stable Gait Generation of A Unilateral Driving Force Invalid 3-link Biped Robot by Upper-body Swinging and period tuning,"

Proceedings of the 32nd symposium on Robotics and Mechatronics, pp. 2P1-J13(1)-2P1-J13(4), 2020. (In Japanese)

[13] Longchuan Li, Cong Yan, Isao Tokuda and Fumihiko Asano, "Energy-Efficient Locomotion Generation and Theoretical Analysis of a Quasi-passive Dynamic Walker," *Proceedings of the 32nd symposium on Robotics and Mechatronics*, pp. 2P2-H01(1)-2P2-H01(4), 2020. (In Japanese)